Chemical Science

REVIEW

View Article Online
View Journal | View Issue

Cite this: *Chem. Sci.*, 2024, **15**, 15023

Received 30th April 2024
Accepted 2nd August 2024

DOI: 10.1039/d4sc02888k

rsc.li/chemical-science

Four-electron reduction of CO_2: from formaldehyde and acetal synthesis to complex transformations

Sarah Desmons,†[a] Julien Bonin,*[bc] Marc Robert *[bcd] and Sébastien Bontemps *[a]

The expansive and dynamic field of the CO_2 Reduction Reaction (CO_2RR) seeks to harness CO_2 as a sustainable carbon source or energy carrier. While significant progress has been made in two, six, and eight-electron reductions of CO_2, the four-electron reduction remains understudied. This review fills this gap, comprehensively exploring CO_2 reduction into formaldehyde (HCHO) or acetal-type compounds ($EOCH_2OE$, with E = [Si], [B], [Zr], [U], [Y], [Nb], [Ta] or −R) using various CO_2RR systems. These encompass (photo)electro-, bio-, and thermal reduction processes with diverse reductants. Formaldehyde, a versatile C_1 product, is challenging to synthesize and isolate from the CO_2RR. The review also discusses acetal compounds, emphasizing their significance as pathways to formaldehyde with distinct reactivity. Providing an overview of the state of four-electron CO_2 reduction, this review highlights achievements, challenges, and the potential of the produced compounds – formaldehyde and acetals – as sustainable sources for valuable product synthesis, including chiral compounds.

1. Introduction

Research in CO_2 transformations conducted by the Carbon Capture and Utilization (CCU) community is driven by both fundamental and applicative motivations. On the fundamental side, the goal is to find the keys to transform this thermodynamically and kinetically stable molecule. On the practical side, there is a desire to emulate nature by using CO_2 either as a synthetic building block or as an energy carrier. These objectives gain urgency due to the increasing concentration of atmospheric CO_2 and the inevitable depletion of fossil

Sarah Desmons

Sarah Desmons is currently a postdoctoral researcher in the Laboratory of Inorganic Synthesis and Catalysis (LSCI) at École Polytechnique Fédérale de Lausanne (EPFL) in Switzerland. She obtained her PhD in Chemistry and Biochemistry for the chemo-enzymatic conversion of CO_2 into carbohydrates from the Laboratoire de Chimie de Coordination (LCC) and the Toulouse Biotechnology Institute (TBI) in Toulouse, France. Her current research focuses on the enantioselective production of chiral amines via tailored bio-catalyzed hydroamination reactions.

Julien Bonin

Julien Bonin received his PhD in molecular physical chemistry from the Université Paris-Sud 11 in 2005. He then joined the Radiation Laboratory at the University of Notre Dame as a Postdoctoral Research Associate for one year. From 2006 to 2024, he has been an Associate, then a Full Professor of Chemistry at the Université Paris Cité, and he has now joined Sorbonne Université. His current research interests are related to photochemistry, redox catalysis and CO_2 reduction.

---

[a]LCC-CNRS, Université de Toulouse, CNRS, 205 route de Narbonne, 31077 Toulouse Cedex 04, France. E-mail: sebastien.bontemps@lcc-toulouse.fr

[b]Laboratoire d'Electrochimie Moléculaire, Université Paris Cité, CNRS, F-75013, Paris, France. E-mail: julien.bonin@sorbonne-universite.fr; marc.robert@sorbonne-universite.fr

[c]Institut Parisien de Chimie Moléculaire, Sorbonne Université, CNRS, F-75005, Paris, France

[d]Institut Universitaire de France (IUF), F-75005, Paris, France

† Present address: Laboratory of Inorganic Synthesis and Catalysis, Institute of Chemical Sciences and Engineering, Ecole Polytechnique Fédérale de Lausanne (EPFL), EPFL-ISIC-LSCI, BCH 3305, Lausanne, CH 1015 Switzerland.

resources. Given its significance and broad scope, the field of CO_2 transformation has been extensively covered in numerous reviews and books. Early reviews[1] and comprehensive perspectives[2] provide authoritative insights. Other reviews focus specifically on the use of CO_2 as an energy carrier[3] or as a synthetic reagent.[4] From an applied perspective, the importance of Life Cycle Assessment (LCA)[5] has been considered to evaluate the industrial potential of various processes.[6] From a thermodynamic standpoint, this expansive field can be categorized into reactions involving a redox event at the carbon atom of CO_2 (CO_2 Reduction Reaction: CO_2RR) or those that do not.[4a] Motivations for the CO_2RR include using CO_2 as an energy carrier, as energy is formally stored during CO_2 reduction, and as a sustainable source of carbon. In the CO_2RR, comprehensive reviews have focused on the type of reduction used, whether it involves thermal reduction with dihydrogen,[7] hydroboranes,[8] or hydrosilanes,[9] (photo)electro reduction[10] or bio-catalysed reduction.[11] Other reviews explore the homogeneous[12] or heterogeneous[13] nature of the catalytic system.

Within the CO_2RR, the level of reduction of CO_2 is arguably the most important parameter to consider. Since the carbon atom of CO_2 is fully oxidized (+IV), it can be reduced by as much as $8e^-$ giving rise to four possible even reduction states shown (Scheme 1). The +II, 0, –II and −IV carbon atom oxidation states can be reached by electroreduction or hydrogenation of CO_2. The corresponding C_1 reduction products are represented in Scheme 1(a): CO[14] and HCOOH[15] ($2e^-$), HCHO and $ROCH_2OR$ ($4e^-$), CH_3OH[15a,16] ($6e^-$) and CH_4 (ref. 17) ($8e^-$). As shown in Scheme 1(b), the same oxidation states are reached with hydroelementation (E–H) reactions. Using mostly hydroborane ($E = BR_2$) and hydrosilane ($E = SiR_3$), HCOOE ($2e^-$), $EOCH_2OE$ and HCHO ($4e^-$), CH_3OE ($6e^-$) and CH_4 ($8e^-$) have indeed been reported. Although it does not correspond to a formal hydroelementation, the catalytic formation of CO ($2e^-$) was reported with hydroborane[18] and with diborane.[19] The $4e^-$ reduction products of CO_2 – namely formaldehyde and acetal compounds – occupy a distinct position compared to other **C1** reduction products (Scheme 1c). The reasons for this are explained below.

1.1. Why reducing CO_2 by $4e^-$ to formaldehyde?

In the context of an increasing demand for complex transformations of CO_2 beyond the simple C_1 building blocks mentioned earlier[20,21] and the desire for long-term CO_2 storage, formaldehyde offers unparalleled potential in terms of reactivity and versatility.[22] More than 30 million tons of formaldehyde are produced and used annually by the chemical industry. This commodity compound is typically synthesized from the partial oxidation of methanol under energy-demanding conditions, representing over 35% of the total methanol transformation.[22a,23] A mild and sustainable synthesis of formaldehyde from CO_2 would thus represent a significant advancement for the chemical industry. Most industrial applications use formaldehyde as a reticulating agent in condensation reactions leading to various C–N, C–O, C–S, and C–C bonds.

Furthermore, formaldehyde serves as a precursor to more complex molecules, including chiral ones,[24] being a C_1 and a C_n source in aldol[25] and formose reactions,[26] notably. These transformations are beyond the reach of other CO_2 reduction products.

However, there is still no selective and sustainable synthesis of formaldehyde from CO_2. This can be attributed to two major issues: (i) the $4e^-$ reduction stage requires any catalytic system to overcome the energy barriers for both the 2 and $4e^-$ reduction steps while preventing the $6e^-$ reduction, and (ii) the detection of formaldehyde (HCHO) is challenging due to its intrinsic instability, limiting further development and optimization. Depending on the reaction media (pH, solvent, co-substrates), formaldehyde can polymerize, precipitate, or react with other chemicals present in the mixture, making its characterization difficult. Several detection methods have been used, such as optical methods, chemical derivatization for HPLC and GC analysis, or chemical conversion for colorimetric method analysis (established by Nash in the 1950s).[27] Recently,

---

Marc Robert

Long time Professor at Université Paris Cité, Marc Robert is now Professor at Sorbonne Université and a Senior member (Innovation Chair) of the Institut Universitaire de France (IUF). His work is dedicated to electrochemical and photochemical approaches of electron-transfer processes and the catalytic activation of small molecules (CO_2, N_2), in an effort to solve contemporary energy challenges. He is an International Advisory Board member at Angewandte Chemie International Edition, ChemSusChem (Wiley), Artificial Photosynthesis and ACS Electrochemistry (ACS).

Sébastien Bontemps

Sébastien Bontemps has received his PhD in 2006 from the University Paul Sabatier in Toulouse and carried out postdoctoral stays at the University of Chicago and McGill University. Since 2009, he has been a CNRS researcher in LCC-CNRS in Toulouse developing research studies directed at CO_2 transformations, boron and hydride chemistry and at the synthesis of new first row metal complexes.

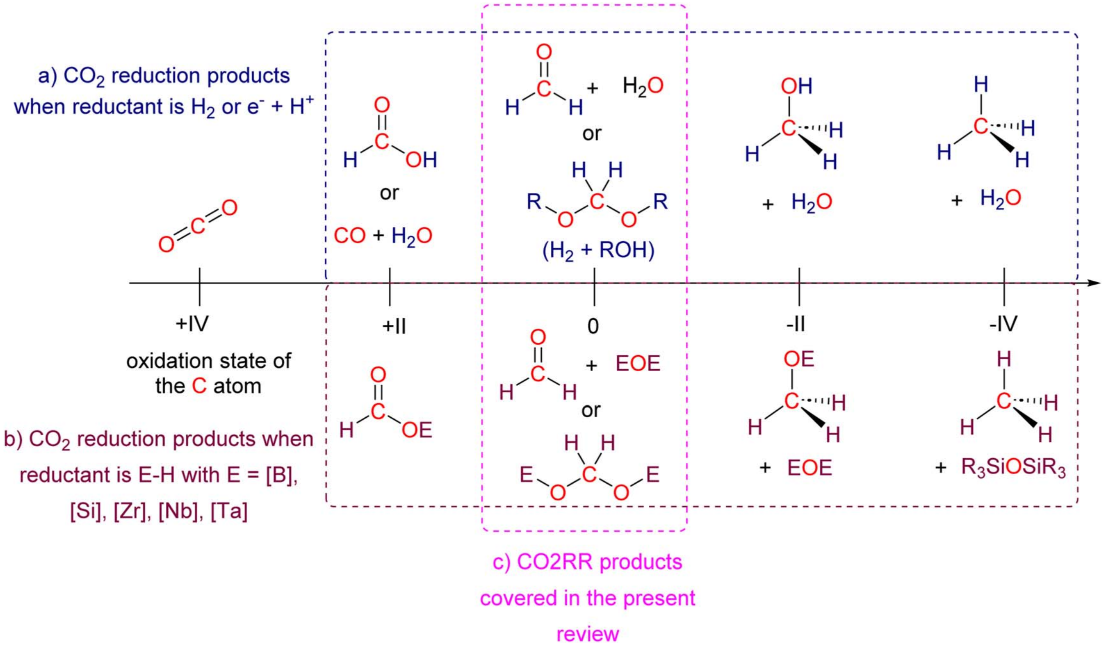

Scheme 1 C_1 products generated from CO_2 reduction by (a) hydrogenation or electroreduction or (b) hydroelementation reactions. (c) Formaldehyde and acetal compounds as the products of four-electron reduction of CO_2 covered in the present review.

a new and simple method for trapping and quantifying formaldehyde in aqueous solutions by ^{1}H NMR was designed, otherwise allowing for isotope labelling experiments and thus unambiguous demonstration that the HCHO production arises from CO_2 reduction.[28]

1.2. Why reducing CO_2 by $4e^-$ to acetal compounds?

The formation of acetal ($EOCH_2OE$) from hydroelementation of CO_2 is an important process linked to formaldehyde, because

(i) Some of these acetal compounds were shown to quantitatively release formaldehyde, offering an efficient and selective access to it under particularly mild conditions and with isotope labelling proving the origin of formaldehyde. The generated formaldehyde was subsequently used as C_1 and also C_n sources,[29] and notably in the first enantioselective transformation of CO_2 into a C_4 carbohydrate,[30] representing the highest level of complexity obtained from CO_2 at that time.[31]

(ii) Beyond the release of formaldehyde, acetal compounds were also involved in transformations related to but distinct from formaldehyde, notably when used as a C_n source. Interestingly, in one case, boryl moieties remained on the product, demonstrating a difference in reactivity compared to formaldehyde.[32] This finding should open opportunities to use the boryl or silyl functional groups as an integral part of new compounds as opposed to a waste moiety.

(iii) Finally, mild conditions and organic solvents used in hydroelementation enable *in situ* NMR monitoring leading to easier proofs of the origin of the acetal or formaldehyde by isotopic labelling experiments.

1.3. Objective and organization of the review

We aim at presenting the challenges and mechanistic considerations associated with formaldehyde[33] and acetal synthesis from CO_2 (Scheme 2a), as well as highlighting the reactions in which these reduction products have been involved (Scheme 2b). This review is organized by the type of reduction system: Hydrosilylation (Section 2), Hydroboration (Section 3), Other hydroelementation reactions (Section 4), Hydrogenation

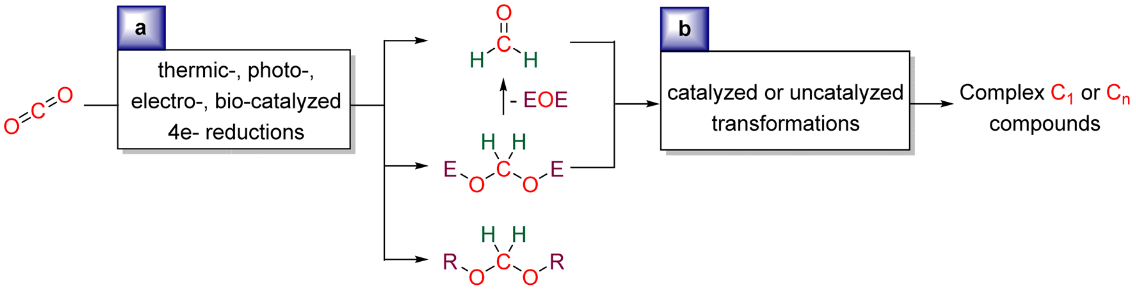

Scheme 2 General scheme presenting the current review: (a) synthesis of formaldehyde or acetal compounds from CO_2RR and (b) utilisation of formaldehyde and acetal as C_1 and C_n sources.

(Section 5), Electroreduction (Section 6), Photo(electro)reduction (Section 7), and Bio-catalysed reduction (Section 8). In each section, the reduction and subsequent transformations of the 4e$^-$ reduction products are presented, with special attention drawn to the mechanisms involved.

2. Hydrosilylation

Hydrosilylation of multiple C=C, C=O and C=N bonds has been intensely investigated, fuelling applications in the silicon industry as well as in synthetic chemistry, in asymmetric reductions in particular.[34] Hydrosilylation of CO_2 involves the addition of a Si–H bond to the C=O bond, transferring the hydride to the carbon atom and forming a Si–O bond. This reaction is favoured kinetically and thermodynamically by the polarity of the Si–H bond (electronegativity (E. N.) of H = 2.2, Si = 1.9) and the formation of a strong Si–O bond (>500 kJ mol^{-1}),[35] respectively. As a consequence, CO_2 hydrosilylation usually operates under mild conditions of temperature and pressure.

CO_2 hydrosilylation was first reported in 1981 with Ru- and Pd-based catalysts, independently.[36] In both cases, the reduction process led to formoxysilane (2e$^-$ reduction product). Hydrosilylation beyond the 2e$^-$ reduction stage was hypothesized in these two initial reports based on the observation of bis(silyl) ether ($R_3SiOSiR_3$) and of a small amount of formaldehyde (<4% yield) with the Ru-based catalyst.[36b] In 1989, an Ir-based catalyst enabled unambiguous observation of the hydrosilylation of CO_2 beyond the 2e$^-$ reduction stage. In this pioneering study, it was remarkable that the 2, 4 and 6e$^-$ reduction products – formoxysilane, bis(silyl)acetal (BSA) and methoxysilane, respectively – were subsequently observed.[37] Finally, the first report of CO_2 hydrosilylation into methane was published in 2006 by Matsuo and Kawaguchi with a $[Zr]/B(C_6F_5)_3$ catalytic system.[38]

Since these initial reports, the reduction of CO_2 by 4e$^-$ with hydrosilane witnessed a growing attention. The present section aims to cover in detail (i) the formation of BSA and formaldehyde in part 2.1, (ii) the mechanisms accounting for their generation in part 2.2, (iii) the proposed origin of the selectivity toward BSA in part 2.3, and (iv) their use as reactive intermediates in reductive functionalization reactions leading to more complex products in part 2.4 (Scheme 3).

2.1. Hydrosilylation of CO_2 into bis(silyl)acetals (BSAs) and formaldehyde

2.1.1. Description of BSA 1 to BSA 11. Bis(silyl)acetals (BSAs) are obtained from the double hydrosilylation of one molecule of CO_2. They feature an acetal core with two stabilizing silyl moieties attached to both oxygen atoms. Reported BSAs are depicted in Scheme 4 and their NMR characterizations are given in Table 1. Currently, eleven BSAs (**BSA 1–11**) have been reported in the literature. **BSA 1–6** have been generated from tertiary silanes $HSiMe_3$, $HSiEt_3$, $HSiPh_3$, $HSiMe_2Et$, $HSiPh_2Me$ and $HSiPhMe_2$, respectively, in excellent NMR yields (79 to 99%) regardless of the nature of silane substituents (trialkyl, triaryl or mixed silanes). Among them, only **BSA 2** and **3** were isolated with best yields of 94 and 95% with **C4** and **C17**, respectively. The utilization of secondary and primary silanes led to the formation of **BSA 7–10**. None of them was isolated. **BSA 10a** was characterized from a quasi-stoichiometric control experiment between a Co–formate complex and phenylsilane.[42] The use of only three equivalents of silane enabled the characterization of **BSA 10a** as the sole (silyl)acetal, in contrast to the observation of several BSA signals under the catalytic conditions. The presence of more than one hydride as reductive entities on the silicon atom with primary or secondary silanes indeed leads to the observation of multiple (silyl)acetal signals. This was clearly exemplified by Eisenberg *et al.* when using the dialkylsilanes, Me_2SiH_2 and Et_2SiH_2 (**BSA 7–8**, respectively).[37] In both cases, three ^{13}C and ^1H NMR signals characteristic of BSA were observed. Despite the ill-defined nature of the acetal mixture, the characteristic NMR chemical shifts and the absence of other signals in this area enable not only the detection but also the quantification of the (silyl)acetal entities. As shown in Table 1, a narrow range of methylene chemical shifts was observed in ^1H NMR (4.96 to 5.80 ppm) and in ^{13}C NMR (83 to 85.7 ppm) with $^1J_{CH}$ coupling constants between 161.5 and 164.4 Hz. In addition, conclusive labelling studies were reported with $^{13}CO_2$. ^{29}Si NMR data are restricted to **BSA 2**, **4–6**, and **11** with chemical shifts of 18.3, 17.7, −2.74, 6.99 and 24.0 ppm, respectively.

Most of the characterized BSA features tertiary silane moieties (**BSA 1–6** and **BSA 11**). Three of them were isolated (**BSA 2**, **3** and **11**) and the latter two were characterized by XRD. The higher stability of (silyl)acetals featuring tertiary silyl moieties is discussed in the mechanism section, Section 2.2. Catalysts were necessary to generate BSA but for **BSA 11**, which was derived from the hydrosilylation of CO_2 by an aluminum complex featuring two hydrosilane pendent moieties. **BSA 11** was generated as a minor product in 24% yield and features an acetal fragment stabilized by the Lewis acidic alane moiety.[43]

2.1.2. Catalytic systems. Selective (**C1–C25**) and non-selective (**C26–C36**) catalytic systems leading to the formation of **BSA 1–10** are described separately below. We consider

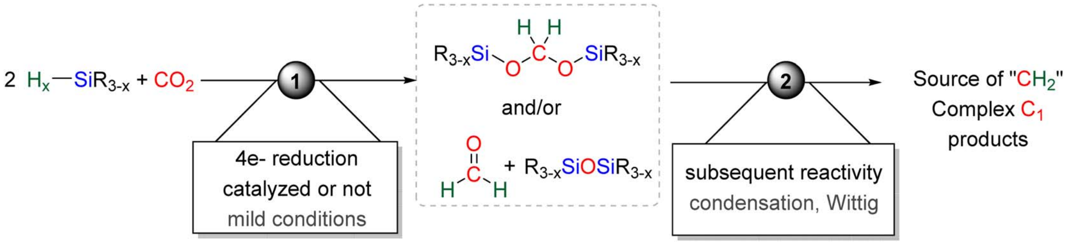

Scheme 3 General scheme of Section 2: CO_2 hydrosilylation.

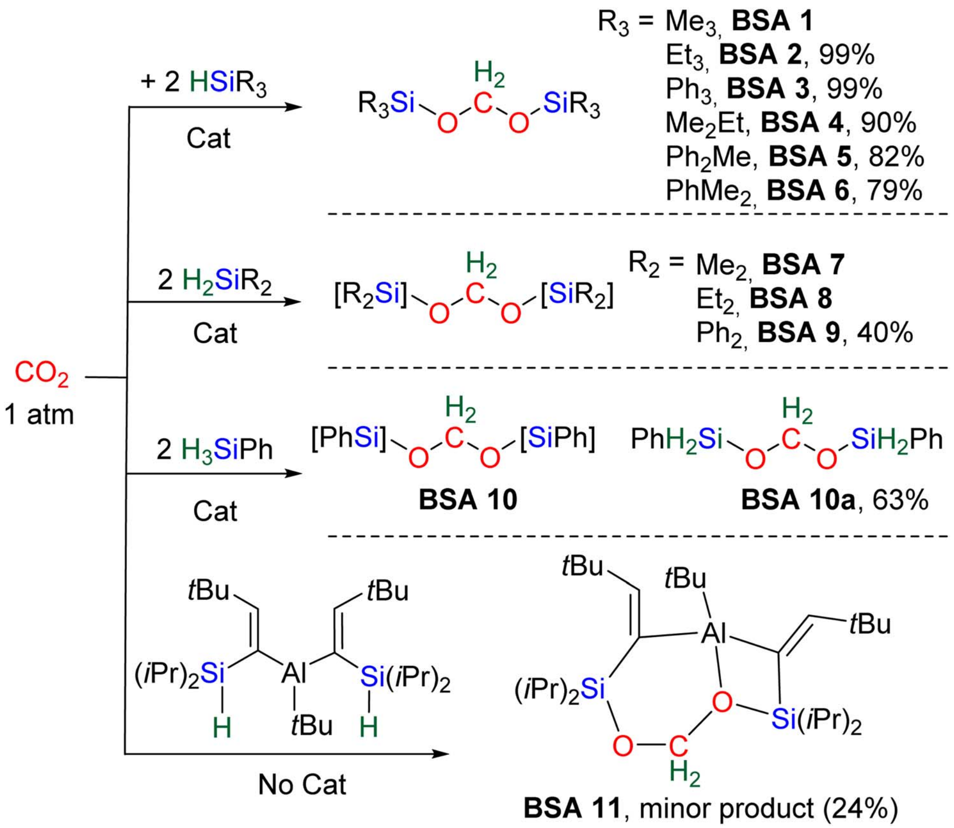

Scheme 4 Synthesis of **BSA 1–11**. The yields indicated are the best reported yields.

Table 1 NMR characterization of **BSA 1–11**

		$^{13}C(CH_2)$				
BSA	Solvent	δ (ppm)	$^1J_{CH}$ (Hz)	$\delta_{^1H}(CH_2)$ (ppm)	$\delta_{^{29}Si}$ (ppm)	Ref.
1	C_6D_6	—	164	5.03	—	37
2 [a]	C_6D_6	84.6	—	5.03	18.3	39
3 [a]	C_4D_5Br	85.5	—	5.55	—	38
	C_6D_6	85.7	164.4	5.45	—	38
4	C_6D_6	84.0	—	5.02	17.72	40
5	C_6D_6	84.9	—	5.21	−2.74	40
6	C_6D_6	84.5	—	5.06	6.99	40
7	C_6D_6	85.4	164	5.02	—	37
		84.5		5.08		
		83.8		5.12		
8	—	—	—	—	—	37
9	CD_3CN	83	—	5.8	—	41
10	C_6D_6	85.6	—	—	—	42
11 [a]	C_6D_6	87.6	—	5.04	24.0	43
				5.18		

[a] Isolated.

a system selective when it affords BSA as the major product even if at a low conversion rate of silane. Catalysts **C1–C25** are depicted in Fig. 1. The specific mode of action of these catalysts indicated with a colour code in Fig. 1 (bottom right) are discussed in detail in the mechanism section, Section 2.2.

Table 2 gathers the catalytic performances (turnover number – TON, turnover frequency – TOF, yield) of catalysts **C1–25**. Key features are the mild conditions in terms of temperature (ranging from 25 to 80 °C) and CO_2 pressure (from stoichiometric quantities to 6 atm). We have selected the conditions affording the best performances in terms of TON, TOF and/or yield for each catalytic system. TOFs are not given at the initial rate because such data were available only for **C5** (Table 2). All BSA derivatives were obtained selectively with the exception of **BSA 1**, **7** and **8**. Most of the TON values are in between 10 and 89. The catalysts **C1**, **C8**, **C11**, **C12**, **C17** and **C25** afford high TONs of 203, 395, 285, 620, 178 and 670, respectively. Only catalysts **C4** and **C8** led to exceptionally high TON values of 3400 and 1200, respectively. Moreover, **C8** and **C25** led to maximum TOFs of 55.8 and 52 h^{-1}, respectively, while all the other catalysts led to TOFs between 0.1 and 10.4 h^{-1}.

In addition to TON and TOF, yields are important to assess the selectivity of a given system. This is particularly important when the synthesized BSA is intended to be used as an intermediate in one-pot transformation (see reductive functionalization, Section 2.4). Most of the catalysts afforded BSA in yields higher than 73%. **BSA 2** was notably isolated from **C8**-catalyzed CO_2 hydrosilylation on the NMR scale, while larger scales of **BSA 2** (570 mg, 2.1 mmol) and **BSA 3** (2.67 g, 4.7 mmol) were isolated with **C4**- and **C17**-catalyzed reactions, in 94 and 95% yield respectively. This preparative scale notably facilitated the utilization of **BSA 3** in subsequent transformations (see reductive

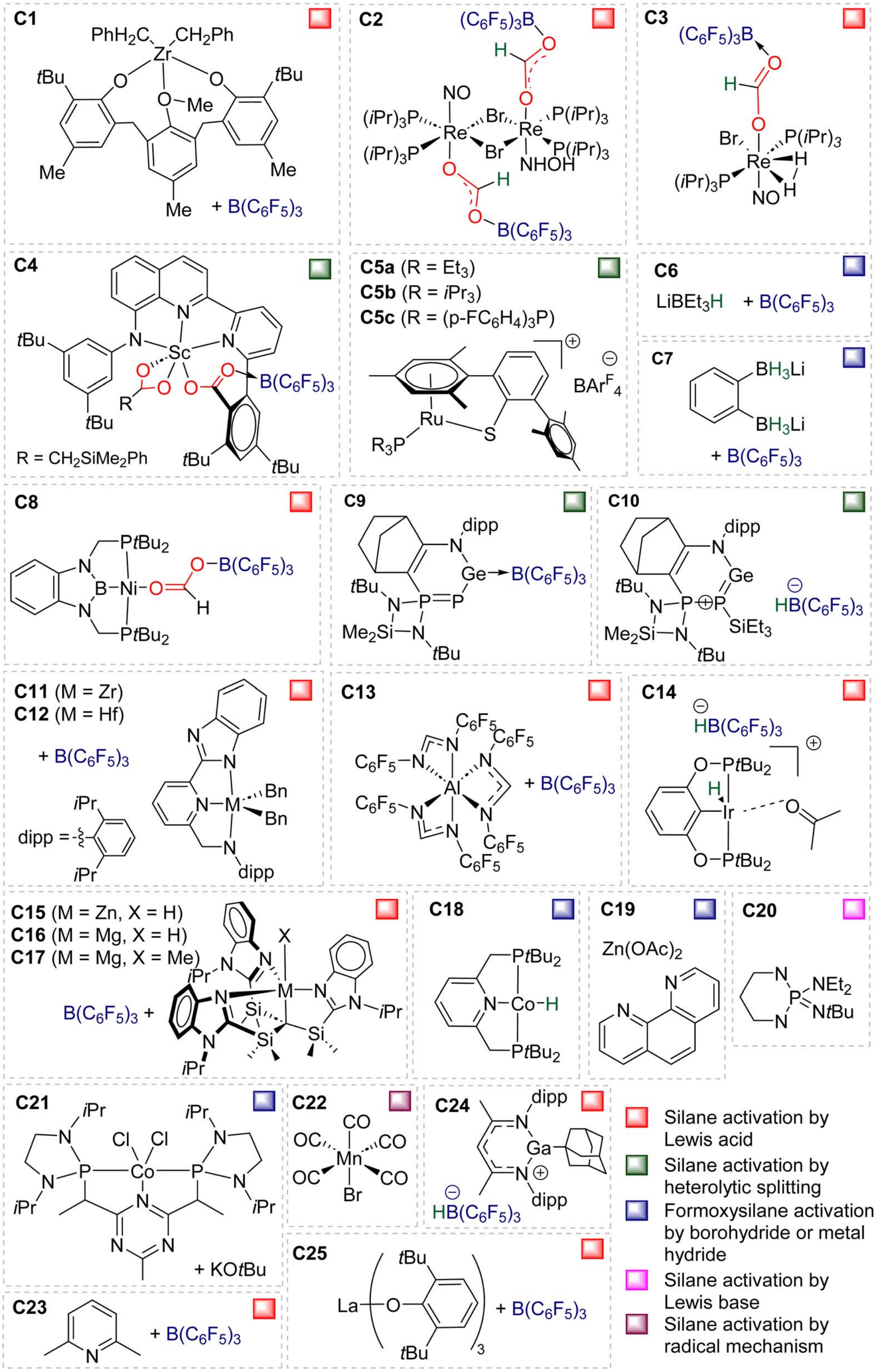

Fig. 1 Catalysts **C1–C25** leading to the selective formation of BSA.

functionalization, Section 2.4). The yields for hydrosilylation of CO_2 are given based on the hydrosilane and not on the CO_2 conversion in the vast majority of the cases. This is due to the difficulty in controlling the amount and conversion of CO_2 as a gas with ^{13}C NMR titration and to the fact that silane is considered to be the most expensive reactant. Yields based on

Table 2 Catalytic performances of the selective catalysts **C1–C25** for the synthesis of **BSA 2–6, 9** and **10**

BSA	Catalyst	TON[a]	TOF (h^{-1})	Yield[b] (%)	P_{CO_2}[f]	T (°C)	Time (h)	[Cat] (%)	Ref.
2	**C1**	203	1.2	82	1	25	165	0.9	38
	C2	89	5.9	87	5	80	15	1	44
	C3	95	7.3	89	5	80	13	1	
	C4	1000	10.4	94[e]	4	65	96	0.1	45
		3400	n.d	94[e]	4	65	n.d	0.02	
	C5a	25	6.2/11[c]	99	5	80	4	4	40
		49	1.5/8.6[c]	80	5	80	32	2	
	C5b	25	0.51/<0.01[c]	89	5	80	48	4	
	C5c	25	0.34/0.00[c]	>99	5	80	72	4	
	C6	n.d	n.d	91	1	50	24	10	46
	C7	n.d	n.d	54	1	50	41	10	
	C8	1200	55.8	60[d]	4	70	21.5	0.05	39
		910	26.8	91[d]	4	70	34	0.1	
	C9	20	0.8	82	3	60	24	5	47
	C10								
	C11	395	6.6	76	1	22	60	0.24	48
	C12	285	5.9	55	1	22	48	0.24	
	C13	9	0.69	60	6	80	13	1.5	49
	C22	57	57.3	86	4	50	1	1.5	50
	C24	17	0.3	85	2	60	58	10	51
	C25	99	99	99	5	25	1	1	52
3	**C1**	50	0.13	64	1	25	384	2	38
	C14	36	2	100	1	23	22.7	2.5	53
	C15	12	0.1	n.d	1	25	120	2 : 10	54
	C16	83	1.2	n.d	1	25	69	0.5 : 2.5	
	C17	178	2.5	n.d	1	25	72	0.5 : 2.5	29*a*
		n.d	n.d	95[e]	1	25	672	1	
	C25	670	52	67	5	80	13	1	52
4	**C5a**	31	0.57/7.8[c]	64	5	80	55	2	40
		25	2.3/12[c]	90	5	80	11	4	
5	**C5a**	17	0.23/3.9[c]	24	5	80	73	2	40
		25	0.69/12[c]	79	5	80	36	4	
	C8	620	16.5	62[d]	4	70	37.5	0.1	40
		137	18.3	82[d]	4	70	7.5	0.6	
6	**C5a**	32	0.44/6.2[c]	55	5	80	73	2	40
		24	0.32/9.5[c]	79	5	80	75	4	
	C8	121	40	78	4	70	3	0.6	39
9 [g]	**C13**	3.5	0.07	31	6	80	48	1	49
	C19	40[i]	1.7[i]	40[i]	1 mmol	25	24	1	55
	C20	5.6	1.4	7	5	25	4	1.25	56
10 [h]	**C18**	32/126[j]	1.2/4.8[j]	63	0.4 mmol	25	26	2	42

[a] TON = silane converted/catalyst loading unless otherwise stated. [b] *In situ* yield unless otherwise stated. [c] Initial rate measured after 1 hour. [d] No other product detected. [e] Isolated yield. [f] atm unless otherwise stated. [g] 2 eq. *vs.* CO_2. [h] 4 eq. *vs.* CO_2. [i] Based on hydrosilane and on CO_2 conversion. [j] Based on CO_2 conversion.

CO_2 conversion are nonetheless significant because (i) it allows for more complete description of a given catalytic system by reporting its performances based on both reactants and (ii) silane is not necessarily the most expensive substrate, notably when isotopically labelled CO_2 is used. Performance data based on CO_2 conversion are particularly important when $^{11}CO_2$ and $^{14}CO_2$ are used for radiochemistry.[57]

Compounds **C26**,[58] **C27**,[37] **C28**,[59] **C29**,[60] **C30**,[61] **C31**,[41] **C32**,[62] **C33**,[49] **C34**,[49] **C35**[63] and **C36**[64] were shown to catalyse the hydrosilylation of CO_2 affording BSA as a minor product (Fig. 2). Most of these systems were optimized for the generation of methoxysilane and/or methane and not for BSA. The observation of BSA as intermediates in many cases confirms that (silyl) acetals are very often on the reaction pathway to the 6 and 8e⁻ reduction products in hydrosilylation processes.

2.1.3. Formaldehyde. The observation of formaldehyde from CO_2 hydrosilylation was only reported at 100 °C with $Ru(Cl)_2(PPh_3)_3$ as the catalyst in 1981 (Scheme 5).[36b] It was however observed in less than 4% yield and detailed experimental data are lacking to know if free formaldehyde was observed by a direct or indirect method after derivatization. Based on current knowledge, one can wonder if the detected formaldehyde may result from BSA evolution, although the authors explicitly indicated that no experimental proofs were found for BSA generation.

More recently, BSA was utilized as an intermediate to selectively access formaldehyde (Scheme 6). The air stable **BSA 3**

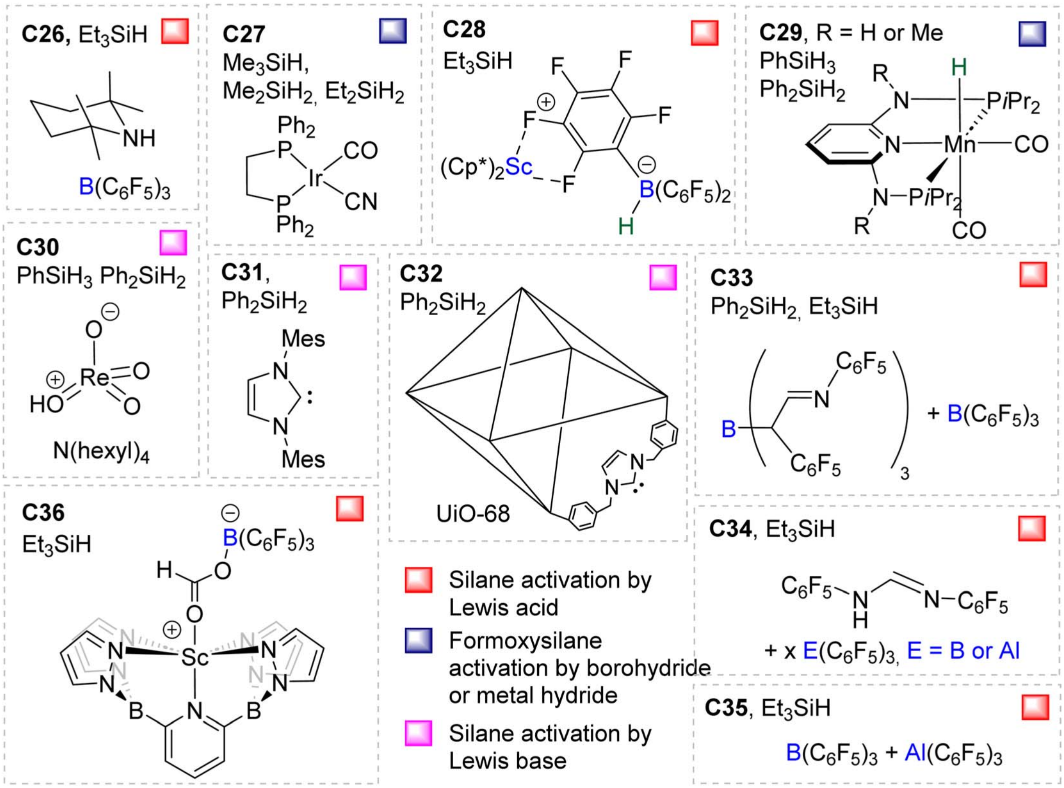

Fig. 2 Unselective catalytic systems **C26–C36** and hydrosilane employed.

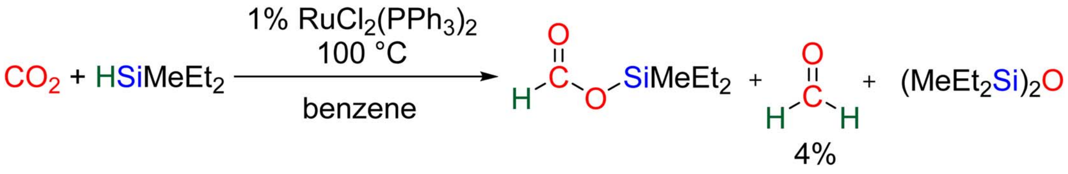

Scheme 5 Early observation of formaldehyde from CO_2 hydrosilylation.

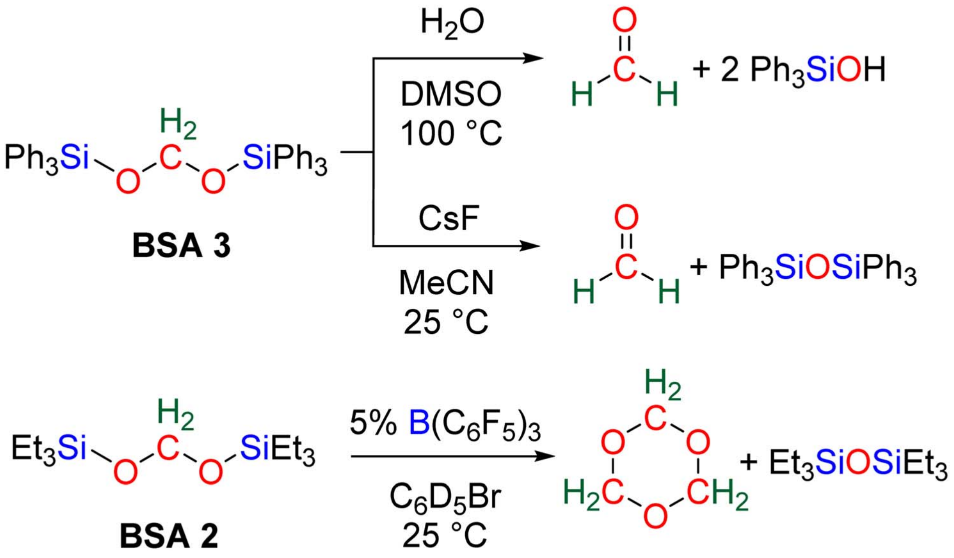

Scheme 6 Quantitative generation of formaldehyde from **BSA 2** and **3**.

featuring triphenylsilyl groups was shown to quantitatively deliver formaldehyde in DMSO/H_2O at 100 °C or in the presence of H_2SO_4 at room temperature.[29a] Alternatively, CsF promoted the generation of formaldehyde at room temperature, presumably *via* the breaking of the Si–O bond after fluoride attack on the silicon centre.

In another study, **BSA 2** featuring triethylsilyl moieties was shown to quantitatively release formaldehyde in the form of trioxane within 1 h in the presence of 5 mol% of $B(C_6F_5)_3$ as the catalyst at room temperature.[63] Conversely, **BSA 3** did not release formaldehyde in the presence of 22 mol% of $B(C_6F_5)_3$ in 10 days at room temperature.[29a] These contrasting reactivities between **BSA 2** and **BSA 3** highlight the influence of the silyl fragment on the reactivity of the BSA.

2.2. Mechanistic considerations

The $4e^-$ reduction of CO_2 into bis(silyl)acetal (BSA) or formaldehyde by hydrosilane takes place along two steps: (i) the $2e^-$ reduction of CO_2 into either formoxysilane or metal formate (Scheme 7, step (i)), followed by (ii) the hydrosilylation of the intermediate into the corresponding $4e^-$ reduction products (Scheme 7, step (ii)). The elementary reactions accounting for step (i) have been already investigated both experimentally and theoretically in reviews focusing on CO_2 hydrosilylation.[9] We will focus here on the less investigated second reduction step leading to the $4e^-$ reduction products. A thorough evaluation of the different mechanisms showed that the role of the catalyst is to activate either the hydrosilane or the formoxysilane, along different activation modes depending on the nature of the catalyst which are described hereafter for the catalysts **C1–36**. A summary of the different activation modes is given in Section 2.2.7 with a general scheme, Scheme 13.

2.2.1. Activation of the hydrosilane by a Lewis base. The N-Heterocyclic Carbene (NHC) **C31** has been shown to catalyse the hydrosilylation of CO_2 into methoxysilane with the observation of BSA as an intermediate.[41] DFT investigations have suggested that the NHC activates the hydrosilane to trigger a hydride transfer to the formoxysilane and the generation of the BSA (Scheme 8).[65] The calculated transition state (**TS1**) of the rate determining step involves three key components: **C31** acting as the LB activator, Ph_2SiH_2 as the reductant and finally the formoxysilane intermediate. A subsequent – almost barrier less – step regenerates the catalyst **C31** along with the BSA release. Although not yet proven, the action mode of **C20**,[56] **C30**[61] and **C32**[62] may be similar to that of **C31** because of their high Lewis basicity. Theoretical investigations on the hydrosilylation of CO_2 catalysed by the perrhenate anion **C30** also support such views with a similar activation pathway of the hydrosilane for the first reduction step to formoxysilane.

2.2.2. Activation of the hydrosilane by a Lewis acid. Hydrosilanes are typically activated by strong Lewis acids promoting the transfer of a silylium "Si^+" moiety. The cationic

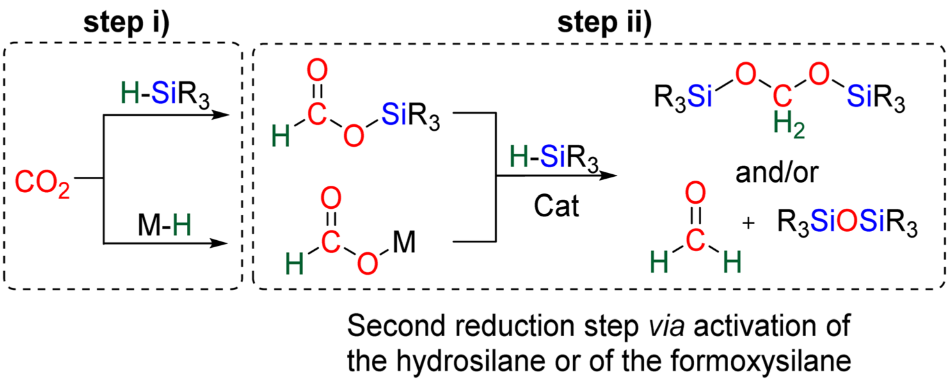

Scheme 7 Two mechanistic pathways for the $4e^-$ reduction of CO_2 by hydrosilanes.

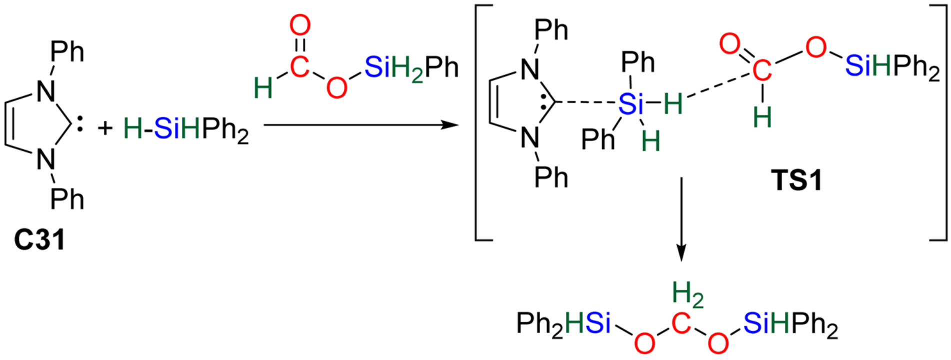

Scheme 8 Schematic view of the computed transition state (**TS1**) of the Lewis basic activation of hydrosilane by catalyst **C31**.

Ir-based complex **C14** and $B(C_6F_5)_3$ are two prototypical compounds known to catalyse the activation of hydrosilanes in various transformations.[66] In such Lewis acid-catalysed generation of BSA, combined cationic TM-based complexes and $B(C_6F_5)_3$ were proposed to catalyse hydrosilylation either of a silylformate or of a metal formate as illustrated in Scheme 9a and b, respectively.

2.2.2.1. *Silyl formate intermediate.* Scheme 9a describes the mechanism associated with a Lewis acidic system promoting the silylium "Si$^+$" transfer to *silyl formate* species. Such a reaction occurred in an S_N2-type activation going through the transition state **TS1a**. The resulting intermediate is then involved in a second elementary step through the transition state in which the hydride abstracted by the Lewis acid (H-LA) is transferred to the carbon atom of the carbonyl function to form the corresponding BSA derivative while regenerating the Lewis acid. Such a mechanism was computed for **C14**,[53,67] **C26**,[58,68] and **C35**.[63]

In the cases of **C14** and **C26**, **TS1a** was found to be higher in energy than **TS2a**, while the reverse was found with **C35**. The catalysts **C1**, **C11–13**, **C15–17**, **C24–25**, **C28** and **C36** are proposed to follow a similar pathway. The catalysts **C18**, **C33** and **C34** could also follow a similar pathway but the observed induction period points toward a more complex process.

2.2.2.2. *Metal formate intermediate.* Scheme 9b describes the mechanism associated with the Lewis acidic system promoting the silylium "Si$^+$" transfer to metal formate species. In the cases of **C2**, **C3** and **C8**, the second reduction step indeed occurred at a metal formate intermediate. The mechanism involving **C8** has been investigated by DFT (Scheme 9b).[69] Both **TS1b** and **TS2b** are similar to **TS1a** and **TS2a** respectively (Scheme 9a). The acetal obtained after these two first steps is a metal silyl acetal. After a second activation of the hydrosilane by $B(C_6F_5)_3$, this metal silyl acetal intermediate is converted into the corresponding BSA derivative along with the regeneration of the

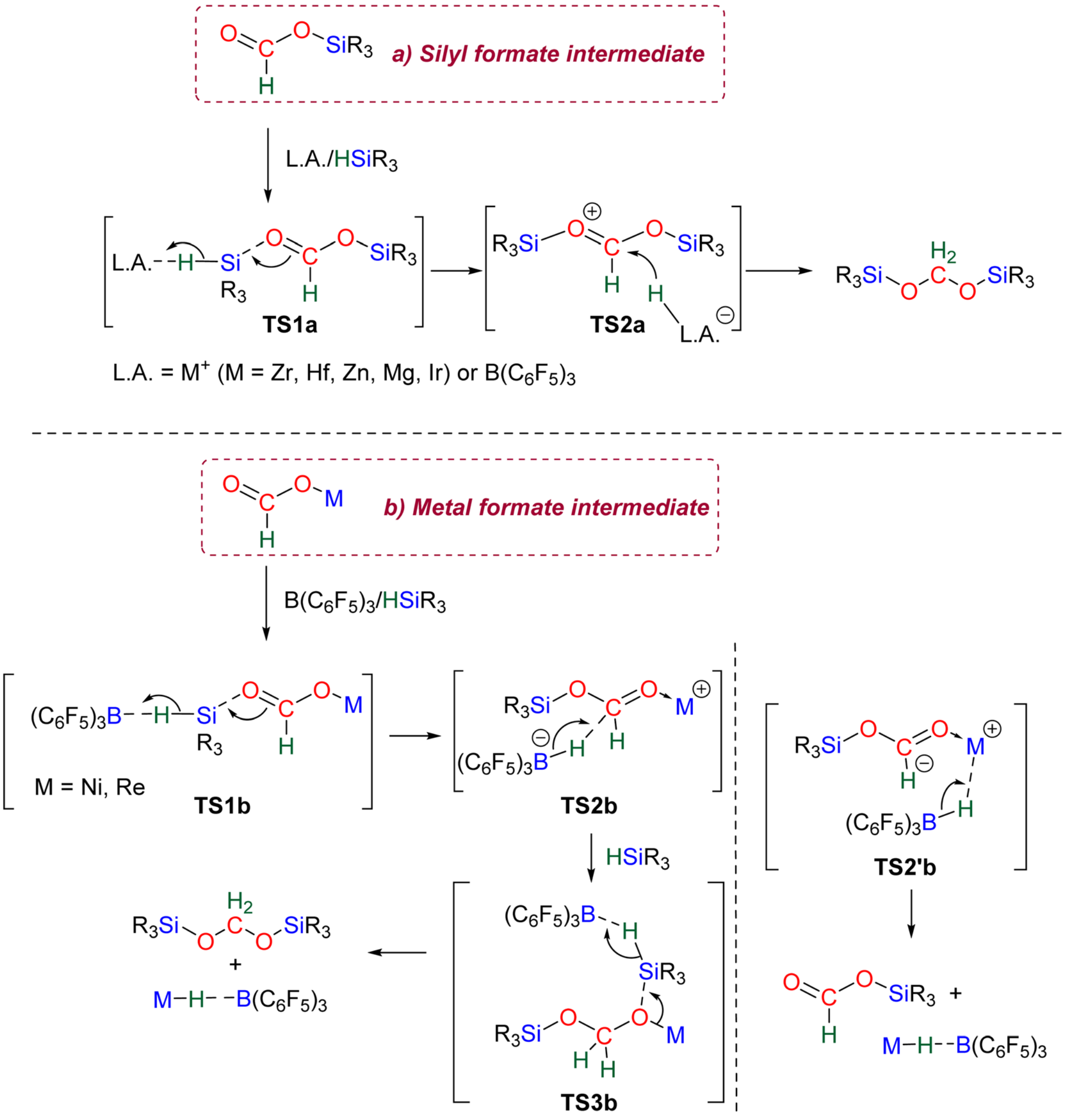

Scheme 9 Calculated Lewis acid activation of (a) silylformate or (b) metal formate intermediates. Only TS are shown for the sake of simplicity, and the movement of the electrons is schematically shown with arrows.

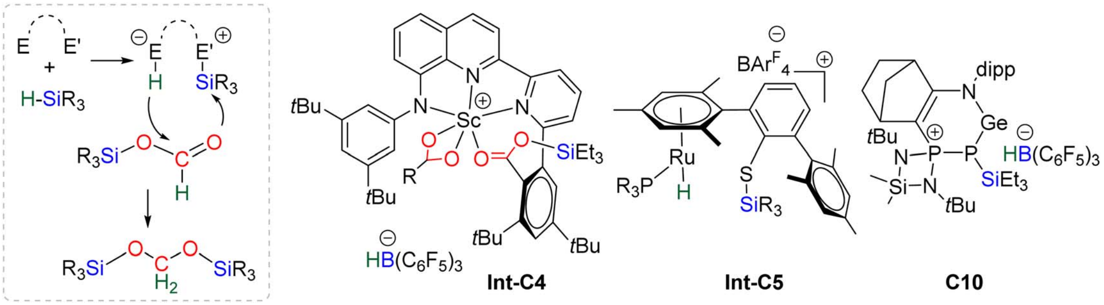

Fig. 3 Complexes resulting from the heterolytic splitting of hydrosilane prior to CO_2 hydrosilylation.

active catalyst. An alternative pathway involving **TS2′b** was also calculated to be iso-energetic.[69]

2.2.3. Heterolytic cleavage of the hydrosilane by bifunctional activation. While the catalytic systems **C4–5** [40,45] and **C9** [47] are structurally different systems, the proposed mechanism of activation is similar: heterolytic cleavage of the hydrosilane prior to the reduction of the formoxysilane (Fig. 3, left). To support this assumption, catalysts **C4–5** and **C9** were shown to heterolytically cleave hydrosilanes to afford the three species **Int-C4**,[45] **Int-C5** [70]) and **C10** (Fig. 3).[47] In addition, **C10** was isolated and used as a catalyst in place of **C9**, showing similar catalytic activity toward CO_2 hydrosilylation to that of **C9**. These compounds are proposed to transfer both silylium and hydride moieties to the formoxysilane intermediate to form the corresponding BSA derivative. Based on previous results concerning the hydrosilylation of other substrates, Oestreich *et al.* proposed the initial transfer of the silylium moiety followed by hydride transfer in a two elementary step mechanism with **Int-C5**.[40] Such a two-step pathway would be very similar to the calculated pathway for the Lewis acid activation of hydrosilane described above.

2.2.4. Homolytic cleavage of the hydrosilane by a radical initiator. $Mn(CO)_5Br$ complex **C22** was shown to catalyse the hydrosilylation of CO_2 into **BSA 2** with triethylsilane.[50] **C22** was proposed to generate a radical complex upon loss of a bromine atom which would then activate triethylsilane in a homolytic manner (Scheme 10). Although no mechanism for the second step was proposed, following the logic of the first reduction step suggests that addition of the silyl radical to the silylformate could take place, followed by hydrogen transfer from a Mn hydride species.

2.2.5. Activation of the formoxysilane by a metal-hydride moiety. As shown in Scheme 11, formoxysilane may be activated by metal hydride species by its formal addition into the M–H bond, leading to a metal(silyl)acetal which will then release the corresponding BSA. Catalytic systems **C18**, **C21**, **C27** and **C29** are proposed to follow this pathway. Detailed pathways were calculated with **C29** [60] and **C21**.[71] The in-depth theoretical investigation on catalyst **C21** points toward the insertion of the formoxysilane into the Co–H bond leading to the formation of a metal silyl acetal intermediate.[71] Following this addition, the metal centre is able to activate the hydrosilane *via* an oxidative addition leading to the transfer of the silyl ligand to produce BSA. Moreover, calculations enabled comparison of the three distinct catalytic cycles leading to the formoxysilane, the BSA and the methoxysilane products. The authors compared the

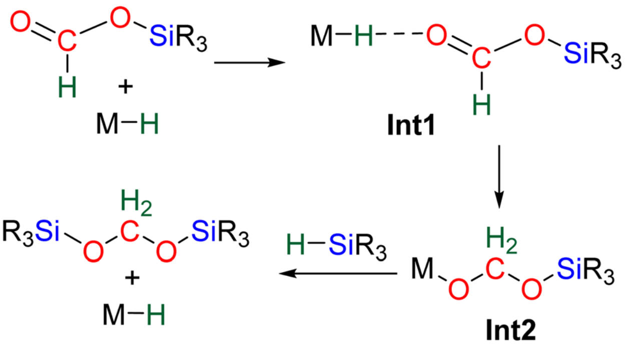

Scheme 11 Computed pathway for the hydrosilylation of formoxysilane to BSA with M-H catalyst **C29** and **C21**.

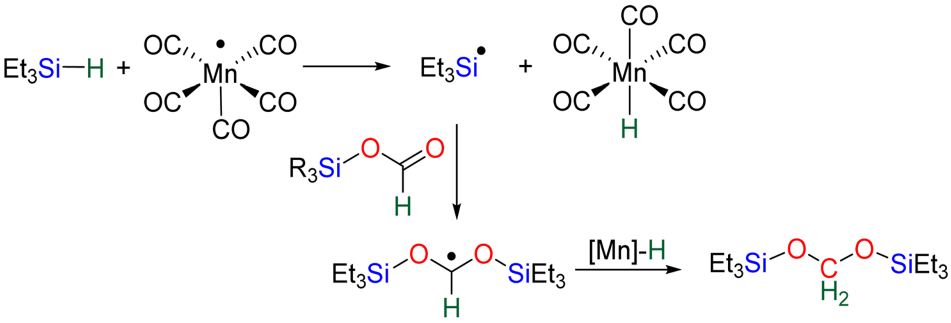

Scheme 10 Proposed mechanism for the radical activation of Et_3SiH by **C22** based on experimental results.

energy gap values δ*E* between the most stable intermediate and the highest transition state for each cycle. The smaller value (24.2 kcal mol^{-1}) found for the formation of the formoxysilane compared to the values for the BSA (28.9 kcal mol^{-1}) and the methoxysilane (29.9 kcal mol^{-1}) explain why formoxysilane could be obtained selectively. The small difference between the δ*E* of BSA *vs.* δ*E* of methoxysilane explains the difficulty in selectively generating BSA in these systems. These calculations reproduced the experimental selectivity obtained under different reaction conditions of temperature and pressure. We hypothesize that the catalytic system **C19** followed this pathway as well, based on the assumption that the combination of the bidentate ligand (*i.e.*, 1,10-phenanthroline) and $Zn(OAc)_2$ would generate a Zn–H moiety in the presence of a hydrosilane under catalytic conditions.

2.2.6. Activation of the formate by a borohydride.

Catalyst systems **C6** and **C7** are the only borohydride compounds reported so far to catalyse the hydrosilylation of CO_2 into BSA.[46] No theoretical investigations were conducted. Based on experimental findings, the proposed mechanism involves the insertion of CO_2 into two B–H bonds of borohydride catalyst leading to a dianionic acetal intermediate (Scheme 12). This assumption is based on the observed reactivity of **C7** with CO_2 and bromobenzoic acid as the CO_2 surrogate. The reactivity of **C7** toward CO_2 was indeed immediate but led to an insoluble material difficult to analyse. However, the reactivity toward bromobenzoic acid led to the reaction of the two borohydride fragments with two equivalents of the carbonyl part. While no further insights were gathered with theoretical investigations for these specific systems, the ability of borohydride to insert CO_2 was observed previously in various studies.[72] An alternative BR_3/SiR_3 exchange after each borohydride addition may also be at play and would avoid any charge build-up.

2.2.7. Summary of the activation modes of hydrosilane or formoxysilane.

Most of the catalytic systems activate the hydrosilane reductant either *via* (i) Lewis base (LB), (ii) Lewis acid (LA), (iii) heterolytic splitting of the Si–H bond in a bifunctional manner or (iv) homolytic cleavage by a radical initiator. The Lewis acid activation is at play in the majority of the examples. In fewer cases, the silyl- or boryl-formate intermediates are activated by (v) a metal or (vi) a borohydride species. The different activation modes are summarized in Scheme 13.

2.3. Origin of the selectivity for BSA

The control or simply the understanding of the selectivity for bis(silyl)acetal (BSA) is a challenge. In this section we describe some of the main parameters which have been shown to favour

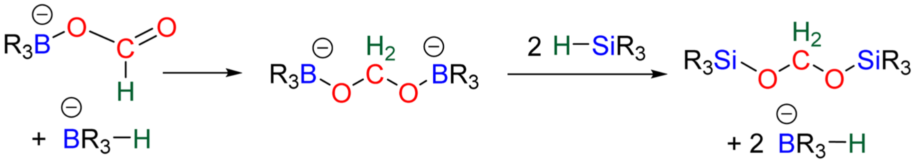

Scheme 12 Proposed mechanism for **C6** and **C7** catalytic systems based on experimental results.

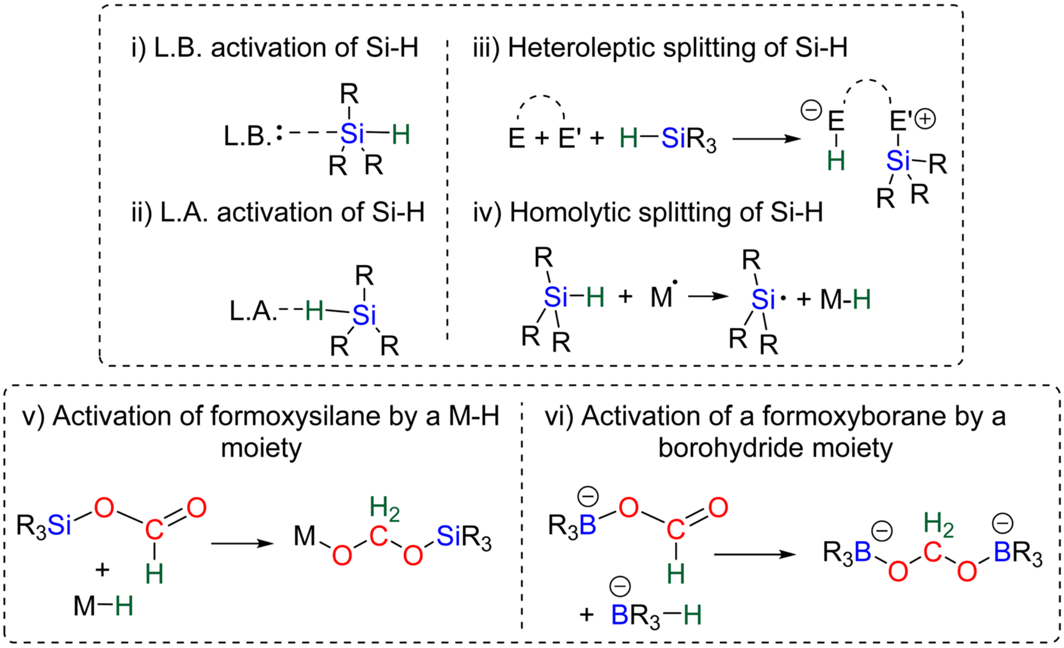

Scheme 13 Activation modes of hydrosilane or formoxysilane leading to (silyl) acetals **BSA** (LB = Lewis base, LA = Lewis acid).

BSA accumulation either upon thermodynamic stabilization or by disfavouring further reduction to methoxysilane or methane.

2.3.1. Thermodynamic and kinetic stabilization of BSA by the nature of the silyl groups. Although no specific study was conducted on the role of the silyl group in the stabilization of BSA, two theoretical investigations provided some reactivity trends. These calculations suggested that BSA evolves to formaldehyde *via* **TS1**, and the formaldehyde is then further reduced to methoxysilane and/or methane (Scheme 14). This process was calculated in two independent studies with phenylsilyl groups (SiH_2Ph) to be thermodynamically favoured by −9.1 and −5.0 kcal mol^{-1}, with an activation barrier of 25.1 and 26.7 kcal mol^{-1}.[65,73] When the same transformation was calculated with triethylsilyl ($SiEt_3$) groups, the reaction was then thermodynamically disfavoured by +1.7 kcal mol^{-1} with a barrier of 37.6 kcal mol^{-1}.[63] It thus appears that $SiEt_3$ groups bring both kinetic (>10 kcal mol^{-1}) and thermodynamic (about 8 kcal mol^{-1}) stability compared to phenylsilyl moieties. Although care must be taken while comparing different theoretical studies, these investigations point toward a higher stability of a BSA featuring tertiary silyl moieties as compared to BSA featuring primary silyl moieties. This corroborates the predominance of tertiary silanes for the selective generation of **BSA 1–6**, and **11**. Moreover, some catalysts were shown to favour BSA when tertiary silanes were employed, but methoxysilane and methane when secondary and primary silanes were employed. This is the case for example with **C1** and **C15–17**, while most of the other selective catalysts have not been tested with primary or secondary silanes. Finally, every isolated BSA featured trisubstituted silyl groups (**BSA 2**, **3** and **11**).

2.3.2. Sequestration of $B(C_6F_5)_3$. The origin of selectivity for BSA of the catalytic systems **C4** and **C8** employing $B(C_6F_5)_3$ is proposed to be the result of the formation of a Lewis pair between $B(C_6F_5)_3$ and an oxygen atom present on the complex. This so-called sequestration of $B(C_6F_5)_3$ during the process is proposed to prevent further reduction.[39,45,69] $B(C_6F_5)_3$ has indeed been shown to favour further reduction to methoxysilane or methane. Two modes of action were calculated (Scheme 15, paths a and b). In path a, $B(C_6F_5)_3$ catalyses the transformation of BSA into formaldehyde *via* **TS1**. This result was obtained within the same study presented just above with **BSA 2** featuring triethylsilyl moieties.[63] The $B(C_6F_5)_3$-catalyzed reaction was calculated to be 10 kcal mol^{-1} lower in energy compared to the uncatalyzed transformation. Moreover, the reaction was probed experimentally: while **BSA 2** was stable for a day in solution, it was transformed into formaldehyde within 1 h in the presence of 5% of $B(C_6F_5)_3$. The second mode of activation b occurs *via* an S_N2-type activation of the hydrosilane by the Lewis acid $B(C_6F_5)_3$ leading to silylium transfer (**TS2**) and finally hydride (**TS3**) transfer to form methoxysilane (Scheme 15, path b). These transformations were calculated in the cases of **C14** (ref. 67) and **C26**.[68] In accordance with this mechanism proposal, various

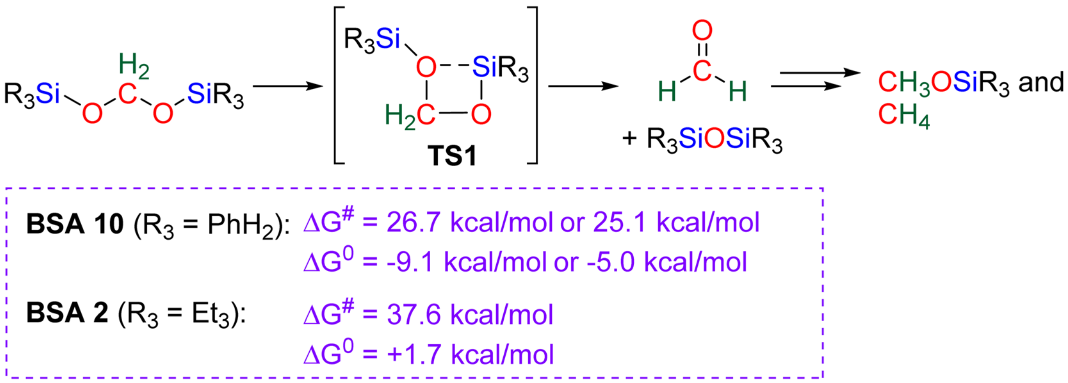

Scheme 14 Computational findings regarding the capability of BSA to liberate HCHO based on the type of silyl moiety.

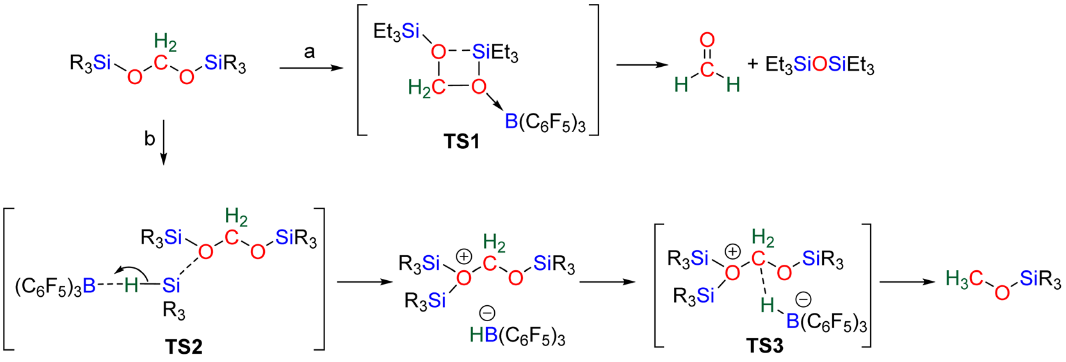

Scheme 15 Computed $B(C_6F_5)_3$-catalyzed conversion of BSA into formaldehyde or methoxysilane.

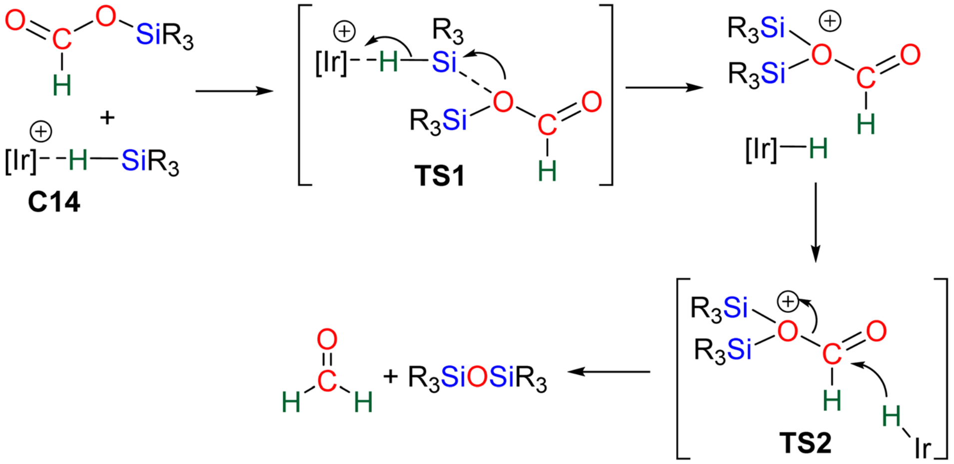

Scheme 16 Calculated pathway for the generation of formaldehyde from formoxysilane with the Ir-based catalytic system **C14**.

selective systems reported further reduction when an additional catalytic amount of $B(C_6F_5)_3$ was added to the system. This was notably the case for **C4**, **C8** and **C15–17**.

2.3.3. **Stoichiometry.** In most of the CO_2 hydrosilylation reactions reported, an excess of CO_2 gas was employed. In order to influence the level of reduction of the hydrosilylation reaction, 2 and 4 equivalents of CO_2 *vs.* silane were used with catalytic systems **C18** and **C19**, respectively. Under such stoichiometric or quasi-stoichiometric conditions, it was possible to observe the formation of BSA in 40 and 63% yields for **C18** and **C19**, respectively. The importance of the stoichiometry conditions was proven for **C18** since a larger ratio of CO_2 gave rise to formoxysilane whereas a larger amount of silane led to methoxysilane.

2.3.4. **Hydrosilylation of CO_2 to formaldehyde without the intermediary of BSA.** While formaldehyde was experimentally shown to be obtained from BSA with further insights from calculations, its generation without the intermediary of BSA remains an open question. Besides its experimental observation early on in less than 4%, there is only one theoretical investigation reporting such generation with the Ir-based catalytic system **C14**.[67] As depicted in Scheme 16, the cationic [Ir]-hydride complex was calculated to promote silylium transfer to the $OSiR_3$ moiety of the formoxysilane intermediate in **TS1**, ultimately leading to formaldehyde *via* **TS2**. However, the same calculation showed that the silylium transfer to the oxygen atom of the carbonyl leading to BSA was favoured explaining why formaldehyde was not observed experimentally during the reaction.

2.4. Bis(silyl)acetal as an intermediate in reductive functionalization of CO_2

The reductive functionalization of CO_2 refers to the reduction of CO_2 combined with the functionalization of the reduced product with a co-reactant. The term was first employed in the case of the hydrosilylation of CO_2 into formoxysilane, intercepted with amines to afford formamide, formamidine or methylamine derivatives.[20c,74] An early reaction of this type can be traced back to a report on the preparation of formamide from CO_2 reduction in the presence of amine in 1988.[75] In this case, the reductant was not hydrosilane but dihydrogen. Although unexpected, the first reductive functionalization of CO_2 *via* the generation of a bis(silyl)acetal (BSA) intermediate was reported in a study devoted to the use of cationic Al-based species for catalysing the hydrosilylation of CO_2 to methane.[76] In the course of the reaction, the formation of deuterated diphenylmethane **1** featuring a bridged-methylene moiety was observed (Scheme 17). Experimental proofs showed that transiently generated BSA reacted with the deuterated solvent *via* electrophilic catalysis by the cationic Al-based compound to afford compound **1** *via* compound **2**.

Following this preliminary report, subsequent studies reported the use of BSA as a key intermediate for the generation of more complex products in the presence of various co-reactants. Such strategies considerably enlarged the scope of compounds obtained from CO_2 in using BSA as a source of methylene for the formation of C–N, C–C, C–S and C–O bonds.

2.4.1. **Reductive functionalization of CO_2 *via* a transient BSA intermediate**

2.4.1.1. $TBD/PhSiH_3$: a pioneering reduction system in reductive functionalization. Formation of C–N and C–C bonds. The first system describing a reductive functionalization of CO_2 with

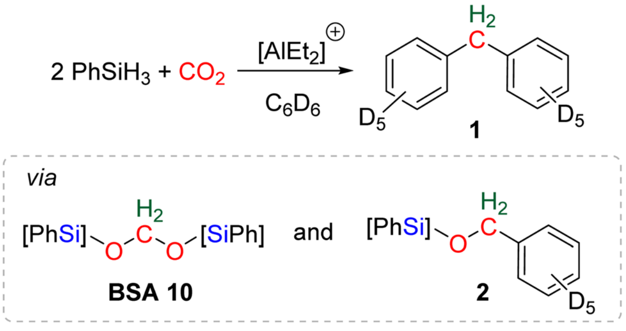

Scheme 17 First example of reductive functionalization of CO_2 into product **1**, involving a BSA intermediate and compound **2**.

hydrosilane with the intermediary of BSA was reported in 2015 (Scheme 18).[77] It included the use of TBD (1,5,7-triazabicyclo[4.4.0]dec-5-ene) which catalysed the hydrosilylation of CO_2 with phenylsilane into the corresponding BSA, although it was never directly observed or characterized. Besides TBD, other Lewis basic catalysts including 1,8-diazabicyclo[5.4.0]undec-7-ene (DBU), Verkade's base and NHC (IPr and I*t*Bu) were tested to catalyse the reduction step. Slightly lower yields of the final products were obtained. Various co-substrates featuring N–H (Scheme 18a) or C–H functionalities (Scheme 18b) acted as functionalizing agents in intercepting the transiently formed BSA leading to the formation of methylene-bridged "N–CH_2–N" and "C–CH_2–C" moieties. In total, 19 cyclic or acyclic symmetrical aminal products **3** were generated selectively with yields ranging from 14 to 99% (larger than 70% in most cases, Scheme 18a). In addition, 5 dissymmetric aminal products **4** were also generated using two different amines with yields ranging from 62 to 94% (Scheme 18a). For the synthesis of these dissymmetric aminal compounds, a key factor was to employ two amines featuring different nucleophilicities, enabling the most nucleophilic amine to first react with BSA, which affords an intermediate aminosilylacetal. Subsequently, the second (less nucleophilic) amine reacts with the aminosilylacetal intermediate yielding the corresponding aminal compound. Replacing the amine co-reactant with 2 equivalents of the nucleophilic malonate compound led to the unique formation of two C–C bonds in 58% yield (compound **5**, Scheme 18b).

2.4.1.2. Extension of the scope with the TBD/$PhSiH_3$ reduction system. The TDB/$PhSiH_3$ system was proven to be reliable and versatile to insert one or two methylene units in complex structures. To do so, 10–20 mol% of TBD was used at temperatures ranging from 100 to 120 °C and reaction times from 6 to 30 h (Scheme 19). Indolepyrrolidine derivatives were engaged as co-reactants leading to cyclisation reactions with the formation of C–CH_2 and N–CH_2 bonds. A second enantioselective reduction step of the pyrrolidine ring afforded spiro-indolepyrrolidine products **6** (Scheme 19), and 17 different compounds have been obtained in good to very good yields (55–92%).[78] Reductive functionalization with amine was then used to incorporate two methylene units from the hydrosilylation of CO_2 (Scheme 19, compounds **7**).[73] Key features of these transformations include the use of (i) a primary amine leading to the generation of an imine intermediate and (ii) a Lewis acid-catalysed cyclization reaction with various enaminones. The scope of the reaction was evaluated with 32 identified examples of tetrahydropyrimidine compounds with isolated yields (based on the enaminone) ranging from 50 to 99% (in most cases larger than 80%). The mechanism for the formation of compounds **7** was also investigated by DFT (Scheme 20). TBD was calculated to catalyse the hydrosilylation of CO_2 into **BSA 10** followed by the liberation of formaldehyde. The imine is then generated from the condensation of the primary amine with formaldehyde (step i). Controlled experiment proved that a stable imine can be formed when a bulky bis(diisopropyl)aniline is used. The enaminone nucleophilically adds to the intermediate imine *via* a Lewis acid/TBD-catalysed reaction (step ii) leading to an aza-diene compound after phenylamine elimination (step iii). The Diels–alder reaction between the aza-diene intermediate and a second equivalent of *in situ* generated imine finally furnishes the tetrahydropyrimidine **7** (step iv). This elegant strategy employing a primary amine as a first functionalization step transformation was further used to generate enaminones (Scheme 19, compounds **8**, 22 examples, 43–94%) and 1,4-dihydropyridines (Scheme 19, compounds **9**, 9 examples, 71–95%).[79]

2.4.1.3. Development of new catalysts. Besides the utilization of TBD as a catalyst, two other catalytic systems were employed for reductive functionalization with hydrosilanes. The

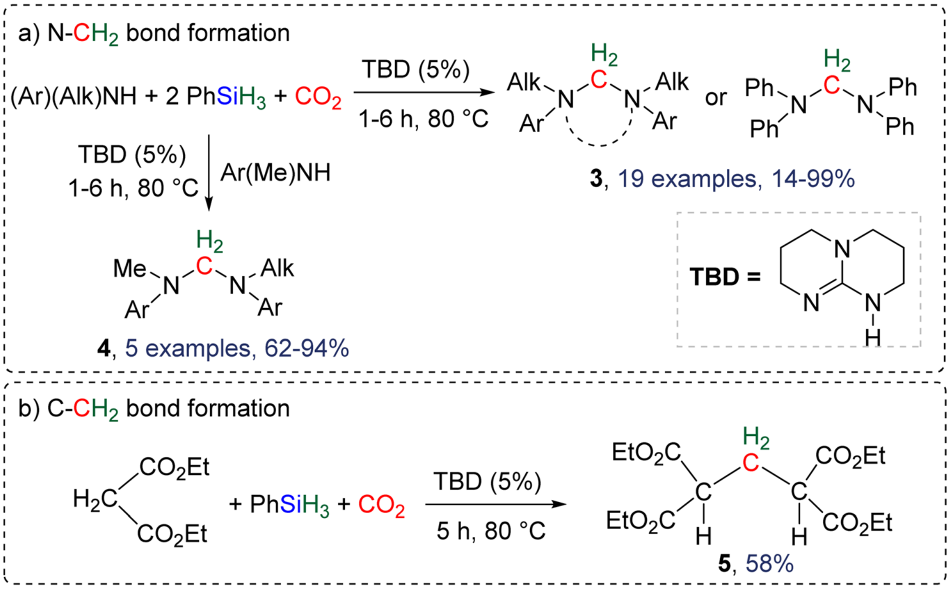

Scheme 18 First selective reductive functionalization of CO_2 *via* the generation of a BSA intermediate leading to the formation of (a) C–N and (b) C–C bonds.

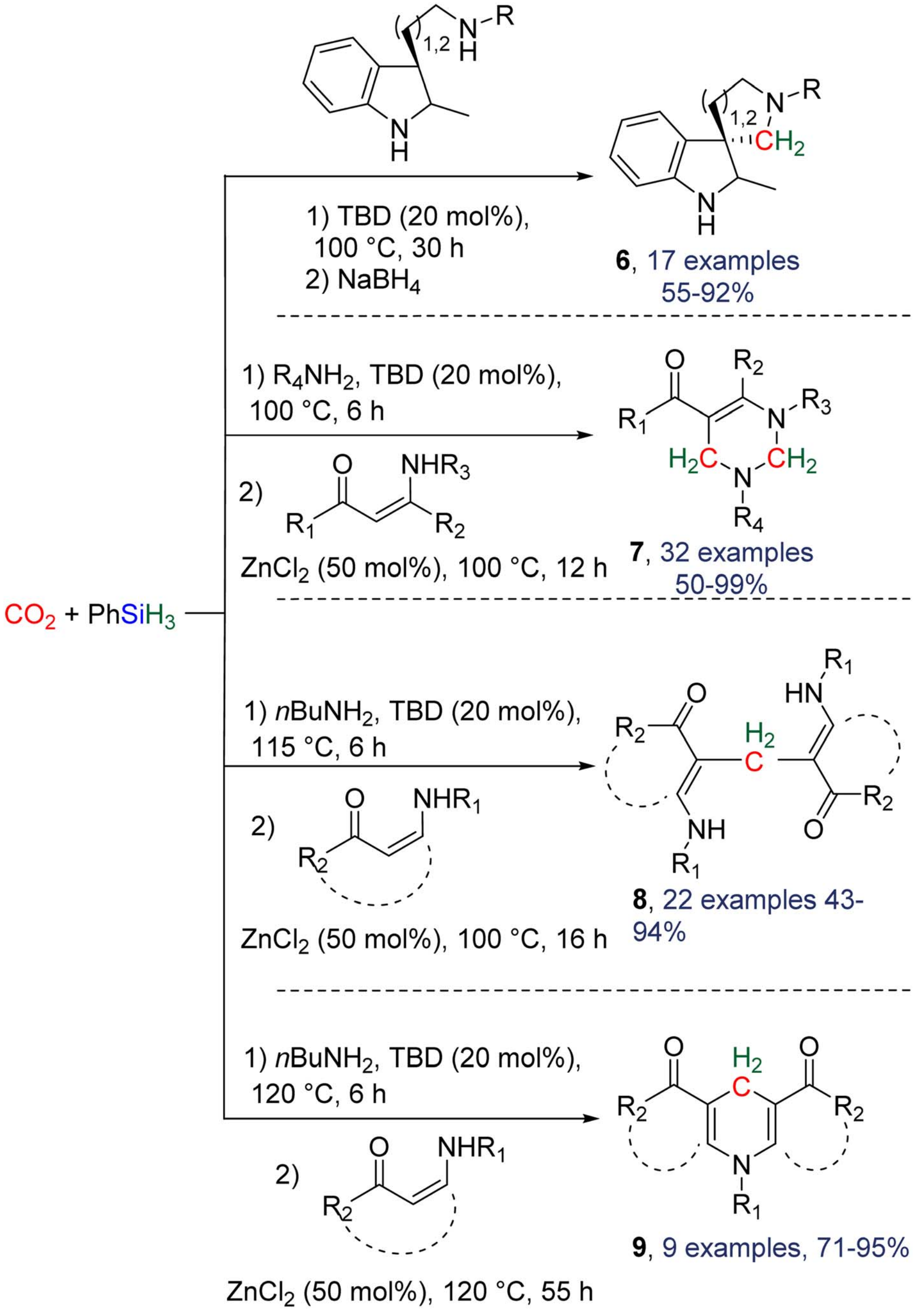

Scheme 19 Extension of the product scope upon reductive functionalization of CO_2 with hydrosilanes.

combination of $[CpFe(CO)_2]_2$ and $P(nBu)_3$ was shown to catalyse the hydrosilylation of CO_2 with phenylsilane in the presence of tryptamine derivatives to afford a variety of tetrahydro-β-carbolines and other nitrogen-containing heterocycles **10** after 36 h at 60 °C (Scheme 21).[80] In total, 19 heterocycles were obtained in yields ranging from 50 to 94%. The $[CpFe(CO)_2]_2/P(nBu)_3$ system is proposed to catalyse the hydrosilylation of CO_2 into BSA which is then involved in a Pictet–Spengler-type cyclization. Other Fe-based precursors did not afford any conversion, while diphenylsilane or other tertiary phosphine afforded the expected compounds although in lower yields. Another report described the use of a phosphorus ylide to intercept the reduction intermediate *via* a Wittig reaction (Scheme 21, compounds **11**).[81]

If the first tests were conducted with the TBD/$PhSiH_3$ system in acetonitrile, optimization conditions revealed the beneficial role of an inorganic base and notably of sodium *tert*-butoxide (NaO*t*Bu) in DMF in catalysing the hydrosilylation of CO_2 with PMHS (polymethylhydrosiloxane) – a waste of the silicone industry. This process led to the synthesis of 20 olefins in yields ranging from 30 to 85%. Ionic liquids[224] and covalent organic frameworks[83] were also employed as catalysts in a similar synthesis of aminal by CO_2 reductive functionalization.

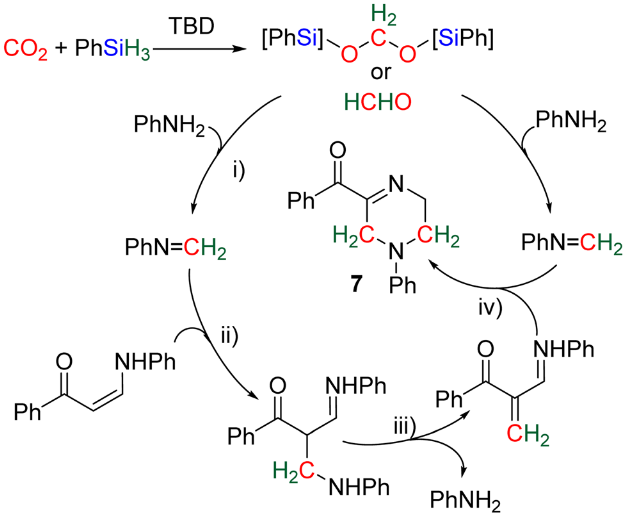

Scheme 20 Proposed mechanism for the synthesis of tetrahydropyrimidine **7**.

2.4.2. **Reductive functionalization of CO_2 *via* an isolated BSA intermediate (BSA 3).** In contrast to the previous examples in which BSA was not isolated or observed, **BSA 3** could be isolated before being involved in subsequent transformations.[29a] Such a process avoids compatibility issues between the reduction and the functionalization steps since they are performed independently. Using the Mg-based catalytic system **C17**, **BSA 3**, featuring triphenylsilyl groups, was isolated in high yield on a 3 g scale (95% yield, Table 2). As presented in Section 2.1.3, **BSA 3** was found to quantitatively release formaldehyde either in DMSO at 100 °C, in the presence of CsF at room temperature or under acidic conditions (H_2SO_4) at room temperature (Scheme 6). Under these conditions, **BSA 3** was then engaged in further transformations (Scheme 22).

In the presence of diol or di-thiol substrates under acidic conditions, the cyclic compounds **12** were generated in good yields forming CH_2–O (69% yield) and CH_2–S bonds (51% yield), respectively. The reaction with hydrazine proved to be efficient to generate a CH_2=N bond (compound **13**, 62% yield), while reactions with molecules comprising primary amine and thiol or secondary amine function led to benzimidazole and benzothiazole compounds **14** (95 and 57% yields), respectively. Finally, the reaction with ammonia afforded hexamethylene tetra-amine **15** in 77% yield. In addition, C–C bonds were also generated (i) with malonate leading to 5,5-dimethylcyclohexane-1,3-dione compound **16** (89% yield), (ii) through a Wittig reaction leading to the acrylate compounds **17** (80 and 87% yields) and finally (iii) through a Pictet–Spengler-type cyclization reaction leading to compound **18** (82% yield). It must be noted that ^{13}C-labelled **BSA 3** could also be efficiently generated and isolated from the catalytic hydrosilylation of $^{13}CO_2$ and was used as a dry source of ^{13}C-labeled HCHO.

2.4.3. **Conclusion on the reductive functionalization of CO_2.** Reductive functionalization of CO_2 with hydrosilanes led to the synthesis of a very broad range of various products in which the intermediate BSA was used as a methylene source to form C–N, C–O, C–S and even C–C bonds. In these reactions, BSA is generated either transiently when $PhSiH_3$ is the reductant – although not observed – or isolated when Ph_3SiH is the reductant.

2.5. Conclusion and perspectives

In conclusion, the four-electron reduction of CO_2 with hydrosilane is noteworthy for several reasons. Firstly, it distinguishes itself with a considerable number and variety of selective

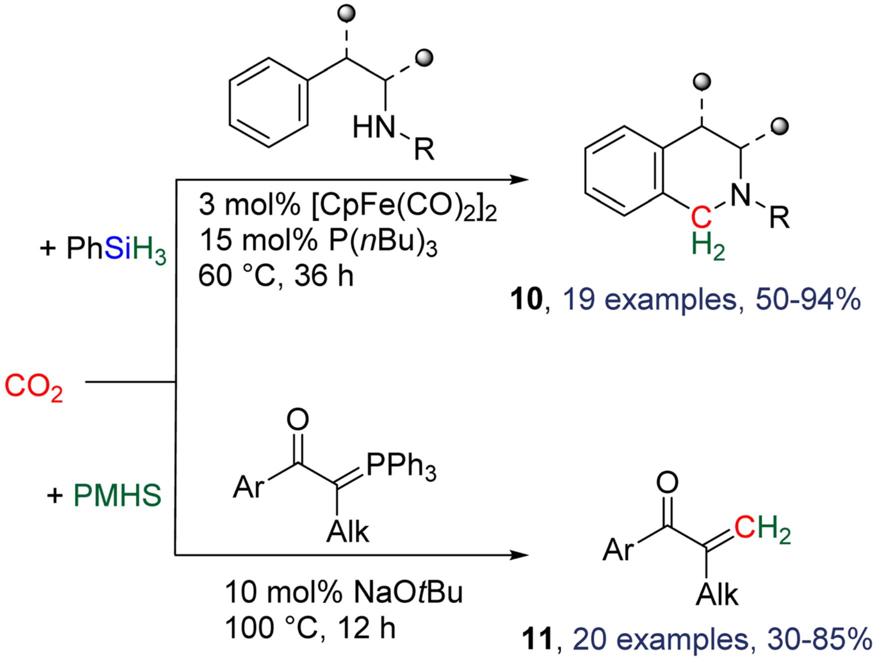

Scheme 21 New catalysts for reductive functionalization with hydrosilanes.

catalytic systems (**C1–24**), primarily based on the combination of transition metal-based complexes and $B(C_6F_5)_3$. Comprehensive experimental and theoretical studies have revealed five distinct activation modes, elucidating the 2 to 4 electron reduction stage. Despite the highest reported TON of 3400 and TOF of 10.4 h^{-1}, there is room for further enhancements. Secondly, it stands out due to the diverse array of characterized and isolated bis(silyl)acetal (BSA) compounds, with a current total of 11 reported. These isolated BSAs were predominantly obtained from tertiary silanes, demonstrating high selectivity (79 to 99% yields) under mild conditions. Finally, the process is notable for numerous transformations involving BSA in reductive functionalization, ranging from simple condensation to multi-step reactions with co-reactants. Interestingly, when primary silanes were employed, BSA formation was never observed, likely due to its high reactivity. In contrast, tertiary silanes led to the isolation of BSA before engaging in subsequent functionalization through formaldehyde release.

Perspectives in the field of $4e^-$ CO_2 hydrosilylation could involve rationalizing the stability of the generated bis(silyl) acetal (BSA) based on the choice of hydrosilane. Generating BSAs with intermediate stability holds particular interest, offering potential for expanding the reactivity scope of BSA compounds. A significant breakthrough would be utilizing BSAs as a C_n source for producing high-value added products, an area yet to be explored compared to their borylated counterparts discussed in the next section. However, the primary challenge remains the treatment of the siloxane by-product produced during CO_2 hydrosilylation, currently considered as waste. Exploring potential uses for these siloxane moieties or designing a regeneration system for the sustainable recycling of hydrosilane presents a promising avenue for further research.

3. Hydroboration

In the realm of hydroelementation reactions, hydroboration holds an important and specific place. Since the discovery of hydroboration of olefins,[84] this reaction has been largely developed for the reduction of unsaturated bonds.[8b,85] Beyond reduction, the formal addition of B–H bonds is used as a privileged access to organoboron compounds which are then used as reagents in coupling reactions.[86] Hydroboration of CO_2 involves the addition of a B–H bond to the C═O bond, transferring the hydride to the carbon atom and forming a B–O bond. It is favoured both kinetically and thermodynamically by the polarity of the B–H bond (E. N. of H = 2.2, B = 2.0) and the strength of the formed B–O bond (BDE(B–O) >500 kJ mol^{-1}),[87] respectively. As a consequence, CO_2 hydroboration reactions, like CO_2 hydrosilylation ones, operate under much milder conditions – usually room temperature and 1 atm of CO_2 – than CO_2 hydrogenation.[8a] However, it is noticeable that the catalytic systems used for the hydroboration or the hydrosilylation of CO_2 are different in most cases.

The first catalytic hydroboration of CO_2 was reported in 2010 with a Ni-based catalytic system and was shown to afford the $6e^-$ reduction product, methoxyborane, readily hydrolysed to methanol.[88] While the $2e^-$ reduction product – formoxyborane – was observed, no $4e^-$ reduction product was detected, although formaldehyde was proposed as an elusive intermediate.[88,89] The Ni-based pincer system used as the catalyst remains one of the most efficient catalyst of CO_2 hydroboration into methoxyborane with TOF and TON of 495 and 495 h^{-1}, respectively. It is worth noticing that an earlier report described the use of borane in the reduction of CO_2. However, it was not a hydroboration reaction, but the reduction of CO_2 into CO by B_2pin_2 and a (NHC)Cu-based catalyst.[19b] It was only in 2012 and 2014 that

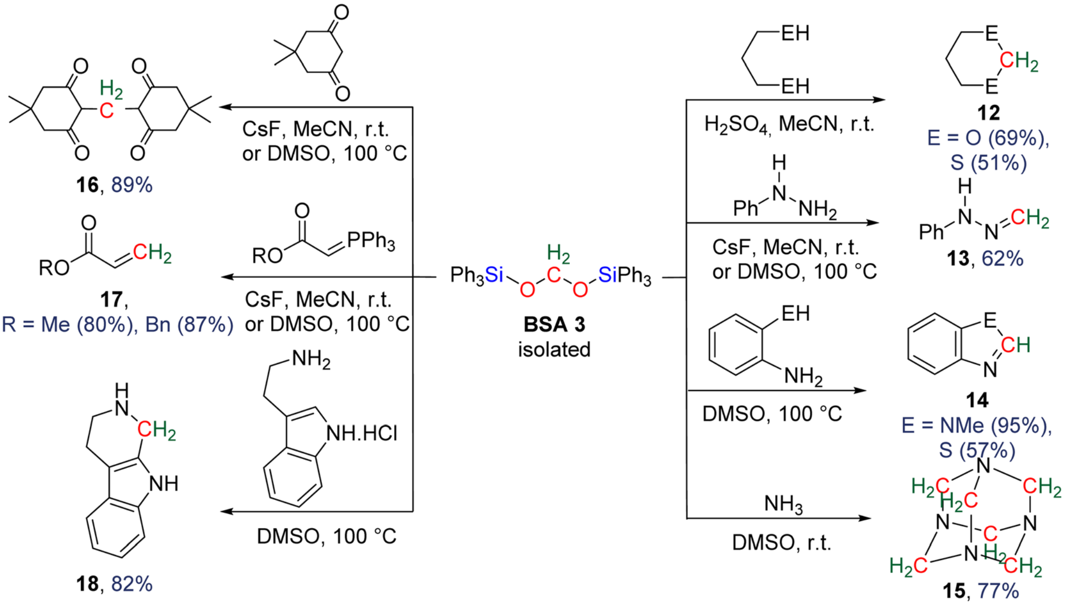

Scheme 22 Products obtained from the functionalization of HCHO released from **BSA 3**.

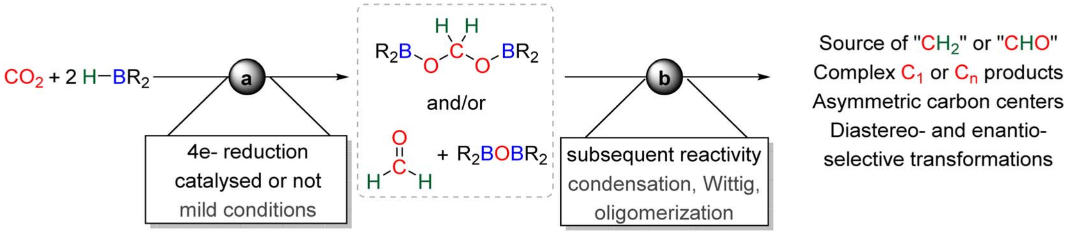

Scheme 23 General scheme for Section 3: CO_2 hydroboration.

bis(boryl)acetal (BBA)[90] and formaldehyde[91] were respectively characterized from the hydroboration of CO_2, although not in a selective manner. Later on, the efficient and selective generation of BBA derivatives was reported using different hydroboranes as reductants. These transformations (Scheme 23, step a) will be presented in the first part 3.1 and the mechanism will be discussed in part 3.2. Finally, the use of these $4e^-$ reduced products as reactants in further transformations (Scheme 23, step b) will be described in part 3.3 and a general conclusion will be drawn in part 3.4.

3.1. Hydroboration of CO_2 into bis(boryl)acetals (BBAs) and formaldehyde

In total, 7 BBA derivatives have been synthesized by the hydroboration of CO_2.[92] **BBA 1–4** were obtained from the hydroboration of CO_2 (Scheme 24) catalysed by compounds **C36–C45** (selective catalysts, Fig. 4) and **C46–C63** (unselective catalysts, Fig. 4). **BBA 5–7** were obtained in the absence of a catalytic system (Scheme 25). **BBA 2** and **4** were shown to be key intermediates leading to formaldehyde in high yields. These transformations are described hereafter.

3.1.1. Catalytic hydroboration of CO_2 into BBA 1–4 catalysed by C36–C63.

BBA 1, featuring pinacolboryl moieties (Scheme 24), was the first BBA reported in the literature in 2012. It was characterized *in situ* as a minor product with Ru-based catalysts **C46–C47** bearing a tricyclohexylphosphine (PCy_3) ligand.[90] Its selective generation was reported with **C38** albeit with a low yield of 30%.[93] It was only in 2017 that the use of 0.2% of the Ni hydride catalyst **C36** led to its selective generation at room temperature, with high *in situ* yields of 84% and 97% after reaction times of 1 h and 4 h, respectively.[94] Such high selectivity enabled the isolation of **BBA 1** by precipitation in 71% yield. This currently remains the only example in which **BBA 1** was isolated. Under optimized reaction conditions, benzene was the solvent of choice. While cyclohexane gave a similar result, the use of THF induced a net decrease (30% yield). **C43** [95] (15 min at room temperature with 2% of the Ni-based precatalyst) and **C44** [96] (2 h at 90 °C with 1% of the Mo-based catalyst) were shown to afford **BBA 1** as the major product. It must be noted that **BBA 1** was observed as a minor product in hydroboration reactions catalysed by compounds **C46–C47**,[90] **C48–C50**,[94,97] **C51**,[98] and **C54–C61**.[99,100]

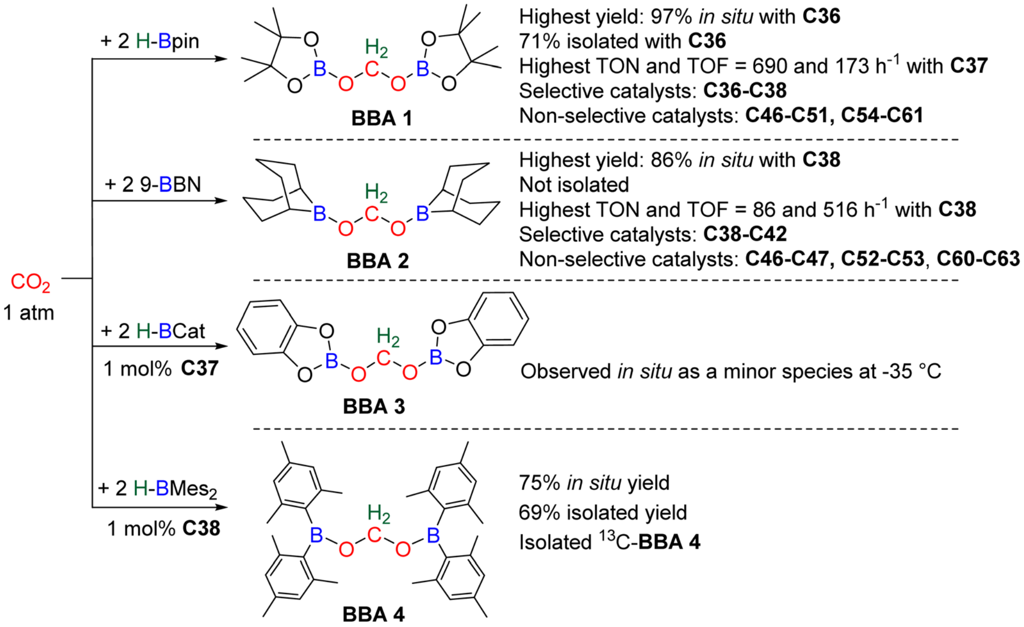

Scheme 24 Catalytic generation of BBA 1–4 with C36–C63 catalysts.

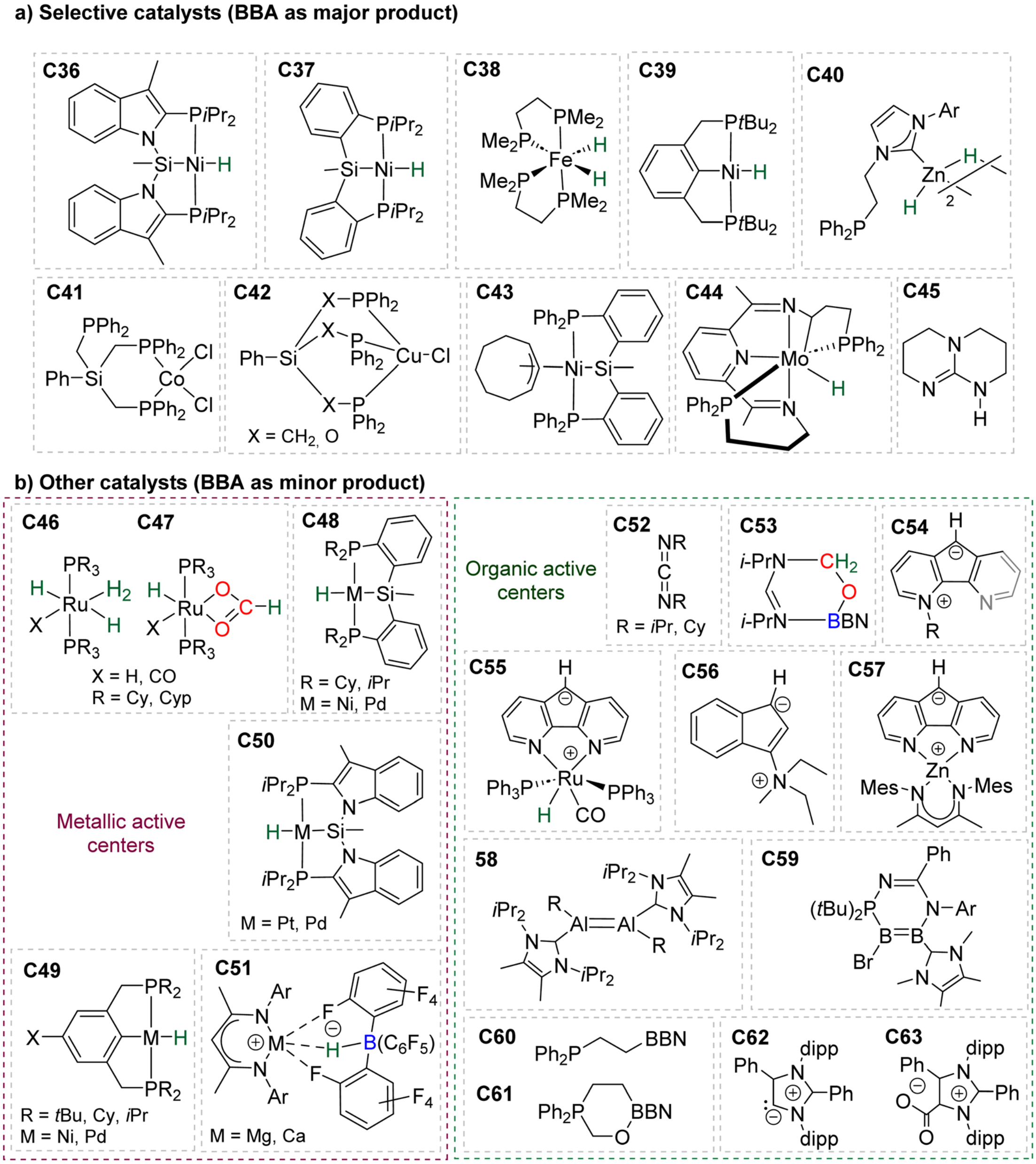

Fig. 4 Catalysts **C36–C63** for the generation of BBA **1–7** and formaldehyde: (a) selective catalysts **C36–C45** and (b) unselective catalysts **C46–C63**.

BBA 2 was reported for the first time in 2014 in CO_2 hydroboration catalysed by the nitrogen-based Lewis base TBD (**C45**).[101] This study focused on the reduction of CO_2 to the methoxyborane compound with various metal-free catalysts and hydroboranes. Using 9-BBN and 2.5 mol% of catalyst **C45**, **BBA 2** was detected as the major intermediate after 1 h (85% ratio) before decaying, leading to the final methoxyborane compound. The selective generation of **BBA 2** and yield quantification (instead of ratio) were then described with **C37–C39**.

In 2015, the well-defined iron dihydride bis-diphosphine catalyst **C38** was used at room temperature and under 1 atm of CO_2 to afford **BBA 2** in 85% yield (TOF = 109 h^{-1}) with a catalyst loading of 1 mol%.[93] The importance of the THF solvent was identified since such selectivity was not observed with benzene or toluene. Moreover, a high TOF of 516 h^{-1} was measured upon increasing the temperature to 60 °C with the generation of **BBA 2** in 86% yield in only 10 min. In 2016, the well-defined [Co]- and [Cu]-precatalysts **C41** and **C42** were shown to generate **BBA 2** as the major product after 24 h at room temperature and 60 °C, respectively.[102] Beyond these selective systems, catalysts **C46–C47**,[90] **C52–C53**,[103] **C60–C61** [104] and **C62–C63** [105] were also reported to catalyze the generation of **BBA 2** as a minor product under mild conditions. **BBA 3** has only been partially characterized once as a minor compound, despite numerous studies using HBCat for CO_2 hydroboration. This is in marked contrast with the selective generation of **BBA 1** and

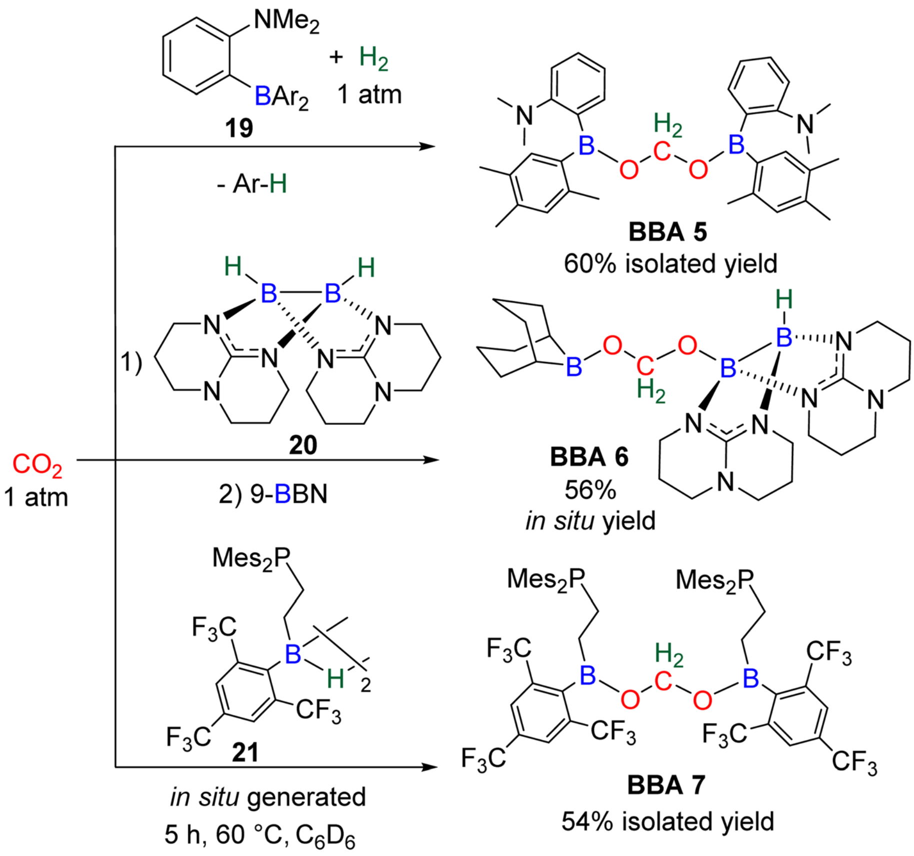

Scheme 25 Catalyst free generation of BBA 5–7.

BBA 2, and might be explained by the ability of HBCat to readily reduce CO_2 to the methoxyborane stage (*vide infra* in mechanistic consideration).

In this context, **BBA 3** was characterized *in situ* as a minor intermediate, during methoxyborane preparation with catalyst **C37**.[97] Following the reaction, a minor signal was observed by ^1H NMR in the characteristic area of acetals. Its broadness suggested the reversible formation of **BBA 3**. This assumption was confirmed by its sharpening at −35 °C leading to the first characterization of the acetal moiety of **BBA 3**. When $^{13}CO_2$ was used, this acetal signal appeared as a doublet, which finally disappeared upon further reduction to the methoxyborane product. **BBA 4** was obtained from the CO_2 hydroboration with $HBMes_2$ catalysed by the iron hydride catalyst **C38** with an *in situ* yield of 75%.[30] This BBA exhibits higher stability as compared to **BBA 1–3**, as shown by an isolated yield of 69% and its characterization by X-ray diffraction analysis.[30] Moreover, **BBA 4** featuring a ^{13}C-labelled methylene fragment was also isolated in similar yield from $^{13}CO_2$ hydroboration. The stability of **BBA 4** was used to perform enzymatic transformations (*vide infra*). It is noteworthy that catalyst **C38** is able to catalyse the selective generation of three BBA derivatives, namely, **BBA 1**, **2** and **4**.

The performances of catalysts **C36–C42** for the selective generation of **BBA 1–2** and **BBA 4** are reported in Table 3. The performances of catalysts **C43–C45** are not indicated because only the ratio between the detected products were measured and not the quantitative yields. The performances of catalysts **C46–C63** are not given since **BBA 1–3** were only observed as minor compounds. Among the seven selective catalytic systems (**C36–C42**), one can notice that all of them are transition metal (TM)-based catalysts and five based on 3d-TM (**C36–C39**, **C41**). The active centre is a metal hydride fragment either present in the initial catalyst or presumably generated *in situ* during the reaction with the hydroborane. The best performances in terms of TON and TOF were obtained with **C37** (487 and 122 h^{-1}) and **C38** (85, 109 h^{-1} at room temperature and 86, 516 h^{-1} at 60 °C) for the generation of **BBA 1** and **BBA 2**, respectively. The best yields were obtained with catalysts **C36** (97% yield) and **C38** (86% yield) for the generation of **BBA 1** and **2**, respectively. The selectivity is an important factor to be considered when the generated BBA is further engaged in additional reactions (see Section 3.3). If a catalytic system exhibits high TON and TOF but poor selectivity, the presence of other products or of the remaining hydroborane may be detrimental for the subsequent reactions.

3.1.2. Catalyst-free generation of BBA 5–8.

Currently, three BBA derivatives, **BBA 5–7**, have been obtained without any catalyst (Scheme 25). **BBA 5** features two different aryl substituents on each boryl moiety, 2,4,5-$Me_3C_6H_2$ and *o*-NMe_2-C_6H_4 groups (Scheme 25). It resulted from the reaction of the ambiphilic ortho amino-borane compound **19** with H_2 and CO_2 (72 h,

Table 3 Catalytic performances of the selective formation of **BBA 1**, **2** and **4** with catalysts **C36–C42**

BBA	Catalyst	TON	TOF (h^{-1})	Yield[a] (%)	P_{CO_2} (atm)	T (°C)	Time[b]	Cat loading (%)	Ref.
1	**C36**	487	122	97 71[c]	1	rt	4	0.2	94
	C37	690	173	69	1	rt	4	0.1	97
	C38	6	1.2	30	1	25	5	5	93
2	**C38**	85	109	85	1	rt	47 min	1	93
		86	516	86	1	60	10 min	1	
	C39	32	2	64	1	rt	16	1	97
	C40	15	3.8	75	1	rt	4	5	106
	C41	25	1	38	1	60	24	1.5	102
	C42	53	2	79	1	rt	24	1.5	
4	**C38**	75	75	75 69[c]	1	25	1	1	30

[a] *In situ* yield unless otherwise stated. [b] Hour unless otherwise stated. [c] Isolated yield.

room temperature). **BBA 5** was isolated in 60% yield as a monocrystal suitable for the first X-ray diffraction analysis of a BBA. DFT investigations suggested that H_2 led to the protodeborylation of compound **19** giving rise to a monohydroborane compound (not observed) which would formally doubly add to CO_2 and generate **BBA 5**. **BBA 6** is a dissymmetric BBA featuring one diboryl and one BBN moieties (Scheme 25).[107] It is the only dissymmetric BBA reported to date and was obtained in two consecutive steps. Compound **20**, so-called diborane (**4**), was proposed to be nucleophilic enough to readily transfer a hydride to CO_2 affording a formoxyborane intermediate, which was characterized *in situ* in a mixture of compounds in 70% yield. In a second step, 9-BBN reduced the formoxy fragment to afford **BBA 6** within 5 h with an *in situ* NMR yield of 80% (56% overall yield). **BBA 7** features boryl units bearing two different substituents at the boron atom, a perfluoroaryl group (1,3,5-tris(trifluoromethyl)phenyl) and an alkyl phosphine group (2-dimesitylphosphino-ethyl, Scheme 25).[108] It was readily synthesized in 5 h at 60 °C and isolated in 54% yield from the *in situ* generated phosphino-hydroborane dimer **21**. **BBA 7** was characterized by XRD analysis.

3.1.3. Summary of the generation of BBA 1–7.

In total, seven BBA derivatives resulting from CO_2 hydroboration have been characterized so far in the literature since the first report in 2012. **BBA 1–4** were obtained using commercially available pinacolborane (HBPin), 9-borabicyclo[3.3.1]nonane (9-BBN) and catecholborane (HBCat) and the non-commercially available dimesitylborane ($HBMes_2$), respectively (Scheme 24). It is worth mentioning that the commercially available hydroborane BH_3 led to the reduction of CO_2 to the methoxyborane stage.[104,109] To our knowledge, detection of a corresponding BBA was never reported. NMR analysis was used as a key tool to characterize these species that are often difficult to isolate. The methylene moiety was indeed easily characterized by ^1H and ^{13}C NMR in a narrow range of chemical shifts: $4.90 < \delta^1H < 5.72$ and $81.9 < \delta^{13}C < 91.3$ (Table 4). Moreover, ^{13}C-labelled control experiments with $^{13}CO_2$ allowed confirmation of the origin of the carbon atom in the product. Boron chemical shift is not characteristic of BBA since the boron atom substituents have a strong impact. They also influence the stability of BBA as observed in the case of BSA derivatives. This general feature is illustrated in BBA compounds by (i) the rather ease of generating **BBA 1** and **2** as opposed to **BBA 3**, (ii) the stability of **BBA 4**, **5** and **7** which could be isolated and crystallized while **BBA 2** was never isolated and (iii) the possibility to generate BBA in the absence of a catalyst in the cases of **BBA 5–7**.

Table 4 Selected NMR chemical shifts for **BBA 1–7**

BBA	Isolated	XRD	Solvent	$\delta^{13}C(CH_2)$	$\delta^1H(CH_2)$	$\delta^{11}B$	Ref.
1	Yes	No	C_6D_6	85.7	5.51	22.8	94
				85.4	5.49 $^1J_{HC} = 167.2$ Hz	—	90
2	No	No	THF-d_8	87.0	5.54 $^1J_{HC} = 165.2$ Hz	58.6 (ref. 100c)	93
3	No	No	C_6D_6	81.9	5.27	n.d	97
4	Yes	Yes	THF-d_8	89.6	5.49	48.5	30
5	Yes	Yes	C_6D_6	90.9	5.72	46.1	110
6	No	No	CD_2Cl_2	91.3	5.20	−5.4 6.8 55.5	107
7	Yes	Yes	C_6D_6	88.5	4.90	51.0	32

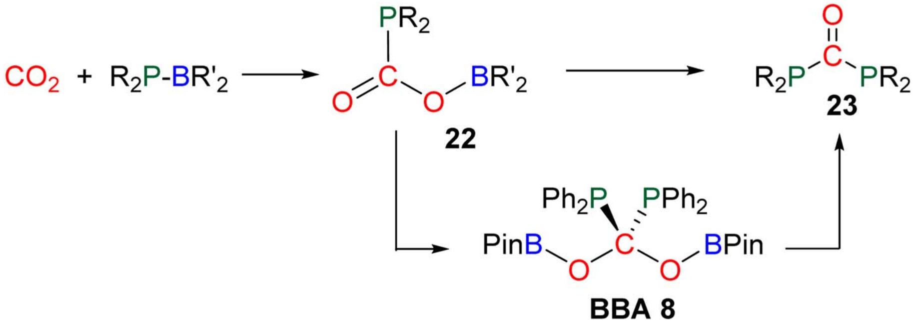

Scheme 26 Synthesis of BBA 8 by the phosphoborylation of CO_2.

3.1.4. Miscellaneous BBA 8. **BBA 8** is an additional bis(boryl)acetal that is not presented with the other BBAs because it does not result from a double hydroboration of CO_2 but rather from formal double phosphoborylation (Scheme 26).[111] This compound features a central acetal core that is substituted by two diphenylphosphino substituents. The reactivity of a series of phosphinoborane compounds (R_2PBR_2) toward CO_2 led to a single insertion (compound **22**) and then ultimately to the formation of diphosphaurea compound **23**. **BBA 8** was shown experimentally, with support from theoretical calculation, to be an intermediate and was synthesized and crystallized enabling its XRD analysis at low temperature. However, its instability precluded any further characterization in solution.

3.1.5. Hydroboration of CO_2 into formaldehyde. The direct observation of free formaldehyde from the hydroboration reaction has been described only once, in 2014, with the ruthenium catalyst **C46** featuring two tricyclopentylphosphine ($PCyp_3$) ligands and HBpin as the reductant (Scheme 27a).[91] Under optimized conditions, HBpin was consumed in 30 min at room temperature with 10 mol% catalyst loading. Formaldehyde was observed as the major reduction product (ratio of 22%) along with other borylated products including **BBA 1** and methoxyborane (CH_3OBPin). Labelling experiments using $^{13}CO_2$ confirmed the generation of free formaldehyde with its characteristic resonances in ^1H and ^{13}C NMR spectra (8.74 and 193.0 ppm, respectively in C_6D_6). In order to drive the selectivity toward formaldehyde, 2,6-bis(diisopropyl)aniline was added in the reaction mixture before CO_2 pressurization. The related imine resulting from the condensation reaction between formaldehyde and the aniline was generated after 1 h at room temperature in 74% and 85% yields based on CO_2 and aniline, respectively (Scheme 27b). Upon hydrolysis of the generated imine, a formalin solution was obtained.

Observation of formaldehyde from CO_2 hydroboration was also mentioned in two other studies.[95,112] In both cases, it appears to result from the evolution of **BBA 1**. Using the selective formation of BBA as a tool to access formaldehyde was further developed recently. **BBA 2** and **BBA 4** were selectively generated with catalyst **C38**, and subsequently hydrolysed with 10 equivalents of D_2O. This led to their complete hydrolysis into formaldehyde at room temperature within 30 min and less than 2 h for **BBA 2** and **BBA 4**, respectively (Scheme 28). The generated formaldehyde was then further transformed in organo-[29b] or enzymatic[30]-catalyzed reactions (see Section 3.3). It is remarkable that **BBA 2** and **BBA 4** were stable enough to be

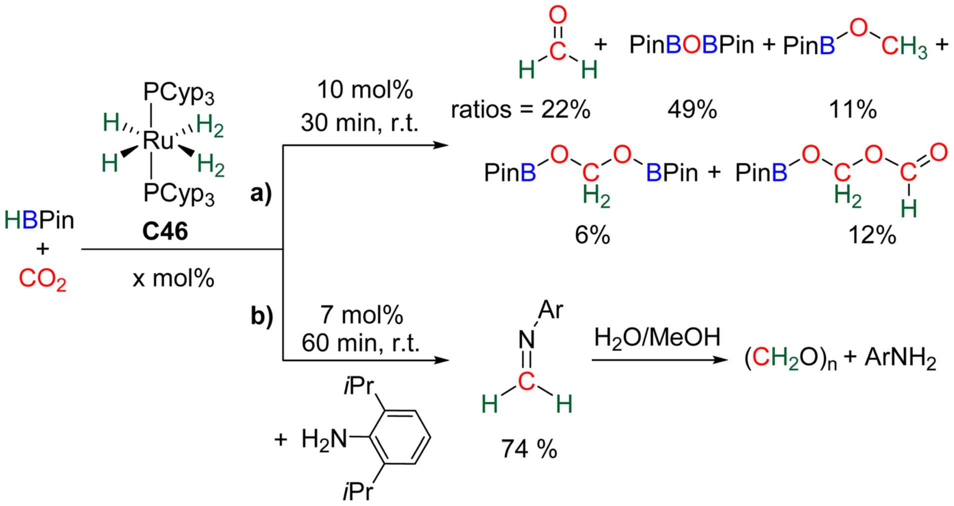

Scheme 27 Hydroboration of CO_2 into formaldehyde: (a) generation and (b) selective trapping of HCHO.

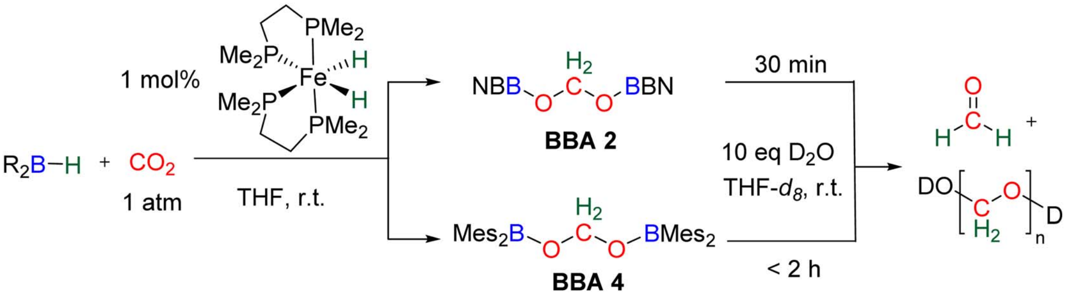

Scheme 28 Generation of formaldehyde from **BBA 2** and **BBA 4** hydrolysis.

generated selectively – and even isolated in the case of **BBA 4** – and yet efficiently released formaldehyde under mild hydrolytic conditions.

3.2. Mechanistic considerations

This section is dedicated to mechanistic considerations for the formation of bis(boryl)acetal (BBA) or formaldehyde. It is divided into three parts: (i) metal-hydride catalysis (**C36–C44**, **C46–C51**), (ii) organic catalysis (**C45, C52–C63**) and (iii) uncatalyzed generation of **BBA 5–7**.

3.2.1. Metal hydride catalysis. The catalysts **C36–C44** and **C46–C51** feature a metal hydride moiety or are believed to generate such a function upon reaction with the hydroborane (**C41–C43**). This hydride is proposed to be the key species of the catalytic process leading to BBA. As shown in Scheme 29, the elementary steps accounting for the $2e^-$ reduction of CO_2 are the insertion of CO_2 into the M–H bond leading to the formate complex **24**, followed by a σ-bond metathesis with the hydroborane leading to formoxyborane **25**. We will not describe further this $2e^-$ reduction of CO_2 since it was reviewed elsewhere.[8] Our discussion will rather concentrate on the ensuing reduction step leading to BBA and formaldehyde. At present, theoretical[89,113] and experimental[90,91,97,112,114] studies are converging on the central role of metal boryl acetal compound **26**, which is proposed to result from the reaction of **25** with M–H (step a, Scheme 29). The corresponding transition state (**TSa**, Scheme 29) is characterized by a hydride attack on the electrophilic carbon atom of **25**, as proposed by several DFT calculations on Ni,[89,115] Ru,[113] Fe,[113a] Os[113a] and Mn[116] systems. The concomitant M–O interaction is often calculated to occur but does not seem mandatory. The likely involvement of a formoxyborane species **25** as an intermediate to the $4e^-$ and $6e^-$ stages was experimentally asserted when a formoxyborane featuring a pinacolboryl moiety was shown to give similar rate and product distribution to that in CO_2 hydroboration with catalyst **C46**.[112]

Numerous experimental proofs demonstrated that formate complex **24** obtained from CO_2 insertion into M–H bond could be used in hydroboration reactions.[8a,90,91] However, although the metal boryl acetal species **26** has been calculated to be central for the $4e^-$ reduction of CO_2, identification and or isolation of these species are still lacking. The aluminum compound **27** is the only metal boryl acetal compound characterized without ambiguity (Scheme 29).[114] It was obtained from the subsequent reaction of the corresponding [Al]–H with CO_2 and then with 9-BBN and **27** was fully analysed by NMR and X-ray diffraction (XRD) studies. It is noticeable that only 9-BBN gave access to this metal boryl acetal structure. Analogous structures could indeed neither be observed with HBpin because of the lack of reactivity nor with HBCat or BH_3 because of subsequent reduction processes. It is also important to notice that like boron, aluminium is a group 13 element and that despite mimicking important steps of CO_2 hydroboration, neither the starting Al hydride complex nor complex **27** catalyses the CO_2 hydroboration reaction because the initial Al–H species is not regenerated under the reaction conditions. Step a′ (Scheme 29) is an alternative step to generate **26** from the direct hydroboration of the formate complex **24**. To the best of our knowledge, it has not been reported in DFT investigations but we believe that it should not be discarded *ipso facto*. Compound **26** is a key intermediate because it serves as a bifurcation point either toward BBA (Scheme 30, step b) or

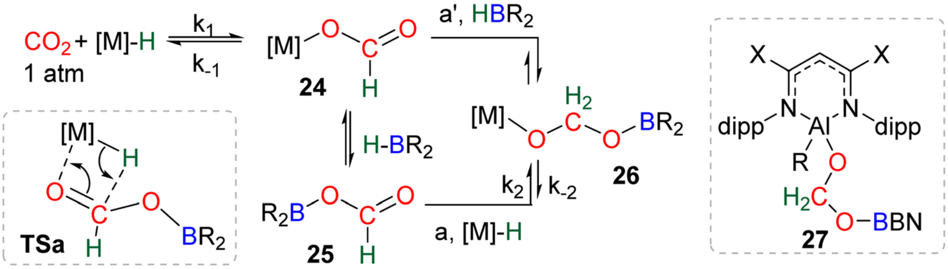

Scheme 29 Calculated elementary steps (a and a′) leading to the generation of the elusive intermediate **26** and structure of the only metal boryl acetal (**27**) so far characterized.

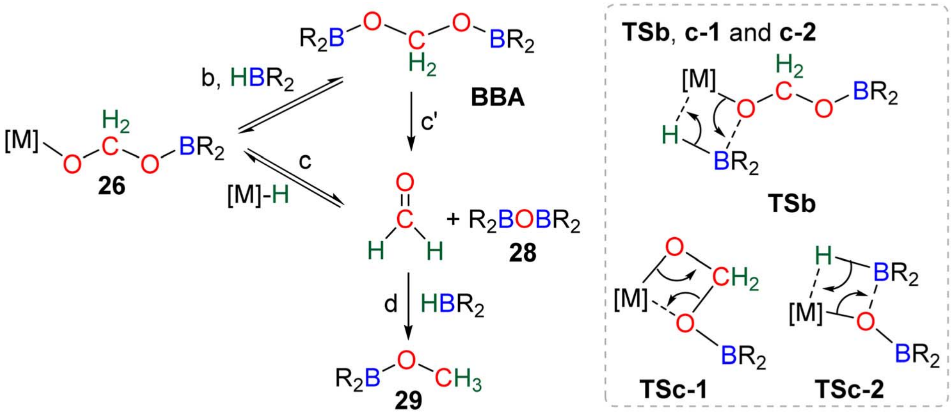

Scheme 30 Calculated elementary steps (b, c, c′, d) and transition states (**TSb**, **TSc-1** and **TSc-2**) from metallic borylacetal.

formaldehyde (Scheme 30, step c). BBA is formed from the hydroboration of the metallic acetal intermediate **26**. **TSb** represents the type of transition state calculated to account for this step. It formally corresponds to an M–O metathesis. Step c illustrates the route leading to formaldehyde and the boryl ether **28** which eventually leads to the 6e$^-$ reduction hydroboration product **29** through step d. This last step was experimentally identified with the Ru–H complex **C46** that was shown to catalyse the hydroboration of formaldehyde into methoxyborane with HBpin. The first transition state **TSc-1** does not involve HBR_2 and is simply a rearrangement of the metal boryl acetal **26**. The aliphatic chain rearranges to enable the interaction of the second oxygen atom with the metal centre. This reorganization weakens the M–O bond of the first oxygen atom and the O–CH_2 bond of the second oxygen atom. This leads to the release of formaldehyde and the formation of an M–OBR_2 intermediate which is subsequently hydroborated to regenerate the metal hydride and affords the ether compound **28** *via* **TSc-2**.

The factors influencing the selectivity have been explored in a thorough study involving the use of various hydride pincers of Ni- and Pd-based catalysts and three different hydroboranes, namely, HBpin, HBCat and 9-BBN.[97] The origin of the selectivity between the 2e$^-$ and 4e$^-$ reduction products was proposed to be dependent on the relative rate of reaction between the metal hydride fragment (M–H) and either (i) CO_2 to afford the formoxyborane **25** (k_1) or (ii) the formoxyborane intermediate **25** to afford the metal boryl acetal **26** (k_2) (Scheme 29). It was indeed shown that a lower pressure of CO_2 led to a higher selectivity toward the 4e$^-$ reduction product presumably by disfavouring k_1. It was also proposed that k_2 could be favoured by (i) increasing the concentration of the hydroborane, (ii) decreasing the steric hindrance of the boryl unit, (iii) increasing its electrophilicity and (iv) using a Lewis acid to co-activate the formoxyborane.

The origin of the selectivity between the 4e$^-$ and the 6e$^-$ reduction products appears to be the preference between the formation of BBA and the formation of formaldehyde, since the latter readily leads to further reduction. However, the factors influencing the preference toward BBA or formaldehyde remain to be disclosed. In addition, the formation of BBA was shown to be reversible which eventually led to the final generation of the more stable methoxyborane in various systems.[90,97] This feature explains the key role that the boryl moieties may play in the kinetic and/or thermodynamic stabilization of the corresponding BBA. Step c′ is an alternative path generating formaldehyde directly from BBA (Scheme 30). Such evolution has not been proposed as a plausible path for M–H catalysis but for organic catalysis (*vide infra*).[96,98] The direct generation of a methoxyborane compound **29** from the metal boryl acetal **26** has not been identified so far.

3.2.2. **Organic catalysis.** As shown in the first section, compounds **C45** (TBD) and **C52–63** are able to catalyse the hydroboration of CO_2 without any metal centre. The metal ions in compounds **C55** and **C57** are not believed to be the active catalytic centres. The suggested mechanism with **C55** and **C57** indeed follows a similar pathway to that with **C54** and **C56**, as it involves the anionic carbon moiety as the active catalytic centre. This was based on the theoretical investigations conducted on the Ru-based system **C55** and is depicted in Scheme 31(a).[82,117]

The carbanion located on the backbone of the ligand of the complex was found to react both with HBPin and CO_2 to produce the catalytic species **30**. Compound **30** was proposed to activate the formoxyborane intermediate **25** and HBPin concomitantly through **TS1** to afford **BBA 1**. The regenerated catalyst **30** could then be involved in the transformation of **BBA 1** into formaldehyde *via* an 8-membered-ring (**TS2**). In this reaction, formaldehyde was not experimentally observed but was proposed to be a transient intermediate *en route* to the observed methoxyborane structure. The ambiphilic phosphine borane **31** was shown to catalyse CO_2 hydroboration into methoxyborane with different hydroboranes (HBCat, HBPin, 9-BBN and BH_3) (Scheme 31b).[118] Although no free formaldehyde nor BBA was observed, a pathway, similar on various aspects to the previous one (Scheme 31a), was proposed. Theoretical investigations notably concluded on the co-activation of HBPin and formoxyborane (**TS**, Scheme 31b) to afford **BBA 1**. **BBA 1** then evolves to formaldehyde which ultimately reacts with compound **31** to form the formaldehyde adduct **32**. Interestingly, labelling experiments proved that the formaldehyde moiety of compound **32** was not reduced further to afford the

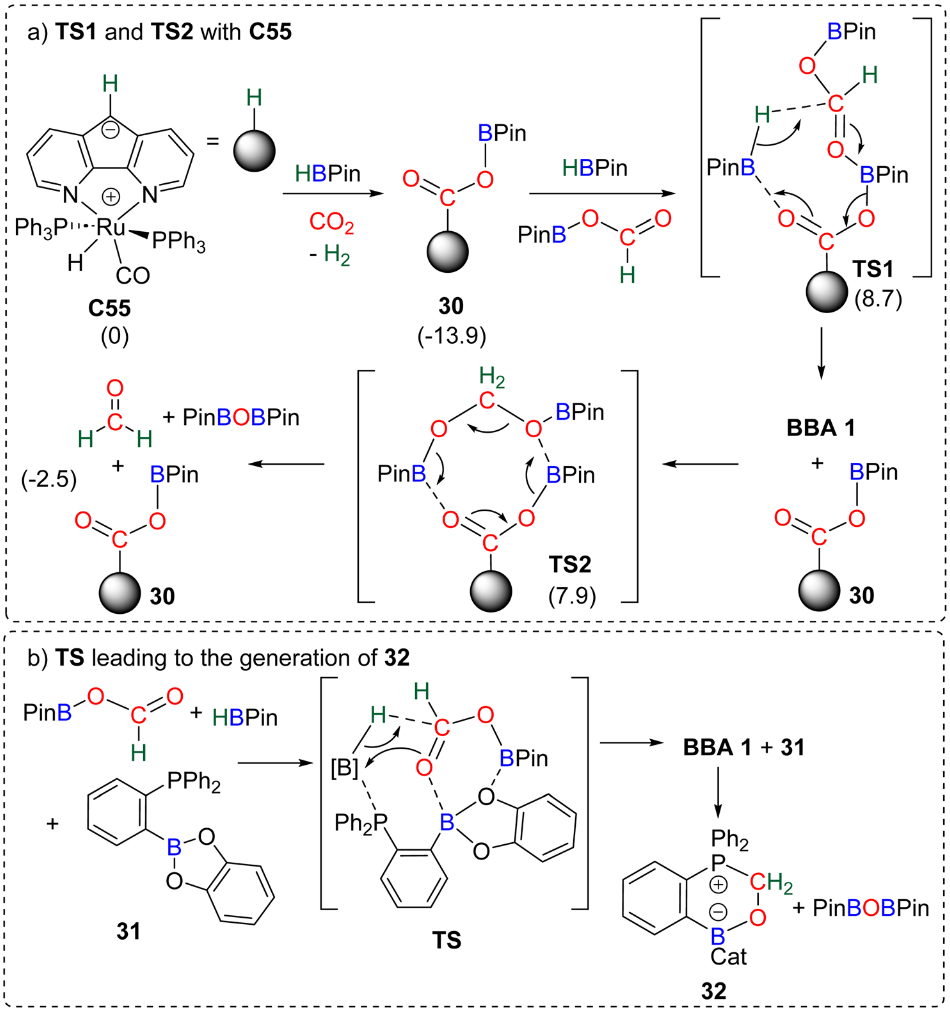

Scheme 31 Calculated elementary steps for the 4e$^-$ reduction mechanism of CO_2 with (a) **C55** (energies indicated in parenthesis are ΔG values in kcal mol^{-1}) and (b) compound **31**.

methoxyborane.[109a] Instead, the adduct **32** acts as a more effective catalyst in the hydroboration of CO_2 into methoxyborane with the various boranes tested. This feature is responsible for an observed induction period, which was also noticed (i) in the CO_2 hydroboration reactions with catalyst **C52** leading to the generation of **C53**,[103,119] (ii) in the hydroboration of CO_2 with $PtBu_3$ in which a formaldehyde derived intermediate (compound **36**, Scheme 33) was also observed,[120] and (iii) when using catalyst **C60** leading to **C61** which was proven to be a more active catalyst.[104] The similar pathway identified in these two studies implies (i) the reduction of CO_2 into formoxyborane as the 2e$^-$ reduction intermediates are observed with metal hydride catalysts and (ii) the subsequent generation of BBA (Scheme 32, step a) and then formaldehyde (Scheme 32, step b) before further reduction to the 6e$^-$ reduction product.[121] This latter feature stands in contrast with the metal hydride systems in which BBA and formaldehyde are not generated along the same pathway (Scheme 30). This common pathway remains to be confirmed by further studies on additional organo-catalysed systems. Generalizing such a mechanism remains highly hypothetical because of (i) the very small number of reported theoretical investigations, (ii) the large variety of organic catalysts **C45** and **C52–C63** and (iii) the difficulty to study very reactive intermediates experimentally. A general trend is the

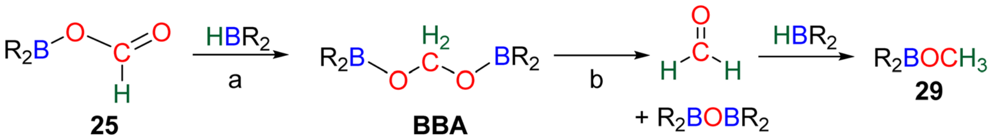

Scheme 32 Elementary steps a and b for the reduction of formoxyborane **25** to methoxyborane **29** calculated with compound **32**.

ability of these main group organic catalysts to co-activate several substrates and/or intermediates (CO_2, hydroborane, formoxyborane). This feature highlights the powerful synergy observed between moderately reactive centres (moderate Lewis acid and Lewis base fragments) for the transformation of very stable molecules such as carbon dioxide.

3.2.3. Uncatalyzed hydroboration for the generation of BBA 5–7. No DFT investigations have been performed to rationalize the catalyst-free generation of **BBA 5–7**. At first glance, the presence of a pendent N- or P-based Lewis base on the boryl unit in all three cases is a striking feature. Based on the ability of main group organic compounds to catalyse CO_2 hydroboration, one could assume that the pendent Lewis base plays a role either in the intramolecular B–H activation or in an intermolecular CO_2 anchoring/activation.[43] Another role could lie in the stabilization of the formed BBA, even though no interaction of the pendant Lewis base was detected in the XRD analyses of **BBA 4**, **5** and **7**. Finally, the uncatalyzed addition of the hydroborane **21** to CO_2 affording **BBA 7** is surprising if one considers the hydride transfer as being the first elementary step for such transformation. Indeed, the presence of a perfluoroaryl substituent on the boron atom certainly decreases the hydricity of the B–H bond.[122] With this reactive trend in mind, one would assume that the B–H bond hydricity in compound **21** is lower than the one in HBPin, HBCat and 9-BBN which were proved unreactive toward CO_2 in the absence of a catalyst. That the empty p orbital at the boron atom might be at play in the first elementary step is worth considering at least in the latter case.

3.3. Use of formaldehyde and bis(boryl)acetal as C_1 and C_n sources

The known high reactivity of formaldehyde was first evidenced in four side reactions involving CO_2 reduction. In these reactions, *in situ* generated formaldehyde reacted with other products or catalysts present in solution (Scheme 33a).

The formation of compounds **32**[109a,118] and **C53**[103] was postulated from calculation to arise from the reaction between transiently generated formaldehyde and the ambiphilic compounds **31** and **33**, respectively. Compounds **34**[90,112,123] and **35**[91] were shown experimentally to arise from the reaction of formaldehyde with **25** and **29**, respectively, which was confirmed by labelling experiments. BBA compounds were also shown to readily react under mild conditions. We believe that the characterization of compound **36** was the first observation of such BBA reactivity (Scheme 33b).[120] Although the authors did not elaborate on the mechanism of its formation, we propose that **36** could be formed from the reaction of **BBA 2** with the phosphine used as the catalyst, on the basis of a similar reaction later observed between **BBA 2** and an NHC leading to compound **48** (Scheme 37) analogous to compound **36**. These examples showed that BBA intermediates or formaldehyde is prone to react. Such "undesired" yet attractive reactivities may pave the way to more controlled transformations. Along this idea, we present hereafter different examples using BBA or formaldehyde in subsequent reactions either (i) as a C_1 source for the formation of C–O, C–N, C–P and C–C bonds, or (ii) as a C_n source in oligomerization reactions leading to the formation of carbon chains and the synthesis of chiral carbon centres.

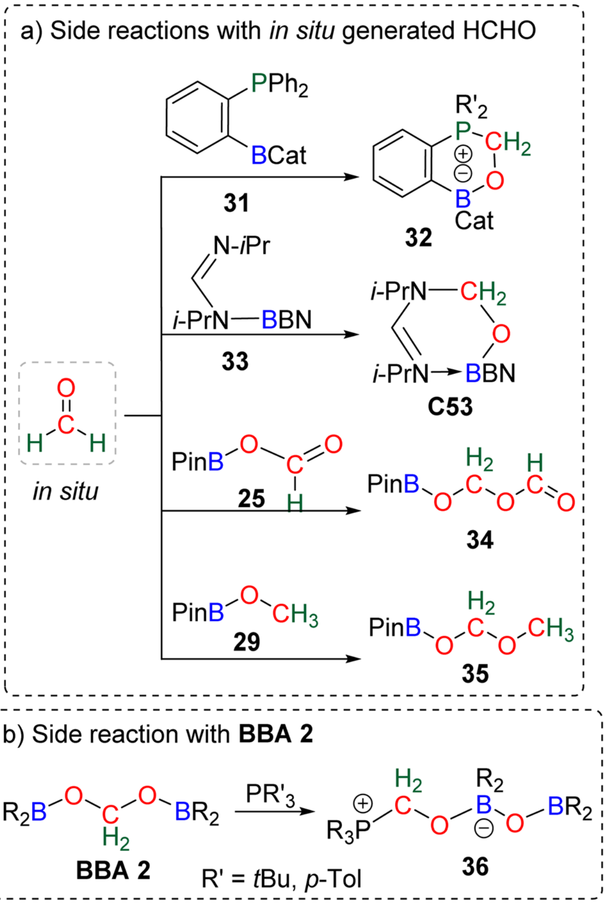

Scheme 33 Side reactions obtained with *in situ* generated HCHO (a) and BBA 2 (b).

3.3.1. BBA as a C_1 source in the formation of H_2C–O, H_2C–N and H_2C–P bonds. **BBA 2** was the first BBA involved in reductive functionalization.[93,124] Although **BBA 2** has never been isolated so far, its selective and efficient generation in 85% yield after 47 min at room temperature from $^{12}CO_2$ and $^{13}CO_2$ hydroboration enabled probing of its reactivity toward various E–H substrates (E = RO or R_2N, Scheme 34).[93] Its reaction with methanol and (diisopropyl)aniline led to the characterization of the hemiacetal compound **37** (89% yield, <5 min) and imine **38** (83% yield, 20 min), respectively. These short reaction times and high yields were the first evidence that **BBA 2** could indeed be used as a formaldehyde surrogate leading to the transfer of a methylene fragment for the formation of H_2C–O and $H_2C{=}N$ bonds. The reactivity was further extended to the generation of the hemiaminal **39** (67% yield, 1 h) and both cyclic and acyclic aminal compounds **40** (77% yield, 3 h) and **41** (84% yield, 1 h), respectively. Finally, the reaction with ammonia afforded the cage compound hexamethylenetetramine **15** in 84% yield after 16 h. In the latter example, it is remarkable that the six fully deoxygenated carbon atoms are issued from **BBA 2** and thus from CO_2. **BBA 1** was also used as a source of methylene in

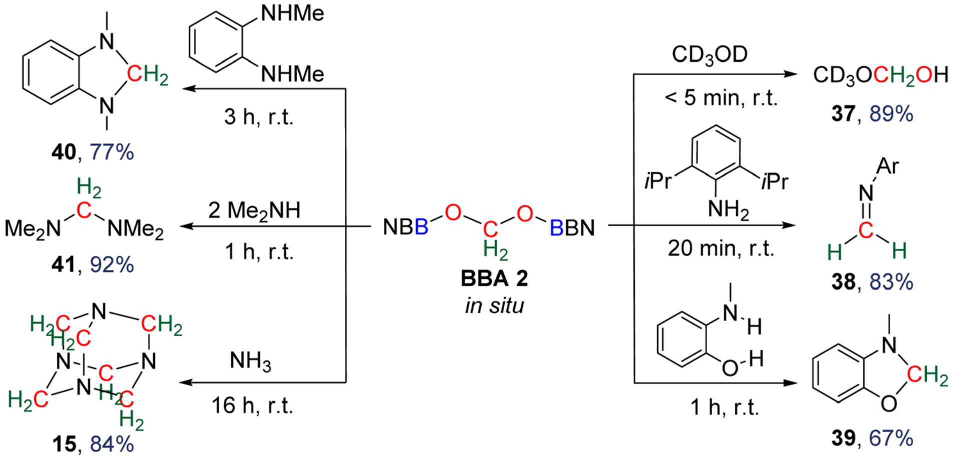

Scheme 34 Formation of CH_2–N, CH_2=N and CH_2–O bonds from **BBA 2**: generation of compounds **15**, **37–41**.

reductive functionalization reactions (Scheme 35).[94] Being selectively generated (71% isolated yield), its reactivity was explored first with (diisopropyl)aniline giving rise to the corresponding imine **38** (86% yield, 24 h). It is interesting to note that similar yields were obtained starting from both **BBA 1** and **BBA 2** (*i.e.*, 83% and 86% yields, respectively) but with longer reaction time with **BBA 1** (24 h) than with **BBA 2** (20 min). The reaction with phenylmethylamine afforded the aminal **42** (79% yield, 24 h). Finally, the reaction with diphenylphosphine gave rise to a single product assigned to compound **43**. Subsequent reaction with phenylamine led to the isolation of compound **44** (78% yield, 48 h) featuring for the first time a C–P bond.

3.3.2. CO_2 as a C_1 source in the formation of C–C bonds. The formation of C–C bonds from CO_2 reduction is of high interest, yet challenging. Such a process was first described with the condensation reaction between **BBA 2** and 2 equivalents of a substituted phenol derivative, leading to the generation of the methylene-bridged compound **45** (46% yield, 36 h, 120 °C, Scheme 36). **BBA 2** was also used in a Wittig reaction, producing styrene **46** (72% yield, 5 h, room temperature). These two examples showed that the formation of C–C and C=C bonds could be successfully achieved from CO_2.[93]

3.3.3. BBA as a C_n source: oligomerization of BBA and formaldehyde. The conversion of CO_2 into C_n compounds by the construction of a carbon chain is an appealing process because of the higher complexity and diversity of the C_n products as compared to the C_1 products. However, this reaction is highly challenging in terms of conditions, selectivity and scope of products.[3b,21a–c] In particular, no asymmetric carbon atom was generated from CO_2. So far, the 4e$^-$ reduction of CO_2 by hydrogenation, hydrosilylation and hydroboration aimed at employing CO_2 exclusively as a C_1 source. While the difficulties encountered in controlling the 4e$^-$ reduction processes may have been the main reason for this, the long-known possibilities of oligomerizing formaldehyde – the so-called formose reaction – were strongly calling for using CO_2 4e$^-$ reduction products as a C_n source.[125] This was first accomplished upon reacting **BBA 2**, generated *in situ* from CO_2 hydroboration, with N-heterocyclic carbene (NHC, Scheme 37).[32] Ender's NHC carbene **47** is a classical organo-catalyst able to catalyse the formation of C–C bonds of carbonyl compounds and notably the oligomerization of formaldehyde.[126] Its stoichiometric reactivity with **BBA 2** was first probed, leading to the formation and isolation of compound **48** (40% yield, 3 h, 10 °C) (Scheme 37). This reaction resulted from the formal isomerization of **BBA 2** triggered by the addition of the NHC on the electrophilic methylene moiety of

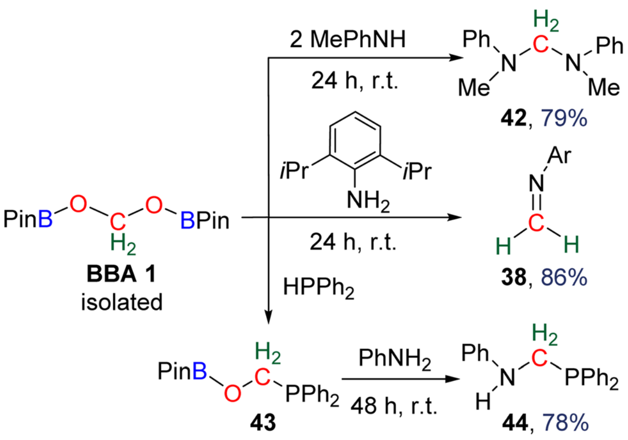

Scheme 35 Generation of CH_2–N and CH_2–P bonds from **BBA 1**.

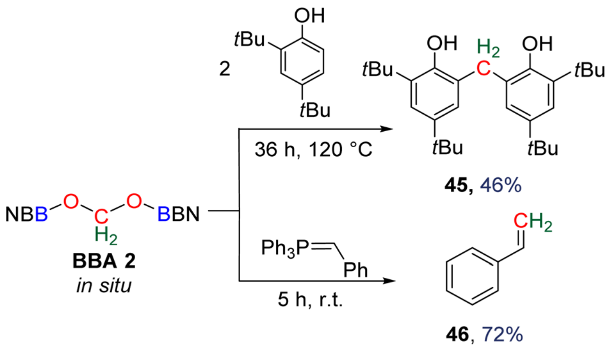

Scheme 36 Generation of C–C and C=C bonds from **BBA 2**.

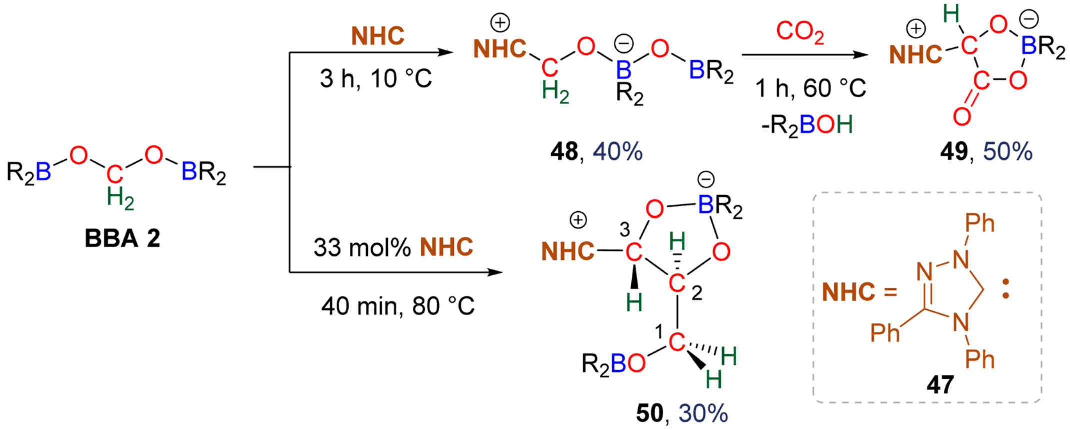

Scheme 37 Homocoupling of **BBA 2** resulting in the formation of compounds **49** and **50**.

BBA 2 *via* an S_N2 type mechanism, as proposed by DFT investigations.[32] This reaction illustrated that a Lewis base can promote the migration of an O-BR_2 fragment onto the other Lewis acid moiety of a BBA molecule, which is reminiscent of the generation of compound **36** from the reaction of **BBA 2** with tertiary phosphines (Scheme 33b). The intermediate **48** was shown to further react with CO_2 to form compound **49** (50% yield, 1 h, 60 °C), which was notably characterized by X-ray diffraction analysis. This compound was obtained from the loss of a borinic acid moiety (R_2BOH), possibly generating a transient original O-borylated Breslow intermediate which was then able to trap a CO_2 molecule in a bifunctional manner.[127]

Compound **49** features a new C–C bond between two carbon atoms arising from two CO_2 molecules. In this reaction, the new C–C bond was formed thanks to the nucleophilic character of the carbon atom linked to the NHC. This Umpolung process – classical of organocatalyzed C–C bond formation with such a carbene – was further used to generate compound **50** from the homocoupling of three **BBA 2** molecules in the presence of 33 mol% of NHC, generating a chain of three carbon atoms (C^1, C^2, C^3) arising from three CO_2 molecules. It must be pointed out that two of the three carbon atoms (C^2, C^3) of the chain are asymmetric carbons and were generated with a high diastereocontrol, thanks to the presence of the boryl moiety. DFT investigations were conducted to get insights on the elementary steps accounting for these transformations,[32] which stand as the first reported example of the generation of asymmetric carbon centres from CO_2. In the process leading to **50**, it should

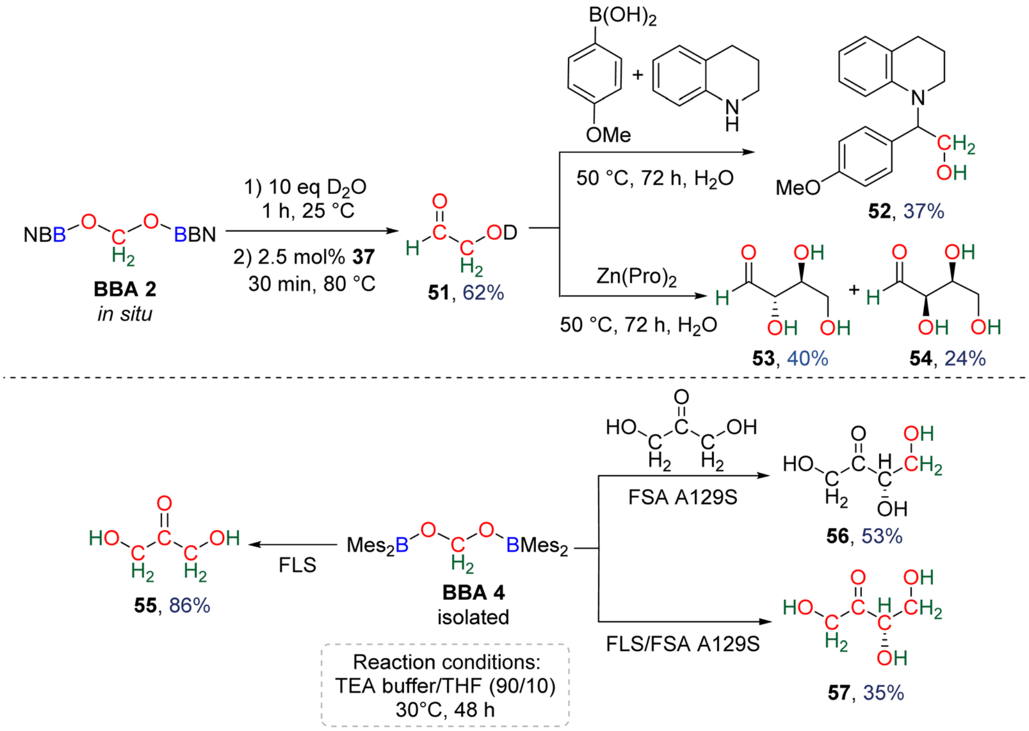

Scheme 38 Chemo- and enzyme-catalysed oligomerization of **BBA 2** and **4**.

be noticed that formaldehyde is never released from **BBA 2**. The oligomerization reaction involves BBA without the intermediary of formaldehyde, as shown from the presence of boryl moieties in the final product **50**. The possibility that formaldehyde could be released from BBA – in the same vein as what was explored with **BSA 3** – before its engagement in the oligomerization process, was recently explored with **BBA 2** and **BBA 4** (Scheme 38). Despite its powerful nature, the formose reaction remains a challenging reaction due to the difficulty in controlling both the length of the carbon chain and the chirality of the generated carbohydrates.[26,126,128]

As presented earlier, **BBA 2** was shown to quantitatively release formaldehyde after 1 h at room temperature in the presence of 10 equivalents of D_2O. Optimization of both the hydrolysis and the formose steps led to the synthesis of the C_2 carbohydrate glycolaldehyde **51** in 62% yield after 30 min at 80 °C using 2.5 mol% of NHC **47** as the catalyst (Scheme 37).[29b] Glycolaldehyde was further engaged in one-pot reactions leading to the formation of compound **52** (37% isolated yield) *via* a Petasis–Borono–Mannich reaction or to the formation of the C_4 carbohydrates erythrose (**53**, 40% yield) and threose (**54**, 24% yield) generated from Zn(pro)-catalysed dimerization reactions (pro = proline).

In a parallel study, **BBA 4** was identified as a promising candidate to conduct enzymatic transformations.[30] Its isolation, in contrast to **BBA 2**, was seen as an important feature toward this aim. If it was stable enough for isolation, **BBA 4** was nonetheless shown to readily release formaldehyde upon hydrolysis under relatively similar conditions to those with **BBA 2**. Enzymatic transformations were then thought about in order to control the length of the generated carbon chain and the chirality of the product. While formaldehyde is usually responsible for enzyme inhibition and even denaturation,[129] D-fructose-6-phosphate aldolase (FSA) and formolase (FLS) were shown to catalyse aldolization and formose transformations of formaldehyde, respectively.[24,130] These enzymes were thus selected to perform the transformation of formaldehyde released from **BBA 4**. The enzymatic transformations were conducted at 30 °C for 48 h in a triethanolamine (TEA) buffered solution (25 mM, pH 7.0 with 1 mM $MgSO_4$ and 0.1 mM thiamine pyrophosphate (TPP)) with THF. The presence of 10% THF was found optimal to ensure the solubility of **BBA 4**, while limiting the detrimental effect of this organic solvent on FLS and FSA activities (Scheme 38).[30] Under these conditions, **BBA 4** was oligomerized by FLS into dihydroxyacetone (**55**) in 86% yield. **BBA 4** was then reacted with commercial dihydroxyacetone in the presence of the mono-mutant FSA A129S[131] to afford the corresponding C_4 carbohydrate, L-erythrulose (**56**) in 53% yield with a perfect enantiocontrolled aldol reaction. In this case, one carbon atom of the carbon chain arose from **BBA 4**. Following recently reported cascade reactions with formaldehyde,[132] these two enzymes were then combined in a one-pot cascade reaction to achieve the transformation of **BBA 4** into L-erythrulose **57** in 35% yield. All four carbon atoms of the carbohydrate arose from CO_2, including the chiral one. This reaction corresponds to the first cell-free enantioselective transformation of CO_2.

3.4. Conclusion and perspectives

In conclusion, the $4e^-$ hydroboration of CO_2 stands out for several reasons: (i) the uncatalyzed formation of three bis(boryl) acetal (BBA) compounds derived from specific hydroboranes; (ii) the highest reported turnover frequency (TOF) at 516 h^{-1} among hydroelementation reactions; (iii) the reactive nature of BBA at room temperature, facilitating condensation reactions or formaldehyde release; (iv) the utilization of BBA as a C_n source with or without formaldehyde release, wherein the reaction without formaldehyde release results in the formation of an O-borylated C_3 compound; (v) the use of BBA in the pioneering enantioselective generation of a carbon centre from CO_2.[30–32] This significant breakthrough was achieved through formaldehyde release and subsequent enzymatic cascade reactions.

As perspectives in CO_2 hydroboration, the primary challenge lies in the stoichiometric utilization of hydroborane and thus the stoichiometric amount of borinic acid (R_2BOH) generated as a co-product following the hydrolysis of BBA compounds. Since there is currently no sustainable process for regenerating hydroborane from this co-product, CO_2 hydroboration is scarcely applicable unless the product synthesized from BBA holds a very high value. For example, carbohydrates, particularly rare and non-natural ones, are of significant interest to the pharmaceutical industry. Their synthesis from CO_2, especially with isotope labelling, could be an avenue worth exploring for generating chiral complex C_n products from CO_2. On the other hand, the prospect of generating O-borylated C_n products could open new avenues to retain boryl moieties in CO_2 transformation products, instead of treating them as waste after B–O bond hydrolysis. This would allow for further functionalization of the generated compounds. To achieve these objectives, future efforts could focus on exploring a broader variety of hydroboranes with diverse properties. Such a range of hydroboranes could lead to the formation of a diverse array of BBA compounds with varying stability and reactivity, suitable for various applications. Additionally, other CO_2 hydroelementation reactions, beyond hydrosilylation and hydroboration, may provide an even greater variety of acetal compounds with unique properties. Specific CO_2 hydroelementation reactions involving early transition-metal hydride species are discussed in the subsequent section of this review.

4. Other hydroelementation reactions

The CO_2 hydroelementation involving metal hydrides and phosphines has seen limited development. We have compiled these results in this concise standalone section, separated from the broader and more extensive sections.

4.1. Hydroelementation with actinide, early TM and rare earth metal hydride species to acetal complexes

Hydride complexes of U, Zr, Ta, Nb and Y were shown to react with CO_2 under mild conditions to afford the bi-metallic acetal or methylene diolate complexes shown in Scheme 39. The reaction of the U(IV) hydride complex $(Cp')_3U(H)$ (Cp' =

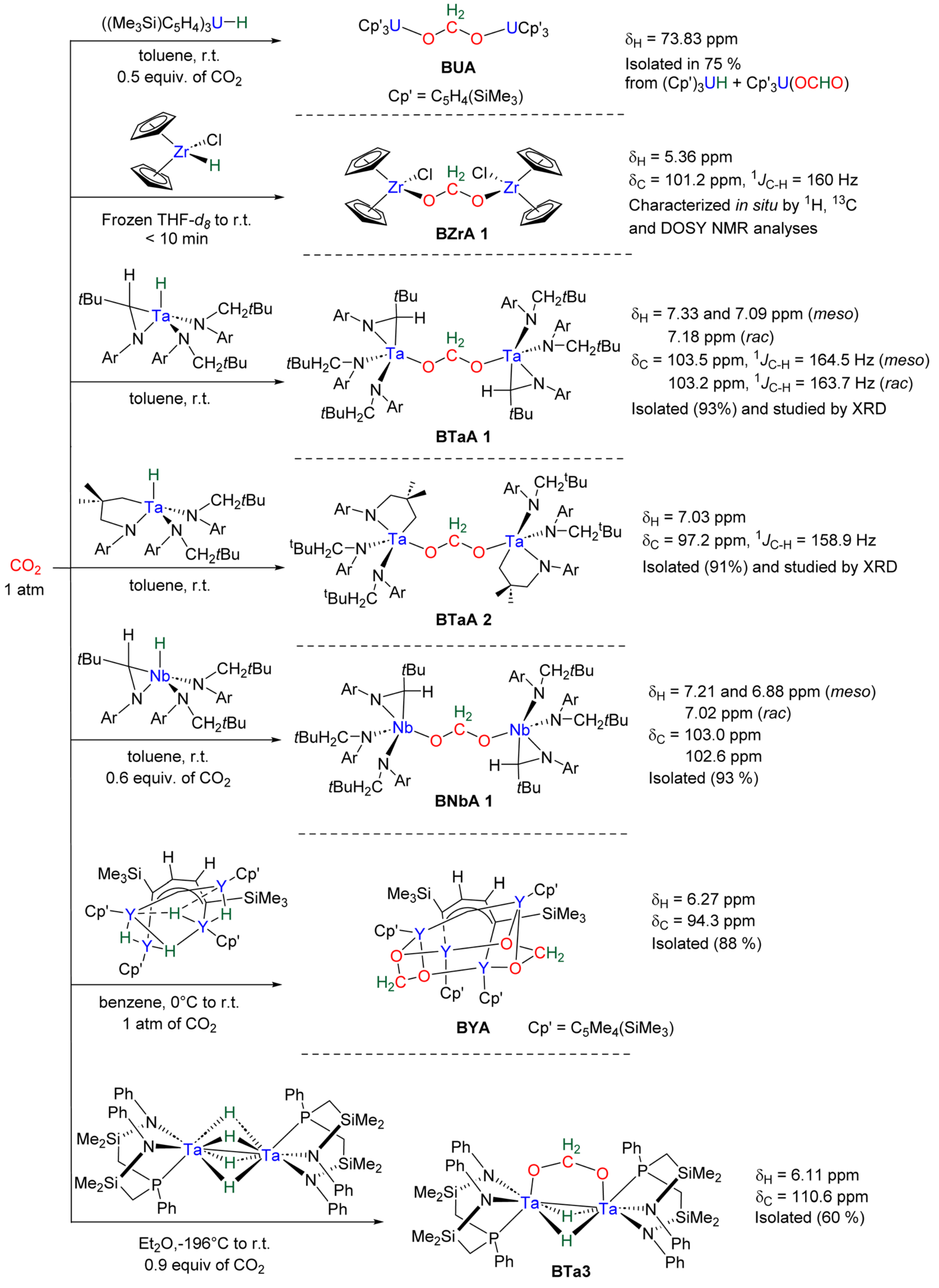

Scheme 39 Generation of BZrA 1, BTaA 1, BTaA 2 and BNbA 1.

$C_5H_4(SiMe_3)$) with 1 atm CO_2 led to the expected formoxy uranium $(Cp')_3U(OCHO)$. However, when only 0.5 equiv. of CO_2 was introduced in an NMR tube, the bis(uranyl)acetal complex (**BUA**) was generated.[131] This complex was also isolated by crystallization from the stoichiometric reaction of $(Cp')_3U(OCHO)$ with $(Cp')_3U(H)$ in 75% yield after 4 h at 70 °C. The methylene fragment was characterized at 73.83 ppm in ^1H NMR due to the proximity with the paramagnetic uranium centre. The reaction of the Schwartz's reagent, $Cp_2Zr(H)Cl$, was investigated with $^{13}CO_2$.[134] A frozen THF-d_8 solution of the Zr complex was prepared and reaction with $^{13}CO_2$ was investigated at an early stage. After initiating the reaction by a gentle shaking of the frozen solution, the acetal **BZrA 1** could be observed by ^1H NMR analysis for only 10 min. To further characterize the acetal

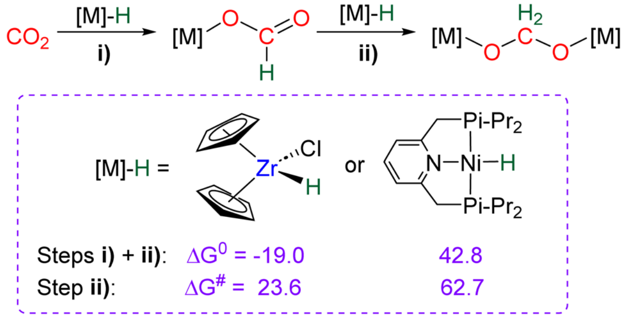

Scheme 40 DFT investigations for the formation of metallic acetal upon reaction of [Ni]–H and [Zr]–H hydrides with CO_2 (free enthalpies in kcal mol^{-1}).

species, ^{1}H and ^{13}C{^{1}H} NMR analyses were conducted at 235 K.[134b] The methylene signal appeared at δ^{1}H = 5.36 ppm and δ^{13}C = 101.2 ppm. Low temperature diffusion ordered NMR spectroscopy (DOSY) confirmed the dimeric nature of **BZrA 1** in solution.[134a] The reduction of CO_2 was also investigated with Ta–H and Nb–H complexes. The acetal complexes **BTaA 1, BTaA 2** and **BNbA 1** were isolated and characterized, notably by XRD in the case of the two former ones (Scheme 39).[135] Two diastereoisomers with diastereotopic methylene protons, the *rac* and *meso* forms, were observed for **BTaA 1** and **BNbA 1**, being the result of a C_2 and C_s symmetry, respectively. The [Ta]- and [Nb]-based hydride complexes featured a peculiar aziridine-metallacycle which was shown to generate a 5-membered cycle leading to **BTaA 2.** Another Ta acetal complex **BTaA 3** was later reported from the reaction of a dinuclear Ta tetrahydride complex with 0.9 equivalent of CO_2 at low temperature.[134] The methylene signal was characterized in solution at δ^{1}H = 6.11 ppm and δ^{13}C = 110.6 ppm and the complex was structurally characterized by X-ray diffraction analysis. Finally, a tetranuclear yttrium tetrahydride complex was also shown to readily react with 1 atm of CO_2 to afford **BYA** featuring two methenediolate bridge fragments maintaining the tetranuclear structure. The complex was analysed in the solid state by X-ray diffraction and in solution by NMR (CH_2 fragment: δ^{1}H = 6.27 ppm and δ^{13}C = 94.3 ppm).[137]

The methylene signal of these acetal products appeared at a lower field in ^{1}H NMR (6.11 ppm < δ^{1}H < 7.33 ppm) as compared to BBA, BSA and **BZrA 1** structures while the ^{13}C{^{1}H} NMR chemical shifts of the early-TM acetals are in a slightly lower field area as compared to the ones obtained from BBA and BSA derivatives (101.2 ppm < δ^{13}C < 103.5 ppm).

DFT investigations[89] were conducted to compare the reactivity of CO_2 toward the Schwartz's reagent [Zr]–H complexes[134] *vs.* [Ni]–H complexes used as catalysts in CO_2 hydroboration,[88] regarding the formation of the corresponding metallic acetal species (Scheme 40). This study disclosed a rare comparison between the reactivities of early and late TM complexes toward CO_2.[138] The formation of the acetal from two equivalents of [M]–H and CO_2 (steps (i) + (ii), Scheme 36) is exergonic with ΔG^{0} = −19.0 kcal mol^{-1} for the Zr complex, while it is endergonic for the Ni analogue by +42.8 kcal mol^{-1}. Replacing the bulky ^{t}Bu group of the pincer system on Ni led to a more accessible, yet still endergonic reaction by +26.9 kcal mol^{-1}. The thermodynamic barriers ($\Delta G^{\#}$) for step (ii) were calculated to equal 23.6 and 62.7 kcal mol^{-1} for the Zr–H and Ni–H, respectively. These calculations explained why the bis-nickel acetal was never observed in contrast to the Zr analogue.[89]

4.2. Hydroelementation to formaldehyde and reductive functionalization

While the formation of **BZrA 1** is favourable as shown in experiments and upon DFT calculations, it is not stable at room temperature, in contrast to **BTaA 1**, **BTaA 2** and **BNbA 1**. The reaction of group IV elements toward CO_2 has been studied for a long time, with an early report in the 1970s.[139] Using Schwartz's reagent as the reductant, CO_2 was readily reduced to formaldehyde at room temperature (Scheme 41).[139a,b] Besides the formation of a [ZrOZr] complex, the proof for the formation of formaldehyde was obtained by *in situ* condensation with 5,5-

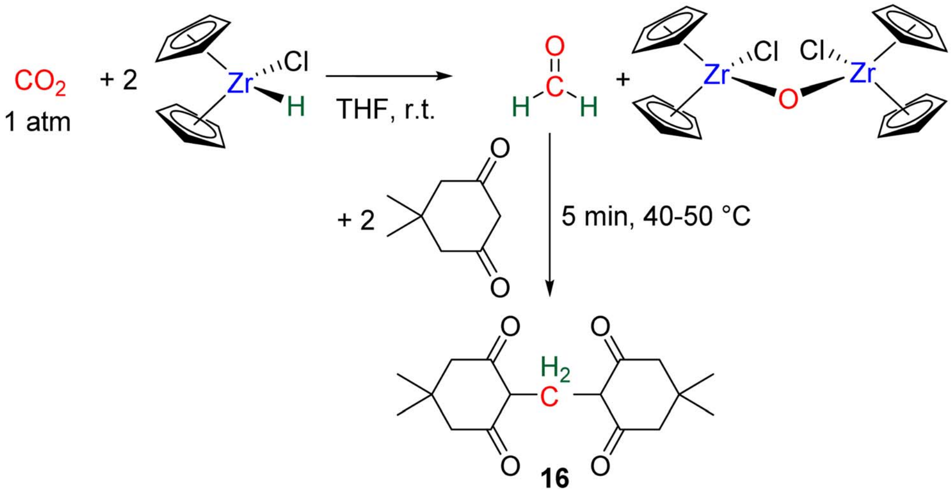

Scheme 41 Condensation of a cyclohexanedione with formaldehyde generated from CO_2 hydrozirconation.

dimethylcyclohexane-1,3-dione to afford the corresponding maledone compound **16** which displays a methylene-bridged structure. This study reported the actual first example of reductive CO_2 functionalization.[139a,140]

4.3. Hydrophosphination

CO_2 hydrophosphination was reported to afford the corresponding formate compound.[141] Despite similar electronegativity values for P and H atoms, 1,3,2-diazaphospholene (NHP–H) exhibits zwitterionic properties[142] leading to the $2e^-$ reduction of CO_2 into a phosphorus formate moiety in high yield (93% isolated yield). However, no further reduction to the 4, 6 or $8e^-$ reduction levels was evidenced. One can imagine that further structural modification would be necessary to achieve further reduction.

4.4. Conclusion

In conclusion, the $4e^-$ hydroelementation with early TM presented in this section stands out by the fact that (i) only four examples were reported so far; (ii) formaldehyde is spontaneously released at low temperature from **BZrA 1**; and (iii) the insertion of CO_2 into the early TM hydride bond is uncatalyzed.

As perspectives, hydroelementation of CO_2 to the $4e^-$ reduction level might offer a wide range of reactivity *via* the modification of the coordination sphere of the metal fragment.

5. Hydrogenation

The hydrogenation of CO_2 into HCOOH, HCHO, CH_3OH and CH_4 are reactions of utmost importance in the actual momentum of producing green H_2 from water electrolysis.[13f,15a,16a,143] As opposed to hydroelementation, hydrogenation of CO_2 is a 100% atom economical reaction making CO_2 perfectly fitted to store energy and/or to afford key C_1 building blocks for the chemical industry. As a consequence, these transformations have been intensively investigated but for formaldehyde synthesis. There are indeed currently only five catalytic systems, including heterogeneous and homogeneous processes, which have reported the generation and detection of formaldehyde in CO_2 hydrogenation (Scheme 42a). These systems are presented in Section 5.1. Three of these examples generated formaldehyde as the major product and none disclosed its isolation. Reasons are because of (i) the disfavoured thermodynamic parameters in gas and in liquid phases, (ii) the highly reactive nature of formaldehyde and (iii) its volatility as a gas under atmospheric conditions.

To circumvent such hurdles, the hydrogenation reaction conducted in the presence of alcohol as the solvent and co-reactant led to the stabilization of the $4e^-$ reduction stage in the form of acetals (Scheme 42b) as described in Section 5.2, which is in line with the formation of BSA and BBA presented in the previous sections. The specific roles of H_2 and alcohol are thoroughly explained in the mechanism described in Section 5.2.3.

5.1. Hydrogenation of CO_2 into formaldehyde

Catalysts **C64–C68** were reported to generate formaldehyde from CO_2 hydrogenation (Scheme 43). The catalytic conditions and performances are presented in Table 5. It is worth mentioning that the origin of the detected HCHO was not confirmed with $^{13}CO_2$ labelling experiments in any of these cases.

C65,[145] **C67**[147] and **C68**[148] gave rise to the generation of formaldehyde as the major product. **C64**[144] is the only reported molecular homogeneous system and operates in liquid media similarly to **C67** and **C68**, while **C65** and **C66**[146] operate in the gas phase. Reaction temperatures range between 40 and 200 °C, while the total gas pressure ($P_{CO_2} + P_{H_2}$) ranges between 4 and 70 atm. The positive impact of a high P_{H_2}/P_{CO_2} ratio on the selectivity toward HCHO formation is a common feature observed for **C64**, **C65** and **C67**. It can also be noticed that both selective systems, **C65** and **C67**, relied on a Pt-based catalyst system. The small number of catalytic systems and their disparities preclude

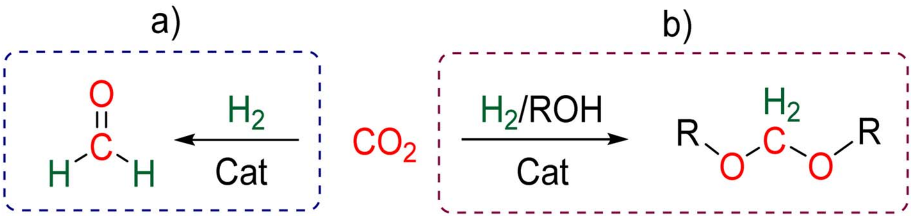

Scheme 42 CO_2 hydrogenation into $4e^-$ reduction products: (a) formaldehyde (Section 5.1) and (b) acetals (Section 5.2).

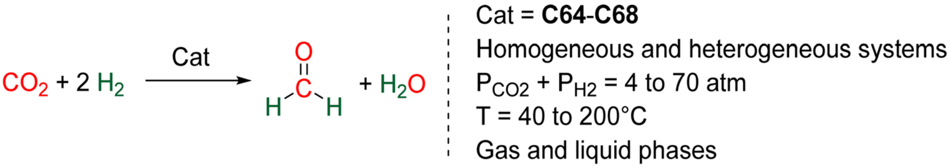

Scheme 43 CO_2 hydrogenation into formaldehyde catalysed by **C64–C68**.

Table 5 Properties of reported systems for CO_2 hydrogenation into formaldehyde catalysed by **C64–C68**

Catalytic systems	K[Ru(EDTA-H)Cl]·H_2O	Pt–Cu/SiO_3	Ni–Co NPs	Pt–Ni and Pt–Cu/Al_2O_3	Ru/LDH
	C64[144]	**C65**[145]	**C66**[146]	**C67**[147]	**C68**[148]
Performances	Rate = 2.79×10^{-2} M h^{-1}	5.22×10^{-3} M g_{cat}^{-1} h^{-1}	CO_2 conv. = 0.24% HCHO ratio = 30%	0.41×10^{-5} M g_{cat}^{-1} h^{-1}	0.037 M g_{cat}^{-1} h^{-1}
T (°C)	40	150	200	25	50
P_{CO_2} (atm)	17	0.3	1	4	10
P_{H_2} (atm)	17	5.7	3	66	10
Medium	H_2O	CO_2 gas	CO_2 gas	CH_3OH	H_2O
HCHO as the major product?	No	Yes	No	Yes	Yes

further general considerations. **C64–C68** systems are described separately hereafter in a chronological order.

The first report of formaldehyde generation dates back to 1989 with the use of the homogeneous Ru-based catalyst **C64.**[144] The reaction was performed in water at 40 °C with a total gas pressure ($P_{CO_2} + P_{H_2}$) of 34 atm. Under these catalytic conditions, CO_2 hydrogenation led to the generation of HCOOH and HCHO which then decomposed into CO and H_2O. The generation of CO was monitored by GC analysis while formation of HCOOH and HCHO was followed spectrophotometrically upon reaction with Nash's reagent.[149] Kinetic investigation showed that the decrease of P_{CO_2} while keeping P_{H_2} constant led to a rate increase in HCHO formation. The initial rate of formation of formaldehyde was measured at 2.79×10^{-2} M h^{-1} using 1 mmol of catalyst loading with an estimated activation energy of 8.3 kcal mol^{-1}. The rate of formation of formaldehyde was found to be lower than its rate of decomposition, explaining the lack of formaldehyde build-up within the system. In addition, the rate of formation of formic acid was always higher than that of formaldehyde explaining the favoured selectivity towards formic acid. In 2001, an impregnated Pt/Cu (ratio = 0.03) on SiO_2 surface (**C65**) was shown to afford formaldehyde and methanol with a total gas pressure ($P_{CO_2} + P_{H_2}$) of 6 atm in the gas phase.[145] The reaction was monitored by temperature programmed surface reaction spectroscopy indicating an optimum temperature of 150 °C for the formation of formaldehyde. While methanol was favoured at a P_{H_2}/P_{CO_2} ratio of 3, the selectivity was reversed when this ratio was increased to 20. At this ratio, the rate of formation reached 0.12 g_{cat}^{-1} h^{-1} for methanol and 5.22×10^{-3} g_{cat}^{-1} h^{-1} for formaldehyde, respectively. In the absence of Pt, the analogous Cu-based catalyst afforded only methanol. The importance of Pt in the formation of formaldehyde was attributed to the known ability of Pt to adsorb H_2. Indeed, the Pt activation of H_2 along with a higher pressure of H_2 was proposed to favour a higher concentration of H_2 in the proximity of the Cu centres, responsible for shifting the product formation from methanol to formaldehyde. These observations suggest that the formation of formaldehyde and methanol follows two distinct competitive pathways and that the accessibility of activated H_2 is part of the rate determining step for formaldehyde but not for methanol. In 2015, bimetallic Ni–Co nanoparticles (NPs) (**C66**) were produced in a bottom-up approach and their ability to catalyse CO_2 hydrogenation was studied.[144] Their catalytic activity was evaluated after deposition of the Ni–Co NPs on a mesoporous silica support and exposition to a $CO_2 : H_2 :$ He (6.6 : 20.7 : 14.7) gas mixture at a total pressure of 6 atm. At 200 °C, a low conversion of CO_2 (0.24%) was observed by GC analysis with 30% selectivity for formaldehyde and 70% selectivity for CO generated as the major product. Only a trace amount of formaldehyde was detected upon increasing the temperature to 350 °C. Pt–Ni and Pt–Cu (**C67**) catalysts selectively afforded formaldehyde in methanol medium at 25 °C and a total gas pressure ($P_{CO_2} + P_{H_2}$) of 70 atm.[147] The catalysts were prepared by a wet impregnation method using γ-alumina as the support. The final Pt–Ni and Pt–Cu supported catalysts contained 10 wt% Ni or Cu content and 1 wt% Pt content. Once again, a high P_{H_2}/P_{CO_2} ratio (16) led to the generation of formaldehyde with a molar yield of

0.9×10^{-4} M g_{cat}^{-1} in 22 h corresponding to 0.41×10^{-5} M g_{cat}^{-1} h^{-1}. This activity is still lower than the one reported with the **C65** catalyst (5.22×10^{-3} M g_{cat}^{-1} h^{-1}).

Compound **C68** is a heterogeneous catalyst consisting of highly dispersed Ru on layered double hydroxide (LDH). The use of 0.5 wt% Ru was recently shown to catalyse the hydrogenation of CO_2 ($P_{CO_2} = 10$ atm, $P_{H_2} = 10$ atm) into 0.446 M g_{cat}^{-1} of formaldehyde in water as the solvent in 12 h, corresponding to 0.037 M g_{cat}^{-1} h^{-1}.[148] The detection and quantification of formaldehyde was performed using the colorimetric method with 3-methyl-2-benzothiazolinone hydrazone (MBTH) and high-performance liquid chromatography (HPLC), respectively. In the same study, dihydrogen was replaced by glycerol as a transfer hydrogenation reagent. In a 0.2 M aqueous glycerol solution, catalytic transfer hydrogenation (CTH) of CO_2 afforded formaldehyde in a slightly better yield at 0.1 and 3 wt% Ru under otherwise the same conditions. It is worth mentioning that in the proposed mechanism, initiation of the reaction *via* the dehydrogenation of glycerol into the C_3 carbohydrate dihydroxyacetone (DHA) or glyceraldehyde is proposed. However, the possibility that glycerol – notably *via* the generation of these carbohydrates – could be a source of formaldehyde prior to the CTH of CO_2 was not investigated.[150]

5.2. Hydrogenation of CO_2 into acetals

As presented above, the selective 4e⁻ hydrogenation of CO_2 into HCHO is still a widely open challenge. In contrast, the selective 4e⁻ hydrogenation of CO_2 into acetal was pioneered rather recently in 2016 and 2017 with homogeneous Ru- and Co-based catalytic systems.[151] The formation of an acetal from CO_2 hydrogenation consists in the addition of alcohol to stop at the 4e⁻ reduction stage with the formation of acetal species (Scheme 42b). Mechanistic investigations have shown that formaldehyde is never formed during the process which alternates between reduction (hydrogenation) and functionalization (with the alcohol) steps giving rise to the acetal. The interest in the formation of dialkoxymethane derivatives is dual. First, it provides a selective access to formaldehyde since some of them were found to release HCHO in strong acidic media,[153] although to our knowledge, the proof of concept from CO_2 has never been reported. Second, dialkoxymethane derivatives are compounds of interest as fuel additives to lower the formation of soot because of their high oxygen content and the absence of C–C bonds.[151,153] The catalytic performances of the reported systems, the in-depth optimization of the catalytic conditions, the proposed mechanism and the extent of the scope of alcohols employed are presented hereafter.

5.2.1. Catalytic systems for CO_2 hydrogenation into dimethoxymethane (DMM). Currently, 10 catalytic systems (**C69–C78**) have been reported for the hydrogenation of CO_2 in the presence of methanol as the solvent and co-substrate affording dimethoxymethane (DMM). Their structures are depicted in Fig. 5 and the catalytic conditions and performances are reported in Table 6. It must be noted that in all reported studies, the reactions were monitored by ^1H and ^{13}C NMR spectroscopy and the products characterized and quantified *in situ*.

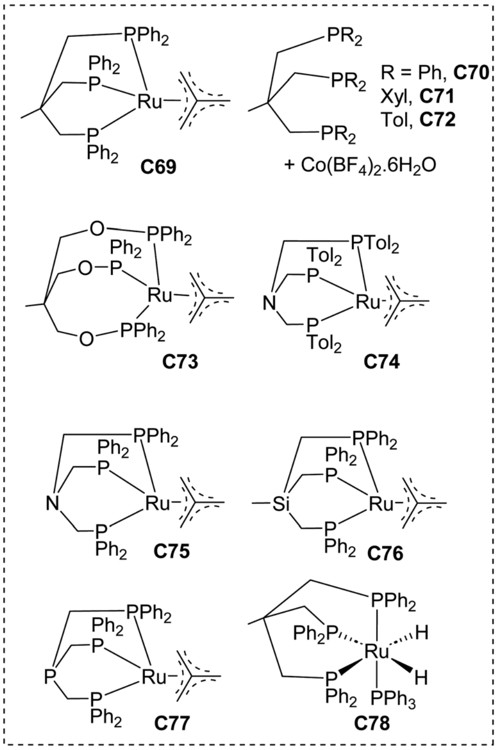

Fig. 5 Catalytic systems **C69–C78** leading to the hydrogenation of CO_2 into DMM.

The characteristic methylene signal of DMM was observed at 4.39 ppm in the ^1H NMR analysis in CD_3OD. With the Ru-based precatalyst **C69** featuring a triphosphine ligand (Scheme 44) and a Lewis acid co-catalyst ($Al(OTf)_3$), the hydrogenation of CO_2 in methanol was shown to afford the 2e⁻ reduction product methoxyformate (MF) and the 4e⁻ reduction product dimethoxymethane (DMM) (Scheme 5).[151a] Among the different conditions tested (variation of the Ru-based precatalyst, temperature, pressure, nature of the acid and time), the best TON of 214 was found with **C69** under the following conditions: $P_{CO_2} = 20$ atm, $P_{H_2} = 60$ atm, 18 h, 80 °C, 2 mL of CH_3OH, 12.5 μmol of Ru-based precatalyst and 25 μmol of $Al(OTf)_3$ (Table 6, entry 1). The selectivity toward DMM *vs.* MF was 67%. Following this initial report, catalytic systems **C70–C78** were investigated in the same reaction (Fig. 5).

Pre-catalysts **C70–C72** are Co-based in contrast to all the other catalysts which are Ru-based.[151b] **C70–C72** were found to generate DMM with slightly lower TON of 92 to 157 than **C69** (Table 6, entries 2–4 *vs.* entry 1, resp.), with an interesting maximal selectivity of 81% for DMM. Better TONs were observed by replacing $Al(OTf)_3$ with $HN(Tf)_2$ as the acid, longer reaction time (22 h) and a higher temperature (100 °C). The impact of the triphosphine ligand was also probed. The use of triphosphine ligands featuring $P(Xyl)_2$ and $P(Tol)_2$ moieties increased the TON to 120 and 157 for **C71** and **C72**, respectively. Optimization of the Ru-based system was further explored in detail by another group.[154–156] **C73–C75** were tested in a first study.[154] While the phosphinite moieties in **C73** gave lower TONs than the other reported catalytic systems (Table 6, entry 5), replacement of the

Table 6 Catalytic conditions and performances of **C69–78**

Entry	Cat, *n* (μmol)	Acid, *n* (μmol)	P_{H_2} (atm)	P_{CO_2} (atm)	V_{CH_3OH} (mL)	Time (h)	*T* (°C)	TON	TOF (h^{-1})	Sel[a] (%)	Ref.
1	**C69**, 12.5	Al(OTf)$_3$, 25	60	20	2	18	80	214	12	67	151
2	**C70**, 15	HN(Tf)$_2$, 45	60	20	2	22	100	92	4	74	151*b*
3	**C71**, 15	HN(Tf)$_2$, 45	60	20	2	22	100	120	5	79	151*b*
4	**C72**, 15	HN(Tf)$_2$, 45	60	20	2	22	100	157	7	81	151*b*
5	**C73**, 1.5	Al(OTf)$_3$, 6.25	60	20	0.5	18	80	32	2	28	154
6	**C74**, 1.5	Al(OTf)$_3$, 6.25	60	20	0.5	18	80	221	12	71	154
7	**C75**, 1.5	Al(OTf)$_3$, 6.25	60	20	0.5	18	80	292	16	72	154
8	**C75**, 1.5	Al(OTf)$_3$, 6.25	90	5	0.5	18	90	97	5	92	154
9	**C75**, 0.38	Al(OTf)$_3$, 1.56	90	20	0.5	18	90	786	44	60	154
10	**C75**, 0.075	Al(OTf)$_3$, 3.576	105	12.5	0.55	21	105	2761	131	61	155
11	**C75**, 0.75	Al(OTf)$_3$, 35.76	100	15	0.5	20	100	3874	194	73	155
12	**C76**, 0.38	Al(OTf)$_3$, 3.13	90	20	0.5	18	90	685	38	60	156
13	**C77**, 0.38	Al(OTf)$_3$, 3.13	90	20	0.5	18	90	439	24	46	156
14	**C78**, 3.1	Al(OTf)$_3$, 25	20	100	5	20	100	1176	59	70	157

[a] Selectivity = TON(DMM)/[TON(MF) + TON(DMM)].

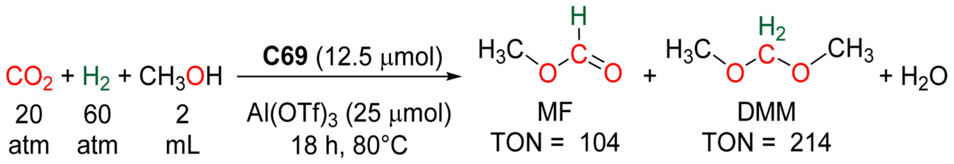

Scheme 44 DMM synthesis with **C69**.

central C atom of the backbone of the ligand by a N atom in **C74** and **C75** enabled slight increase of the TON to 221 and 292, respectively (Table 6, entries 6 and 7). With **C75**, the optimization conditions led to a net increase of either the selectivity for DMM to 92% but with a TON of 97 (Table 6, entry 8) or of the TON to 786 but with a selectivity for DMM reduced to 60% (Table 6, entry 9). The quantities of the catalyst and co-catalyst were shown to be the main factor enabling this TON increase. In this optimization study for **C75**, all possible parameters were carefully optimized individually (univariate optimization) to improve the TON from 214 to 786 (Table 6, entries 1 and 9, resp.) which represents a 367% increase in TON. A subsequent study using a multivariate optimization led to a larger improvement of TON. The pre-catalyst **C75** indeed provided TONs of 2761 and 3874 with a 10 fold increase of the scale of the reaction leading to the formation of 2.88 mmol of DMM (Table 6, entries 10 and 11, resp.).[155] This corresponds to a significant improvement of further 493% from the univariate optimization (Table 6, entry 9). These impressive results were made possible mainly by acting on the quantities of the catalyst and co-catalyst. In another report, the replacement of the heteroelement of the backbone by Si or P atoms (**C76** and **C77**, respectively) did not enable any further increase of the catalytic performances or selectivity (Table 6, entries 12 and 13).[156] In order to have a closer look at the active catalyst, dihydride compound **C78** was synthesized and tested (Table 6, entry 14).[157] Pre-catalysts **C69–77** are indeed sought to generate M–H species which act as the active catalyst in the reaction. This study showed the beneficial aspect of adding tertiary phosphine or phosphite in order to prevent catalyst deactivation by the formation of a carbonyl ligand from the CO_2 decarbonylation. Overall, optimization strategies presented with catalysts **C69–C78** were dedicated to the improvement of TON as the most important parameter. Although interesting selectivities of DMM *vs.* MM were obtained, the lesser attention to this parameter can be explained by the possibility of hydrogenating MF into DMM in a second step.[154,156] However, the TOF parameter was not optimized. As indicated in Table 6, it ranges between 2 and 194 h^{-1}, leaving room for improvement in these systems.

5.2.2. **Extension to other dialkoxymethanes (DAMs).** Other alcohols beside methanol were tested to generate dialkoxymethane (DAM) compounds. Using **C69** [151a] and **C70** (Fig. 5),[151b] 11 examples were obtained and characterized with TON ranging from 16 to 118 (Scheme 45a). Aliphatic alcohols used included linear chain (containing 2 to 10 carbon atoms), branched (^{t}BuOH and ^{i}PrOH) and benzyl alcohol. In a subsequent study, the authors used bio-sourced diols to increase the sustainability of the process and the product scope.[158] These diols were shown to afford either a cyclic acetal (C-DAM) or a linear acetal (L-DAM) (Scheme 45b). In total, eight products were characterized and selectivity toward either C-DAM or L-DAM was reached depending on the nature of the diol substrate ($n = 1–6$). A selectivity of 92% was notably observed toward the formation of the C-DAM, 4-methyl-1,3-dioxane, while reversed selectivity of 99% to L-DAM was obtained with the diol featuring a 5-carbon linker.

5.2.3. **Mechanism.** In the initial description of the formation of DMM from CO_2, the intermediary of methoxyformate (MF) and methoxymethanol (MM) was demonstrated

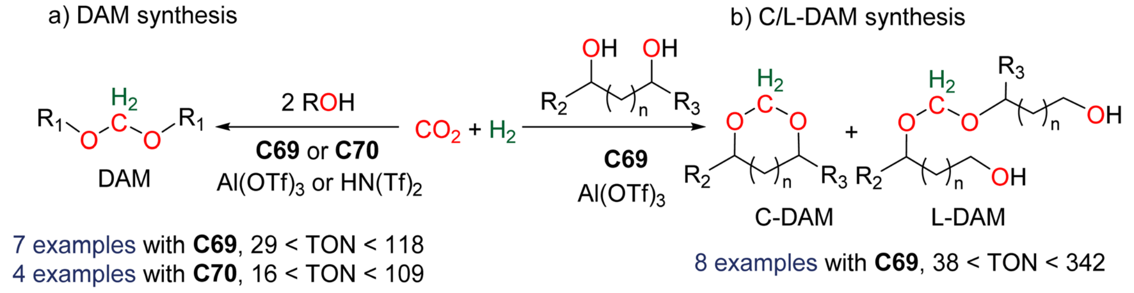

Scheme 45 Synthesis of (a) linear DAM with **C69** or **C70** and (b) cyclic or linear C-DAM or L-DAM, respectively, with **C69**.

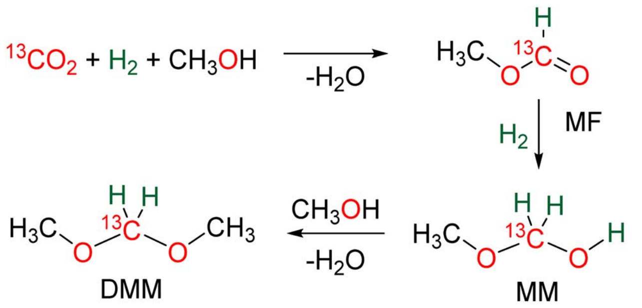

Scheme 46 Proposed mechanism for the formation of DMM.

(Scheme 46).[151a] MF and MM were indeed observed during the reaction and the expected ^{13}C-labelled products and intermediates were characterized when starting from $^{13}CO_2$ and $^{12}CH_3OH$ reactants. In this reaction mechanism, formaldehyde was not an intermediate. One methanol molecule was indeed involved in the first reduction step leading to MF. Compared to formic acid, the methylated analogue MF was hypothesized to "activate" this reduction stage enabling further hydrogenation into MM under rather mild conditions compared to the CO_2 hydrogenation reaction to methanol in the absence of alcohol. It is reminiscent of pioneering strategies using alcohol[159] or amine[20b,160] to promote the hydrogenation of CO_2 into methanol under mild conditions in cascade reactions. One additional molecule of methanol is finally reacted with the MM intermediate affording DMM.

Two recent in-depth studies published concomitantly in 2021 proved to be particularly complementary since one is an experimental investigation of the most used **C75**/Al(OTf)$_3$ catalytic system,[161] while the other is a DFT investigation on the Co-based **C70**/HN(Tf)$_2$ system.[153b] It is noteworthy that these studies confirmed the elementary steps proposed initially in 2016. The **C75**/Al(OTf)$_3$ catalytic system was investigated by *in situ* infrared (IR) spectroscopy at three relevant temperatures: 333 K, 353 K and 373 K enabling the determination of rate constants and activation parameters for the three steps: CO_2 to MF, MF to MM and MM to DMM.[161] These key steps were included in a reaction network analysis. The rate determining step (rds) was shown to be the first CO_2 to MF step with an activation parameters $\Delta G^{\#}$ (333 K) of 119.0 kJ mol^{-1} and the lowest rate constant of 1.41×10^{-6} s^{-1} M^{-2} at the same temperature. In accord with the experiment, the competitive formation of CH_3OH from the hydrogenation of MM was shown to be accessible at higher temperature and the formation of DMM was favoured by the large excess of CH_3OH used as the solvent. Furthermore, this reaction network analysis was also used as a predictive tool to propose new experimental conditions that would favour one product over the other. The positive effect of H_2O removal on the formation of DMM was notably proposed.

The DFT study of the **C70**/HN(Tf)$_2$ system proposed a detailed kinetic and thermodynamic analysis of each elementary step accounting for the formation of DMM but also for the over-reduction to CH_3OH.[153b] The thermodynamic values ΔG^0 for the subsequent formation of formic acid, MF, MM and DMM, indicated in Scheme 47, have been calculated to be 34, 19, 53 and 41 kJ mol^{-1}, respectively. A major input of this study was to define the exact role of the TM-based catalyst and the acid co-catalyst. The active Co-based species were calculated to be the monohydride cationic Co complex ([$P_3Co–H]^+$) depicted in Scheme 47 (purple box) and was calculated to be the catalyst responsible for the hydrogenation of CO_2 into formic acid and of MF into MM. The two steps (i) and (iii) have been calculated with $\Delta G^{\#}$ of 79 and 98 kJ mol^{-1}, respectively. On the other hand, the esterification of formic acid into MM (step ii) and the etherification of MM into DMM (step iv) are catalysed by the acid catalyst HN(Tf)$_2$. It was found that the methylating agent responsible for the etherification of MM to DMM was not directly methanol, but CH_3O-NTf$_2$ *in situ* generated from the reaction of CH_3OH with HN(Tf)$_2$. Nonetheless, the calculated Gibbs free energy barrier from the most stable Co-formate species is 179 kJ mol^{-1} for the last step (iv), making it the rate determining step (rds) of the whole process. As in the previous study, the access to DMM *via* formaldehyde was calculated to be higher in energy and thus discarded. The formation of formaldehyde as an intermediate to DMM was proposed in a related Ru-based system using ethanol instead of methanol, but not with the same level of kinetic or thermodynamic investigations.[162]

5.3. Conclusion

In conclusion, the selective 4e$^-$ reduction of CO_2 by hydrogenation stands out for several reasons: (i) the development of highly active catalytic systems resulting in the reduction of CO_2 into acetals, achieving the highest reported turnover number (TON) of 3874 for this reduction stage, following extensive

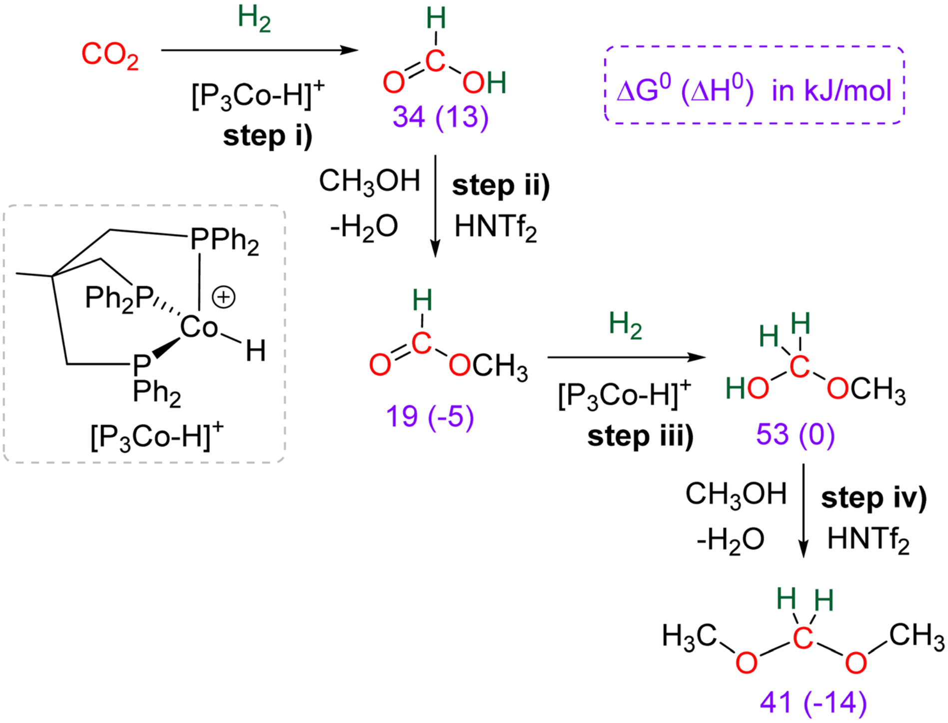

Scheme 47 Mechanism of formation of DMM based on calculations.

optimization studies; (ii) the synthesis of acetals, which are of interest as fuel additives, in contrast to bis(silyl)acetal (BSA) and bis(boryl)acetal (BBA) compounds that lack known applications. Consequently, a variety of DAM derivatives have been synthesized, utilizing various alcohols, particularly those derived from biomass.

As perspectives, future endeavours could focus on broadening the applicability of DAM, encouraging additional investigations into acetal syntheses *via* CO_2 hydrogenation, and exploring diverse catalytic processes beyond [P_3Ru] and [P_3Co] systems.[163] It would be intriguing to explore the potential use of the generated acetal as both C_1 and C_n sources, similar to what has been described with BSA and BBA. However, the hydrogenation of CO_2 into formaldehyde is still in its early stages, with only three selective systems described so far, operating in gas or liquid phases, involving catalysts **C65**, **C67**, and **C68**. Moreover, no isolation or utilization of the generated formaldehyde has been reported to date. Given its perfect atom efficiency and the reactive nature of formaldehyde, the primary challenge lies in developing an efficient system for hydrogenating CO_2 into formaldehyde, enabling its isolation and/or utilization.

Finally, although the processes of $4e^-$ reduction of CO_2 into formaldehyde and into acetal are at very different stages of maturity, it is noteworthy that the stabilization of the $4e^-$ reduction stage in the form of acetal parallels the stabilization of monomeric formaldehyde (HCHO) in the form of acetals of various lengths in formalin solution – the common commercial source of formaldehyde for chemical or biochemical transformations.[24–26,128a–130,132,164] It is indeed noticeable that the two examples described in liquid medium for the hydrogenation of CO_2 with **C64** and **C67** were conducted in H_2O, CH_3OH or glycerol. Presumably, these solvents stabilize the reactive *in situ* generated monomeric formaldehyde in the form of methanediol or acetal derivatives while avoiding its polymerization as paraformaldehyde.

6. Electroreduction

Electrochemical CO_2 reduction reaction (eCO_2RR) offers a green and sustainable approach for converting this gas into various products, under mild conditions (room temperature and pressure) and both in organic or aqueous media. Regarding C_1 products, while the formation of $2e^-$ reduction products has been performed with several catalysts with high selectivity and rate,[10a] the formation of 4, 6 and $8e^-$ reduction products has been much more rarely observed (Scheme 48).[165] If methanol and methane have been produced in a few cases, formaldehyde remains an elusive product to date.

6.1. Electrocatalytic systems

One of the early examples of CO_2 electrochemical reduction to formaldehyde concerned the use of a Ru based complex with a terpyridine–bipyridine ligand (Fig. 6) which was shown to produce a small amount of HCHO, through the formation of a formyl complex, in a mixture of water and ethanol, at low temperature (−20 °C) upon electrolysis at an Hg pool working electrode ($E = -1.70$ V *vs.* Ag/AgCl).[166] A faradaic efficiency (FE) of *ca.* 5% was obtained for HCHO, while methanol and remarkably C–C coupling products were also identified (H(O)CCOOH, $HOCH_2COOH$). Unexpectedly, a metal-free organic

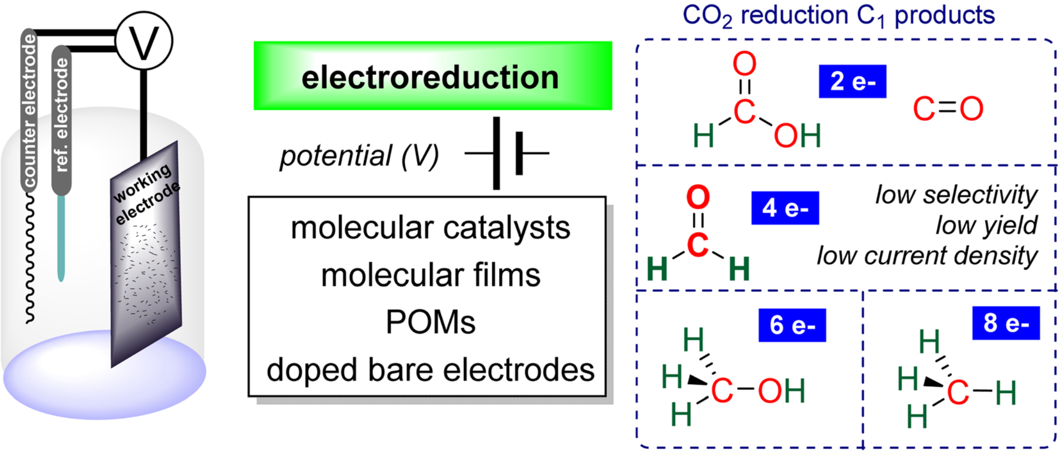

Scheme 48 Electrochemical reduction of CO_2 into C_1 products.

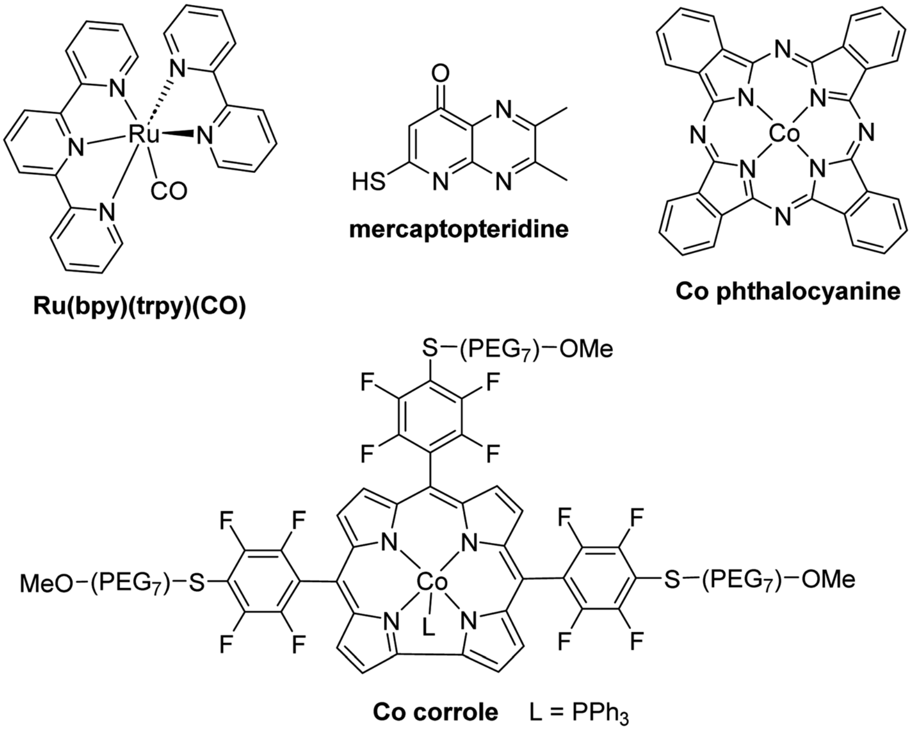

Fig. 6 Examples of molecular catalysts capable of generating formaldehyde from CO_2 electroreduction.

catalyst, 6,7-dimethyl-4-hydroxy-2-mercaptopteridine (a natural cofactor, Fig. 6) was reported to electrocatalyze CO_2 reduction to various products, including not only formate, but also methanol and formaldehyde (not quantified).[167] The reaction was conducted in a phosphate buffered solution at a reticulated vitreous carbon electrode ($E = -0.65$ V *vs.* Ag/AgCl), and it was suggested that CO_2 was first reduced to formate, which was subsequently reduced to formaldehyde and methanol (the latter product was obtained with FE 10–23%) *via* a carbamate compound. Recently, a transition metal based polyoxometalate $(TOA)_6[a\text{-}SiW_{11}O_{39}\text{-}Co(\_)]$ (TOA: tetraoctyl ammonium, _ = vacant position at the Co atom) was shown to electroreduce CO_2 under homogeneous conditions in dichloromethane as the solvent, and a potential of −1.5 V *vs.* Hg_2Cl_2/Hg at a Hg electrode.[168] In the presence of an acid as a co-reactant (water and H_2SO_4), the products were identified as CO, with about 13% FE, and formaldehyde with a maximum efficiency (FE) of *ca.* 25%. The use of an organic and reducible solvent (which is shown to generate HCHO under an Ar atmosphere), limits the development of the process but this example is an interesting case of molecular electrochemical approach for CO_2-to-HCHO conversion. Another molecular cobalt complex, a Co corrole (triphenylphosphine 5,10,15-tris(2,3,5,6-tetrafluoro-4-(MeO-PEG(7)thiophenyl)), Fig. 6) modified at the para positions with thiol bound poly(ethylene glycol) chains terminated by methoxy groups was adsorbed at the carbon paper electrode and then investigated for the eCO_2RR into methanol and ethanol.[169] In 0.1 M phosphate buffer solutions with 0.1 M $NaClO_4$ at potentials ranging from −0.51 V to −0.8 V *vs.* NHE, low formaldehyde efficiencies from 10 to 1%, respectively, were obtained among other liquid phase products (formate, acetate, glyoxal), corresponding to low current densities (from 0.2 to 0.02 mA cm^{-2} respectively).

Another strategy was developed upon polymerizing electrode films of metal complexes at the surface of conductive carbon. Cr, Co and Fe bis-terpyridine complexes bearing the vinyl group were used to grow electroactive films upon oxidation, which were further employed as catalysts in aqueous solutions with 0.1 M $NaClO_4$.[170] At potentials close to −1.1 V *vs.* Ag/AgCl, faradaic yields of 28% (Fe), 39% (Co) and 87% (Cr) were reported for formaldehyde, thus showing very high activity for first row transition metals while second and third row transition metals (Ru and Os respectively) gave barely any reactivity, which was assigned to the presence of metal-based redox processes in the former cases compared to ligand-based redox processes in the latter. The CO_2 to CO conversion being now a well-controlled reaction, and CO being a possible intermediate towards formaldehyde production, a parallel approach was developed using CO directly as the reactant and supramolecular catalysts: thin films of Co phthalocyanine and 4,4′,4″,4‴-tetracarboxyphthalocyanine made at the carbon fibre were investigated and shown to produce mainly formaldehyde as the CO reduction product with very little methanol, at a potential of −0.7 V *vs.* SCE (Saturated Calomel Electrode) in sulfuric acid solutions.[171] Recently, it was further shown that CO reduction with a phthalocyanine monomer complex also led to formaldehyde with unambiguous confirmation from labelled studies.[172] These results opened the door to understanding the mechanism of formaldehyde pathway from both CO_2 and CO as reactants, with possibilities of tuning the quantity of formaldehyde being produced and the ratio between HCHO and methanol. It also opens the possibility of setting a cascade approach in which the CO produced from CO_2 reduction could further be used to generate HCHO. A very recent study explored such electroreduction of CO to HCHO with Co phthalocyanine deposited at a carbon paper electrode. Upon optimization of the pH (12) and of the electrode potential, a partial current density of 0.64 mA cm^{-2} (17.5% faradaic efficiency) was achieved for HCHO, with a maximum ratio between HCHO and CH_3OH of *ca.* 7.5. Mechanistic insights illustrate that the binding of CO to the metal cobalt site is strong enough for further reducing it, while controlling the amount of protons and the electrode potential is key to favouring formaldehyde formation and release at the expense of methanol production.[173] A puzzling discovery was made upon direct electroreduction of CO_2 in various solutions (methanol, water and even sea water) at boron doped diamond (BDD) electrodes without any additional catalyst.[174] These materials have several advantages, including a large potential window, high stability and furthermore the presence of sp^3-bonded carbon atoms on BDD which are believed to be active sites for triggering chemical transformations. Upon 1 h electrolysis at $E = -1.7$ V *vs.* Ag/AgCl, a maximum yield (FE) of 74% was obtained for formaldehyde, along with formic acid and a very small amount of dihydrogen as a by-product. The formaldehyde was deemed to be formed from the $2e^-$ reduction of formic acid initially obtained from CO_2 conversion, while current densities were low, typically in the range of 0.1 to 0.2 mA cm^{-2}. Finally, an elegant indirect approach has been proposed with methanol as the solvent. While methanol itself was oxidized to formaldehyde in the anodic compartment, electroreduction of CO_2 at the Sn electrode led to formic acid, which reacted with the solvent to give methyl formate. Finally, the latter was reduced to formaldehyde, with faradaic efficiencies for HCHO from 10 to 50% depending on the electrolyte conditions.[175]

6.2. Conclusion and perspectives

In conclusion, the electrochemical reduction of CO_2 to formaldehyde poses a formidable challenge, with only a limited number of examples identified thus far. These cases exhibit low yields, low current density, and, in many instances, uncertainties regarding the origin of the produced formaldehyde. The challenge of obtaining formaldehyde also arises from its susceptibility to further transformation at the electrode into more reduced products, such as methanol. Additionally, the precise catalytic mechanisms involved in these processes remain elusive with only very few mechanistic studies.[173]

As perspectives, the prospect of *in situ* generating a substantial quantity of formaldehyde under mild conditions across a range of precisely controlled potentials is enticing. This potential development could pave the way for utilizing formaldehyde in subsequent chemical reactions, particularly in coupling reactions. As an early illustrative example, co-reduction scenarios involving CO_2 (or CO) with nitrogen-containing species like nitrite (NO_2^-)[176] or nitrate (NO_3^-)[176b,177] could facilitate C–N bond formation, yielding a diverse array of products, including amines and urea. The exploration of these processes, along with related ones, under the controlled conditions afforded by electrochemistry is poised to yield new and stimulating results.

7. Photo(electro)reduction

The photochemical (PC) and photoelectrochemical (PEC) reduction of CO_2 (Scheme 49), mostly using semiconducting materials, have been extensively studied in the last four decades.[178] However, if compared to other reduction products such as CO or formate, only a limited number of studies so far reported the formation of formaldehyde as a major product and even less studies report a selective HCHO production, mainly because of its high reactivity.[179] Moreover, very few of these studies conducted proper isotope labelled measurements to confirm the origin of the carbon atom, which constitutes a severe drawback.[180]

A very early report questioned the possible formation of formaldehyde from water and CO_2 as the first stage of the photosynthetic process forming carbohydrates.[181] This study showed that an aqueous solution, free of catalyst, containing carbon dioxide gives formaldehyde when irradiated with

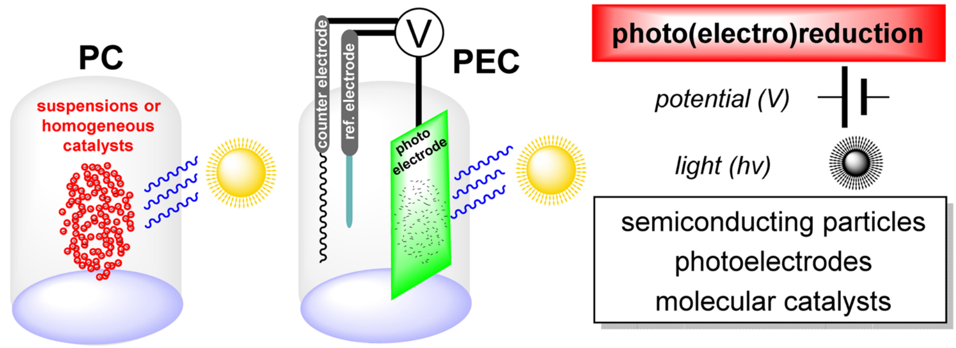

Scheme 49 Photochemical and photoelectrochemical reduction of CO_2.

UV-light ($\lambda = 200$ nm) in a first stage, and that subsequent irradiation with lower energy light ($\lambda = 290$ nm) induced the polymerization of HCHO to sugars. It also showed that the formation of HCHO can be photocatalyzed under visible light through the use of "coloured basic substances" such as malachite-green or methyl-orange. Remarkably, the role of HCHO in the course of the photochemically induced formation of highly reduced compounds from CO_2 was thus already questioned a century ago. Later, a pioneer work reported that using suspensions of various semiconductors (TiO_2, ZnO, CdS, GaP and SiC, Table 7, entries 1–5) in CO_2-saturated purified water, the generation of formic acid, formaldehyde and methanol was observed up to the millimolar concentration range after 7 h of visible light illumination (500 W Xe or Hg lamp).[182] Trace of methane was also detected. The reduction products were quantified by gas chromatography although no labelled experiment was conducted to assert the origin of the products. The yield in methanol was observed to increase as the conduction band (CB) of the material was more negative compared to the reduction potential of the CO_2-to-CH_3OH reaction. A quantum yield of *ca.* 5×10^{-4} was reported for the formaldehyde production with both TiO_2 and SiC photocatalysts. Using semiconductor electrodes polarized at −1.5 V *vs.* SCE, CO_2 reduction to formic acid, formaldehyde and methanol was also observed with non-illuminated TiO_2 and illuminated GaP. Since this seminal paper, the majority of studies published so far have explored various semiconductors,[198] based on metal and metal oxides, doped or not, eventually in combination with co-catalysts,[3c,199] in the form of suspensions, bulk materials or thin films. Some other examples, albeit quite rare, employed either a fully molecular, a heterogeneous material or even a photo-enzymatic approach.

7.1. Suspension of a semiconductor

Aqueous suspensions of semiconducting $SiTiO_3$, WO_3 and TiO_2 under both Hg lamp or natural sunlight were reported to generate a mixture of methanol (a few μmol per hour) and formaldehyde (a few tens of μmol per hour) from dissolved carbon dioxide, as quantified by gas chromatography (CH_3OH) and colorimetric (HCHO) measurements (Table 7, entries 6–8).[183] Traces of methane were also detected. In a follow-up study,[184] aqueous suspensions of strontium titanate ($SrTiO_3$) treated with various transition metal–TiO_2 deposits, namely Rh, Pt, In and Au, and saturated with CO_2 were irradiated with a 75 W Hg-lamp or a solar concentrator. When using Ir oxide as an additive (4.55 mol%), formic acid was the main product with a rate of *ca.* 1 μmol h^{-1}. With Ru oxide (4.55 mol%) as the additive, methanol was the main product. The highest rate for formaldehyde formation was obtained with $SrTiO_3$ with 0.5 mole % of lanthanum chromite ($LaCrO_3$) as an additive (Table 7, entry 9). However, the change in selectivity with the nature of the additive was not discussed. Aqueous suspensions of n-type semiconductors such as bismuth (Bi_2S_3) and cadmium (CdS) sulphides were reported to generate formic acid and formaldehyde at *ca.* 10^{-5} M concentration after 1 h under wide spectrum irradiation (55 mW cm^{-2}) when H_2S was present in the system (Table 7, entries 10 and 11).[185] This was explained by a sequential process producing first formic acid by $2e^-/2H^+$ transfers then formaldehyde by additional electron transfers. The catalysis, which was shown to be proportional to the light intensity, stopped due to the poisoning deposition of elemental sulphur at the surface of the particles. The formation of HCHO as the only CO_2 reduction product was also observed at a rate up to 0.25 μmol h^{-1} with a CO_2 saturated aqueous suspension of TiO_2 at 333 K under 500 W high pressure Xe lamp irradiation (Table 7, entry 12), but the origin of such selectivity is unknown.[186] TiO_2 doping with 0.1 mol% WO_3 further increased this rate up to 0.42 μmol h^{-1} (Table 7, entries 13 and 14). The deposition of Rh on TiO_2 led to the formation of HCOOH (major), CH_3OH (secondary) and HCHO (minor) up to a total rate of 0.67 μmol h^{-1} (Table 7, entry 15). The doping of TiO_2 with Au was more thoroughly studied. At 7 bars and 80 °C, a reactor containing 0.6 g of 0.1–0.5 wt% loading of Au/TiO_2 composites led to the highest yield of formaldehyde (270 mmol kg_{cat}^{-1} h^{-1}, Table 7, entry 16).[187] Another study reported the use of a gold nanoparticle decorated TiO_2 photonic crystal as the photocatalyst (Au-PMTiNTs).[188] When irradiated with an AM1.5 G source, methane was the main reduction product (302 μmol g_{cat}^{-1} h^{-1}, 89.3% selectivity), whereas, under the irradiation of a UV-poor white lamp, formaldehyde (420 μmol g_{cat}^{-1} h^{-1}) and CO (323 μmol g_{cat}^{-1} h^{-1}) were the major products (Table 7, entry 17). This so-called optical control of selectivity was explained by the plasmonic effects of the gold surface involving hot electrons but no discussion was made on the hydrogen atom source.

Table 7 Catalytic performance of photochemical and photoelectrochemical systems for CO_2 reduction to formaldehyde[a]

Suspensions

Entry	Catalyst	Loading	Conditions	Light source	Products	Yield (μmol h^{-1} g_{cat}^{-1})	Ref.
1	TiO_2	1 g/100 mL	Water	500 W Xe or h.-p. Hg arc lamp	HCOOH CH_3OH HCHO	n.d 3.3 15.7	182
2	ZnO	1 g/100 mL	Water	500 W Xe or h.-p. Hg arc lamp	HCOOH CH_3OH HCHO	n.d 5 17.1	182
3	CdS	1 g/100 mL	Water	500 W Xe or h.-p. Hg arc lamp	HCOOH CH_3OH HCHO	n.d 16.7 28.6	182
4	GaP	1 g/100 mL	Water	500 W Xe or h.-p. Hg arc lamp	HCOOH CH_3OH HCHO	n.d 15.7 13.3	182
5	SiC	1 g/100 mL	Water	500 W Xe or h.-p. Hg arc lamp	HCOOH CH_3OH HCHO	n.d 15.7 13.3	182
6	$SrTiO_3$	4–10 g L^{-1}	Water 67 °C	70 W h.-p. Hg lamp (>300 nm)	CH_3OH HCHO	1.79 0.01	183
7	WO_3	4–10 g L^{-1}	Water 67 °C	70 W h.-p. Hg lamp (>300 nm)	CH_3OH HCHO	1.26 0.05	183
8	TiO_2	4–10 g L^{-1}	Water 34 °C	70 W h.-p. Hg lamp (>300 nm)	CH_3OH HCHO	0.51 0.08	183
9	$SrTiO_3$ + 0.5 mole % $LaCrO_3$	1 g/160 mL	Water 60 °C	70 W h.-p. Hg lamp	HCOOH CH_3OH HCHO	0.98 0.065 0.042	184
10	CdS	0.33 g L^{-1}	Water H_2S 0.097 M	100 W quartz-iodine lamp (>350 nm)	HCOOH HCHO	1.22 1.95	185
11	Bi_2S_3	0.5 g L^{-1}	Water H_2S 0.097 M	100 W quartz-iodine lamp (>350 nm)	HCOOH HCHO	1.0 1.58	185
12	TiO_2 (MCB)	0.3 g	Water 60 °C	500 W h.-p. Xe lamp	HCOOH HCHO	0.94 1.98	186
13	TiO_2 + 0.1 mole % WO_3	0.3 g	Water 60 °C	500 W h.-p. Xe lamp	HCHO	1.18	186
14	TiO_2 + 2 mole % WO_3	0.3 g	Water 60 °C	500 W h.-p. Xe lamp	HCHO	1.4	186
15	1 mole % Rh/TiO_2	0.3 g	Water 60 °C	500 W h.-p. Xe lamp	HCOOH CH_3OH HCHO	0.69 0.53 0.37	186
16	0.1 wt% Au/TiO_2	0.6 g/1.2 L	Water, Na_2SO_3 0.85 g L^{-1} 80 °C 7 bar CO_2	med.-p. Hg lamp (254–364 nm)	HCOOH CH_3OH HCHO	148 721 270	187

Table 7 (*Contd.*)

Suspensions							
Entry	Catalyst	Loading	Conditions	Light source	Products	Yield (μmol h^{-1} $g_{cat}{}^{-1}$)	Ref.
17	Au/TiO_2 NT photonic crystals	85 μg Au per TiO_2 wafer	Water vapor	50 W white-cold LED (>400 nm)	CO HCHO	323 420	188
18	TiO_2	0.5 g L^{-1}	Water 80 °C 7 bar CO_2	125 W med.-p. Hg lamp (254–364 nm)	H_2 HCOOH HCHO	102 2954 16 537	189
19	TiO_2/ZrO_2 (ZrO_2 40 weight%)	0.2 g spread on a Cu plate	"Wet" (70% humidity)	Real sunlight	CH_3OH HCHO	732 1392	190
20	$NaTaO_3$–C (annealed at 650 °C)	100 mg/200 mL	Water	Pen ray lamp (254 nm)	HCHO	19.5	191
21	Pd/TiO_2–Fe_2O_3	0.05 g/50 mL	Water pH 8.5 Na_2CO_3	500 W Xe lamp	HCHO C_2H_5OH CH_3CO_2H	33.5 101.7 51	192
22	CoPc/TiO_2 (1% mass ratio, calcined at 400 °C)	10 g/100 mL	0.1 N NaOH aq. sln	500 W tungsten–halogen lamp	HCOOH CO CH_3OH CH_4 HCHO	15.7 1 0.5 0.8 2.5	193
23	RuL1OH/TiO_2 (0.125 μM Ru complex per g_{cat})	10 mg/10 mL	0.8 mM TEOA aq. sln	250 W lamp (>420 nm)	CO CH_4 HCHO	2.1 1 11.3	194
24	Sn_{75}–Cu_{25}/C_3N_4	1.5 mg/3.5 mL	0.1 M $KHCO_3$ 10v vol% TEA aq. sln	300 W Xe lamp (>420 nm)	HCOOH HCHO	6.9 10.8	195
25[b]	$K_2Ti_6O_{13}$ + 0.3 wt% Pt	0.3 g/4 mL	Water r.t	150 W Hg-lamp	H_2 HCOOH CH_4 HCHO	68 0.23 0.2 0.476	196
26[b]	Cu/ZnO/$K_2Ti_6O_{13}$ + 0.3 wt% Pt	0.3 g/4 mL	Water r.t	150 W Hg-lamp	H_2 HCOOH CH_4 HCHO	17 3.04 0.27 0.57	196
27[b]	$K_2Ti_6O_{13}$ + 0.3 wt% Pt	0.3 g/4 mL	Water 274 °C	Concentrated sunlight	H_2 HCOOH CH_4 HCHO	32.8 20.7 0.23 5.59	196
28	TiO_2	30 mg/20 mL	Aq. sln pH 6.5, NADH 5 mM, $[Cp^*Rh(bpy)(H_2O)]^{2+}$ 0.25 mM	23 W UV lamps (max 365 nm)	HCHO (PB buff.) HCHO (NaOH-EDTA buff.)	27.6 548	197

Table 7 (*Contd.*)

Suspensions

Entry	Catalyst	Loading	Conditions	Light source	Products	Yield (μmol h^{-1} $g_{cat}{}^{-1}$)	Ref.
29	TiO_2 coupled to FDH : FADH (ratio 1 : 03) loaded membrane	30 mg/20 mL	Aq. sln pH 5.5, NADH 5 mM, $[Cp^*Rh(bpy)(H_2O)]^{2+}$ 0.25 mM	23 W UV lamps (max 365 nm)	HCHO (PB buff.) HCHO (NaOH-EDTA buff.)	13.5 345	197

Photoelectrodes

Entry	Catalyst	Bias (V)	Conditions	Light source	Products	Yield (μmol h^{-1} cm^{-2})	Ref.
30	Polyaniline coated p-Si	−1.9 V *vs.* SCE	0.1 M $LiClO_4$ aq. sln	Xe lamp (150 mW cm^{-2})	HCOOH HCHO	60.5 15	200
31	*p*-GaAs	−0.5 V *vs.* SCE	4 M HCl aq. sln with 0.32 M V(II)/V(III) couple, 50 °C	150 W tungsten or Xe lamp	HCOOH CH_3OH HCHO	n.d	201
32	Bifunctional TiO_2 with Ru N719 dye	No bias	2 M NaOH aq. sln pH 10	300 W Xe lamp (cutoff > 420 nm)	HCOOH CH_3OH HCHO	16.7 35.6 25.8	202
33[b]	Cu_2O film on Cu	No bias	0.1 M $Na_2CO_3/NaHCO_3$ aq. sln pH 9.0	125 W h.-p. Hg lamp	CH_3OH HCHO	9.5 125	203
34	040-$BiVO_4$|Cu	+0.9 V *vs.* RHE	0.5 M NaCl aq. sln	300 W Xe lamp with an AM 1.5G filter	HCHO CH_3OH C_2H_5OH	108[c] n.d n.d	204
35	Cu/rGO/PVP/Nafion	+0.68 V *vs.* RHE	0.1 M NaOH aq. sln	300 W Xe lamp with a KG3 filter	HCHO	1.18	205

[a] n.d: not determined. [b] Catalyst deposited on a wet paper filter at the bottom of the reaction vessel. [c] In μmol L^{-1} h^{-1} cm^{-2} (reactor volume not specified).

Another example of TiO_2 based photocatalysis was reported in which sodium sulfite was used as the reducing agent in order to fill in photogenerated holes. Under 7 bars of CO_2, at 80 °C and at a TiO_2 loading of 0.5 g^{-1} in basic (pH 14) aqueous solutions, the formation of H_2 (102 μmol h^{-1} $g_{cat}{}^{-1}$), formaldehyde (16 537 μmol h^{-1} $g_{cat}{}^{-1}$) and formic acid (2954 μmol h^{-1} $g_{cat}{}^{-1}$) were measured depending on experimental conditions (time and pH) under UV irradiation from a medium pressure Hg vapor 125 W lamp introduced into the photoreactor (Table 7, entry 18).[189] The higher formation rate for formaldehyde was observed at the beginning of the reaction (few hours), which was explained by a branched mechanism, with on one hand a CO_2-to-formic acid reduction later generating gaseous products (only detected after several hours of irradiation once the hole scavenger is consumed), and on the other hand the direct reduction of carbonates into HCHO. Composites made of nanometre-sized TiO_2 particles and micrometre-sized zirconium oxide (ZrO_2) particles have been reported to generate high yields of formaldehyde and methanol (maximum 300 μmol $g_{cat}{}^{-1}$ total after only 300 s) under real solar light illumination (Table 7, entry 19).[190] For that, the composite was scattered on a copper plate and allowed to humidify in a fridge to form a thin layer of water on the composite surface. The assembly was then placed in a gas-barrier plastic bag (allowing CO_2 diffusion only) containing ambient air and then was illuminated with solar light. It was proposed that reduction products originated from the reduction of bicarbonate ions resulting from the dissolution of CO_2 contained (from ambient air) in the thin layer of water. A highly crystalline carbon-doped $NaTaO_3$ perovskite was also reported to reduce CO_2 to formaldehyde in neutral aqueous solutions at room temperature and under 254 nm irradiation (4.4 mW cm^{-2}), at the optimal rate of 39 μmol $g_{cat}{}^{-1}$ after 2 h (Table 7, entry 20).[191] This rate, determined through complexometric measurements, was shown to be dependent on the annealing temperature used to prepare the material as well as the carbon content since the undoped material showed very low formaldehyde yield. Three hematite-based materials, namely Fe_2O_3, TiO_2–Fe_2O_3 and Pd/TiO_2–Fe_2O_3 were suspended as nanoparticles in an aqueous sodium carbonate solution (pH 8.5) and illuminated with a 500 W xenon lamp. After 2 hours, the highest rate for formaldehyde was obtained with Pd/TiO_2–Fe_2O_3 (1338 μmol L^{-1} $g_{cat}{}^{-1}$, Table 7, entry 21), when compared with the simple Fe_2O_3 (878 μmol L^{-1} $g_{cat}{}^{-1}$) and TiO_2–Fe_2O_3 (399 μmol L^{-1} $g_{cat}{}^{-1}$) and was explained by the hydrogenation of formic acid with hydrogen atoms on the photocatalyst surface.[192] An example of a system combining a semiconducting material and a molecule consisted of cobalt phthalocyanine loaded TiO_2 nanoparticles (CoPc/TiO_2) of *ca.* 11 nm diameter prepared by a sol–gel method and dispersed in alkaline (NaOH) aqueous solutions under a CO_2 atmosphere.[193] When irradiated with a tungsten–halogen 500 W lamp, a mixture of products containing CO, HCOOH, CH_3OH, CH_4 and HCHO was produced at a maximum yield of 407 μmol $g_{cat}{}^{-1}$ after 20 h under optimized conditions (CoPc/TiO_2 mass ratio, calcination temperature), the latter accounting for *ca.* 50 μmol $g_{cat}{}^{-1}$ (Table 7, entry 22). The CO_2 reduction to formaldehyde utilizing a heteroleptic ruthenium metal complex covalently linked to TiO_2 nanoparticles was also reported to occur in aqueous medium at pH 7 under visible light (λ > 420 nm) illumination.[194] When the hybrid catalyst was dispersed in neutral water, in the presence of TEOA (triethanolamine) as a sacrificial donor agent, the formation of formaldehyde as the major product (maximum TON of 720 after 5 h, corresponding to a formation rate of 18 μmol h^{-1} $g_{cat}{}^{-1}$, Table 7, entry 23) was observed in the liquid phase as determined by HPLC, with CO and CH_4 as minor (TON 136 and 64, respectively), gaseous, products. Moreover, recyclability tests showed that the loss of activity was limited to 10–15% after the sixth cycle, due to some material loss during washing steps. In addition, this system used the *in situ* generated formaldehyde in a condensation reaction with amine, generating new H_2C–N bonds (Scheme 50). To the best of our knowledge, this represents the only example of reductive functionalization of CO_2 *via* formaldehyde in (photo)electroreduction systems.

Very recently,[195] a single-atom catalyst with dual-atom sites (DAS) composed of neighbouring Sn(II) and Cu(I) centres embedded in a C_3N_4 framework was reported to generate HCHO from CO_2 with a selectivity of 61% and a productivity of 259.1 μmol g^{-1} (Table 7, entry 24) after 24 h irradiation. The catalyst was dispersed in a CO_2-saturated 0.1 M aqueous $KHCO_3$ containing 10 vol% triethylamine (TEA) as the sacrificial electron donor and was irradiated using a 300 W Xe lamp equipped with a 420 nm cut-off filter. The best productivity was obtained with the Sn_{75}–Cu_{25}/C_3N_4 composition, and the production of HCHO from CO_2, asserted by ^{13}C labelled experiments and FTIR and NMR characterization, was attributed to the $2e^-$ reduction of HCHO through the synergetic action of the two metals.

An original strategy was also tested with a Pt-loaded potassium hexatitanate (Pt–$K_2Ti_6O_{13}$) photocatalyst (0.3 mg) deposited on a filter at the bottom of a flask containing 4 mL of water under a CO_2 atmosphere.[196] Upon illumination with a 150 W Hg-lamp, formaldehyde was detected as a secondary reduction product (H_2 as the main one) by GC at a rate of 0.48 μmol h^{-1}

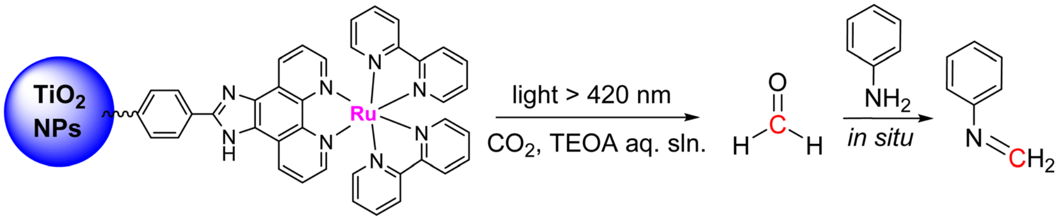

Scheme 50 Visible light reduction of CO_2 into formaldehyde followed by *in situ* condensation with an amine.[194]

g_{cat}^{-1}, together with CH_4 and HCOOH (Table 7, entry 25). When combined with a Cu/ZnO catalyst, the resulting composite produced HCHO as the secondary product (H_2 – major) at a rate of 0.57 μmol h^{-1} g_{cat}^{-1} along with CH_4 and HCOOH (Table 7, entries 26 and 27).

Finally, semiconductors can also be associated with an enzymatic process. For example, a very recent study reported the immobilization of two kinds of dehydrogenases, namely formate dehydrogenase (FDH) and formaldehyde dehydrogenase (FADH) (see Section 8 for more details on these enzymes), on the surface of polyethylene hollow fibre membranes, coupled with UV induced, TiO_2-based photocatalytic coenzyme regeneration.[197] In this system, the excitation of TiO_2 causes charge separation and electrons are transferred to the NAD^+ formed during the enzymatic cascade CO_2 reduction, for coenzyme NADH regeneration, using EDTA as the electron donor and pentamethylcyclopentadienyl rhodium bipyridine ($[Cp^*Rh(bpy)(H_2O)]^{2+}$) as the redox mediator. In the absence of an enzyme, HCHO was formed at a maximum rate of 0.207 mM (with H_2O as the electron donor) and 4.11 mM (with EDTA as the electron donor), at pH 6.5 and after 5 h UV irradiation (365 nm max). With the photo-enzyme assembly, the best results were obtained at pH 5.5 with EDTA as the electron donor, reaching 2.59 mM of formaldehyde after 5 h of reaction (Table 7, entries 28 and 29). The production of HCHO proceeded for 48 h with limited loss of activity.

7.2. Photoelectrodes

A p-type Si photoelectrode was coated with a polyaniline film of *ca.* 50 nm thickness upon electro polymerization. Under illumination with a Xe lamp (150 mW cm^{-2}) at a bias potential of −1.9 V *vs.* SCE, the photocathode immersed in a CO_2-saturated 0.1 M $LiClO_4$ aqueous solution generated several micromoles of formic acid and formaldehyde as determined by a colorimetric method (Table 7, entry 30).[200] The bare photoelectrode did not show any activity towards CO_2 reduction. The total faradaic yield reached 20 to 28% even though no methane or methanol could be detected by gas chromatography. In the presence of the V(II)–V(III) chloride redox couple presumably acting as an electron relay, a p-type GaAs photoelectrode was reported to generate formic acid, formaldehyde and methanol in low yields (from 1 to 3% faradaic yields) in an acidic (4 M HCl) aqueous solution under visible light illumination (tungsten–halogen lamp, 980 mW cm^{-2}) at a bias potential of −0.5 V *vs.* SCE and at 50 °C (Table 7, entry 31).[201]

The sequential formation of formic acid (detected by HPLC), formaldehyde (UV-Vis) and methanol (GC) was reported with a bifunctionalized TiO_2 film under visible-light irradiation (300 W Xe lamp with a cut-off filter) in acetonitrile solution containing DMPImI electrolyte and the iodide/triiodide couple as a redox mediator.[202] The film was separated into two zones, a sensitized area containing a ruthenium complex (N719) as the dye and a catalytic area composed of a pure TiO_2 zone. Under illumination, electrons generated in the sensitized zone migrate to the catalytic one through TiO_2 particles. This film was used as the reduction half-cell in a H-type reactor with Pt as the anode material, in order to prevent re-oxidation of CO_2 reduction products. Formic acid was generated first, then formaldehyde and methanol, with a respective yield of *ca.* 0.05 mmol cm^{-2} after 5 h (Table 7, entry 32). This yield was enhanced when an external voltage was applied between the reference electrode and the anode thus enabling the regeneration of the redox mediator and consequently of the dye. The effect of the bias potential and the pH on the product distribution was studied with a PEC assembly composed of the Cu/Cu_2O electrode irradiated with a 125 W high pressure mercury lamp.[203] In 0.1 M Na_2CO_3/$NaHCO_3$ electrolyte (pH 9.0) saturated with CO_2, a high rate for HCHO was observed at 0 V bias (Table 7, entry 33), whereas methanol was the main product at +0.2 V bias. At the positive potential bias, some HCHO was also observed at pH 8 to 11 as a minor product.

A PEC assembly consisting of a (040)-facet engineered $BiVO_4$ plate as the photoanode (040-BVO) and a Cu plate immersed in NaCl electrolyte as the cathode has been reported to generate various C_1 products from CO_2 when illuminated with solar light under an external bias potential.[204] Depending on the applied potential, the selectivity could be tuned towards a specific product, with a general trend showing that at low potentials, kinetically favourable products are dominant, whereas at high potentials, thermodynamically stable products are dominant. Formaldehyde is produced with 85% faradaic efficiency at an applied potential of 0.90 V *vs.* RHE, corresponding to a yield of 143 μM h^{-1} (Table 7, entry 34). Very recently, it has been shown that a system combining calcium and iron co-doped TiO_2 films as the photoanode and multilayered Cu based dark electrode as the cathode was able to selectively generate formaldehyde and/or acetaldehyde at the cathode surface by tuning the anode bias potential.[205] Both electrodes were immersed in a 0.1 NaOH aqueous electrolyte saturated with CO_2, and formaldehyde was detected as the only product with a reduced graphene oxide (rGO) coated copper electrode (Table 7, entry 35). The highest yield was 470 μM cm^{-2} after 8 h (25% faradaic efficiency) under solar simulated irradiation with an applied bias of 0.68 V *vs.* RHE. It is important to note that in the last example ^{13}C labelled experiments were conducted to confirm the origin of the products.

7.3. Solid material approaches

Some studies were also conducted with catalytic solid materials. Two Mo-based heterogeneous catalysts, namely a mixed-valence polyoxomolybdate cluster and composite consisting of a molybdenum keplerate cluster embedded in reduced graphene oxide (RGO), were shown to reduce CO_2 and oxidize water at the same time, generating sub-mmol amounts of formic acid as the main product and formaldehyde as the secondary product, as quantified by HPLC.[206] Experiments were conducted in pure water with no sensitizer and light irradiation was set at 373 nm (19 mW cm^{-2}). The turnover number and frequency for formic acid (not calculated for formaldehyde) were claimed to reach *ca.* 10^6 and *ca.* 6×10^2 s^{-1}, respectively. This study shows the possibility of using cheap metal oxides such as oxometallates as catalytic materials for both CO_2 reduction and water oxidation.

7.4. Molecular approaches

To the best of our knowledge, only two studies employing a fully molecular approach have been reported. A homogeneous system employing pyridine as a catalyst in aqueous solution in the presence of $Ru(phen)_3$ photosensitizer, ascorbic acid as an electron donor and KCl as an electrostatic stabilizing agent reported the formation, under 470 nm monochromatic illumination, of formate (NMR quantified) as the main product with methanol (GC-MS) as the minor product and traces of formaldehyde detected by NMR.[207] Two ruthenium(II) polypyridyl complexes covalently modified with a pendant pyridyl function have also been shown to be active towards CO_2 reduction under both electrochemical and photochemical conditions in a DMF : water mixture. In the presence of TEA (triethylamine) as a sacrificial donor agent and under 470 nm irradiation, the formation of formate (main product), formaldehyde and methanol (minor) was observed after 1 h irradiation albeit with a very low TON of 16, 7 and 1, respectively.[208] The rapid loss of activity was attributed to ligand photolabilization leading to complex degradation. In neither of these examples has the mechanism been elucidated.

7.5. Conclusion and perspectives

In conclusion, achieving the selective conversion of CO_2 into formaldehyde (HCHO) using light as the primary, if not the sole, energy source is far from realized, as outlined in Table 7 with key examples. The predominant outcome in the majority of studies involves a product mixture, lacking control over selectivity, with low yields and demonstrating limited mechanistic understanding. The inherent high reactivity of HCHO poses a clear challenge to its detection. Therefore, improvements in analytical detection methodologies are imperative. The use of visible (solar) light still remains scarce, with most systems requiring UV light.

As perspectives, functionalized materials, in particular associating a photoactive material and molecular tuneable unit, open new possibilities to finely control the local environment of the catalytic site and thus to favour the formaldehyde pathway.

8. Enzyme-catalysed CO_2 reduction into formaldehyde

Biological fixation of CO_2 occurs through six major pathways including the Calvin–Benson–Bassham (CBB) cycle which represents the most common pathway.[209] Interestingly, the transformation of CO_2 into carbohydrates in the CBB cycle was initially hypothesized to occur *via* a formaldehyde pathway.[181,210] However, it was later demonstrated that the CBB cycle does not involve the intermediate formation of formaldehyde, but the CO_2 fixation to form a carboxylate which is then further reduced in subsequent steps.[211] It is only with isolated enzymes that HCHO and CH_3OH were obtained from CO_2. The dehydrogenases, formate dehydrogenases (FDHs, EC 1.2.1.2),[212] formaldehyde dehydrogenase (FaldDH, EC 1.2.1.46)[211] and alcohol dehydrogenase (ADH, EC 1.1.1.1)[213] are able to catalyse the reduction of CO_2, HCOOH and HCHO into HCOOH, HCHO and CH_3OH, respectively.[11b,214] Although most of the reports focused on the selective generation of formate, notably because of its implication as an intermediate in the Wood–Ljungdah pathway in acetogens[215] or methanol,[216] only a handful of studies focused on the selective generation of formaldehyde. The two-step enzyme cascade combining formate dehydrogenase (FDH) and formaldehyde dehydrogenase (FaldDH) is currently the only reported process (Scheme 51) for the enzymatic conversion of CO_2 into HCHO. Both enzymes are commercially available and

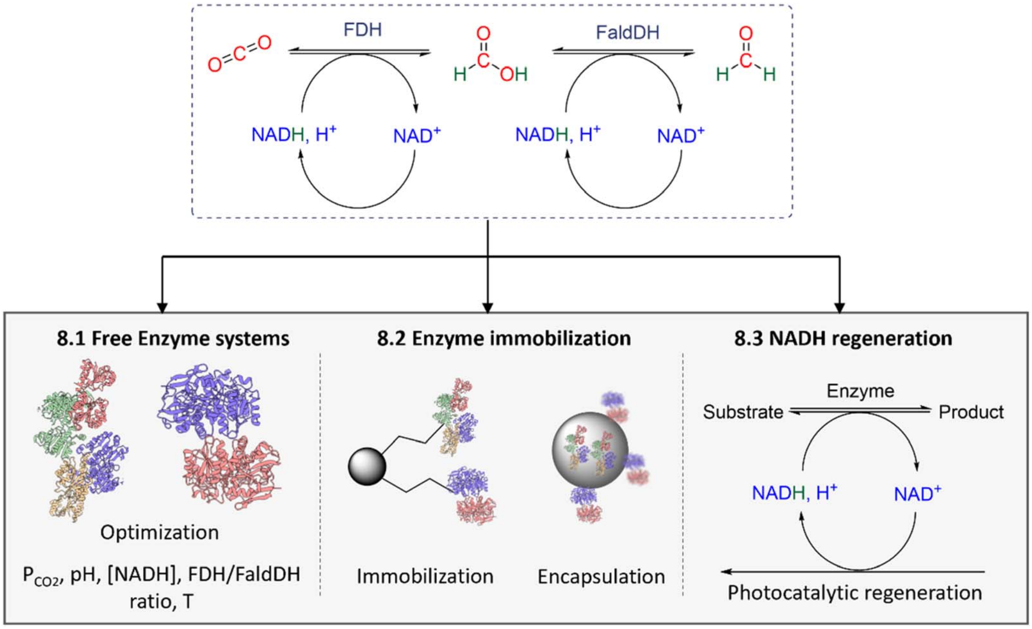

Scheme 51 Enzymatic sequential generation of formate and formaldehyde with FDH (formate dehydrogenase) and FaldDH (formaldehyde dehydrogenase).

Table 8 Conditions and performances of bio-cascade systems for CO_2 reduction into formaldehyde[a]

Entry	Immobilization	Substrate	P or [C]	NADH regeneration	Time (h)	HCHO generation (mmol L^{-1})	Ref.
1	Free enzymes	$KHCO_3$	100 mM	No	72	0.060	217
2	Free enzymes	$CO_{2(g)}$	0.5 MPa	No	12	0.901	218
3	HDMMC-based system	$CO_{2(g)}$	0.3 MPa	No	8	0.022	219
4	TiO_2-NPs	$CO_{2(g)}$	0.3 MPa	No	4	—	220
5	NPSCs	$CO_{2(g)}$	0.3 MPa	No	4	0.125	221
6	MCF-MP	$KHCO_3$	200 mM	No	—	0.037	222
7	3% TCPP@ZIF-8	$NaHCO_3$	10 μM	Yes	8	0.008	223
8	PE-HFMs	$CO_{2(g)}$	3 mL min^{-1}	Yes	4	0.034	197

[a] HDMMCs = hybrid double membrane microcapsules, NPs = nanoparticles, NPSCSs = nanoparticle-stabilized capsules, MCF-MP = siliceous mesostructured cellular foams functionalized with mercaptopropyl groups, TCPP = 5,10,15,20-tetrakis(4-carboxyphenyl)porphyrin, ZIF = zeolite-like imidazole framework material, PE-HFMs = polyethylene hollow fibre membranes.

have similar pH and temperature optima. Each step of the cascade is endowed with a $2e^-$ reduction of CO_2 and requires one equivalent of NADH (nicotinamide adenine dinucleotide hydride) as a co-factor, serving as the reductant. Two molecules of NADH are thus oxidized into the corresponding NAD^+ during the biocatalyzed reduction of CO_2 to formaldehyde.

The main parameters and performances of these selective catalytic systems are summarized in Table 8. The results are described in three sections: (i) optimized reaction conditions with free enzyme systems, (ii) immobilized and compartmentalized enzymes and, finally, (iii) systems coupled to the NADH regeneration process.

8.1. Optimization of the reaction conditions with free enzyme systems

Studies have shown that FDH/FaldDH ratio lower than 1 is beneficial for the production of formaldehyde over formate since the formate is a good substrate for the FDH (Table 8, entry 1).[217] In the same vein, an excess of NADH (NADH/NAD^+ molar ratio > 2000) was also found necessary to drive the reaction. Under optimized conditions, 60 μM of formaldehyde was produced from $KHCO_3$ instead of CO_2 in 72 h with 15 g L^{-1} of FaldDH and 1 g L^{-1} of FDH. The formaldehyde concentration was quantified using a colorimetric test (Nash reagent)[149] as it was found that indirect detection through UV quantification of NADH disappearance could be erroneous due to interaction with CO_2. Following this study, the same cascade was explored with gaseous CO_2 (Table 8, entry 2).[218] Higher amount of FaldDH as compared to FDH was again necessary and the study disclosed the positive impact of a high CO_2 pressure (from 0.2 to 0.5 MPa) to generate a high amount of formaldehyde. Under optimized conditions, 901 μM of formaldehyde was produced (0.5 MPa of CO_2) after 12 h. A plateau was found at 10–12 h before a net decrease of formaldehyde, tentatively explained by the consumption of formaldehyde *via* the reverse reaction (*i.e.*, oxidation of HCHO into CO_2) and/or the instability of formaldehyde in the reaction medium.

8.2. Enzyme immobilization and compartmentalization

Immobilized systems were explored to improve the performances of the FDH/FaldDH cascade with the aim to increase enzyme stability, activity[224] and reusability compared to the enzymes freely diffusing systems. FDH and FaldDH were immobilized and spatially separated at organic–inorganic hybrid double membrane microcapsules (HDMMCs) (Table 8, entry 3).[219] FDH was encapsulated in the lumen of the HDMMCs while FaldDH was encapsulated in the intermembrane space. The study showed an improved activity with formaldehyde production of 22 μmol compared to the control experiment with free enzymes (9 μmol). The same group encapsulated FDH in Ti nanoparticles (NPs) while FaldDH was immobilized at the surface of the particles (Table 8, entry 4).[220] The size of the NPs (from 75 to 375 nm) was shown to have a significant impact on the reaction. The best performances were obtained with NP size of 75 nm. The recycling stability of the enzyme-containing NPs was evaluated and displayed a loss of half of the initial performance after 10 cycles. It was improved in a following report describing the preparation of nanoparticle-stabilized capsules (NPSCs) containing FDH entrapped in the capsule and FaldDH conjugated on the capsule surface (Table 8, entry 5).[221] Furthermore, the distance between both enzymes was evaluated using Förster resonance energy transfer (FRET) analysis on the enzyme labelled with carbocyanine dyes (Table 8, entry 6).[222] While no detectable FRET was observed free in the enzyme system with an estimated distance of 40 nm between the two enzymes, co-immobilization of the enzymes in the silica materials displayed an increased transfer efficiency >50% with an estimated distance of less than 10 nm. This feature was proposed to be responsible for the enhanced activity in the particles compared to the enzyme free system, due to probability increase of direct substrate transfer between the two enzymes.

8.3. NADH regeneration

NADH is a co-factor that is regenerated in biological systems. When implemented *in vitro*, its stoichiometric use negatively impacts the atom-efficiency of any given transformation. The regeneration of NADH from NAD^+ has thus been the subject of intense investigation with the development of bio-, electro- and photo-regeneration systems.[225] In the case of the FDH/FaldDH cascade reaction transforming CO_2 into formaldehyde, only two reports described the combination of the cascade with a regeneration process. FDH and FaldDH were co-immobilized in the cavities of the zeolitic imidazolate framework-8 (ZIF-8) combined with 5,10,15,20-tetrakis(4-carboxyphenyl) porphyrin (TCPP) as a photosensitizer fixed to the surface of the zeolite (Table 8, entry 7).[223] Triethanolamine (TEOA) was used as an electron donor, Cp*Rh(bpy)Cl (M, Cp* = pentamethylcyclopentadienyl, bpy = bipyridine) as an electron mediator and water as a proton donor. Under optimum conditions (1 mg mL^{-1} 3% TCPP@ZIF-8, pH = 8.0) the NADH regeneration reached 75% yield after 3 h under visible-light exposure. Combining this regeneration system with FDH/FaldDH (2 : 1 ratio) afforded the conversion of 10 µM of $NaHCO_3$ into 7.74 µM of formaldehyde (conversion rate 77%) after 8 h under visible-light exposure. The use of titanium dioxide (TiO_2) in a photocatalytic system[182] was also probed with immobilized FDH/FaldDH on the surface of polyethylene (PE) hollow fibre membranes (HFMs) (Table 8, entry 8).[197] Despite side reactions due to the known ability of the UV/TiO_2 system to photoreduce CO_2 into various products (*e.g.*, CO, HCOOH, HCHO, CH_3OH, CH_4),[182] NADH regeneration was observed and 34 µM of formaldehyde was generated under the best conditions (ratio FDH : FaldDH = 1 : 0.3, CO_2 3 mL min^{-1}, H_2O as the electron donor, PB buffer, pH 7.0, [NADH] = 1 mmol L^{-1}, exposure to two 23 W UV lamps at λ = 365 nm).

8.4. Conclusion and perspectives

In conclusion, the enzymatic conversion of CO_2 into formaldehyde is still at an early stage of development. Only a few reports have highlighted the selective formation of formaldehyde in cascade reactions involving FDH and FaldDH. Strategies for enzyme immobilization were identified to enhance both the reusability and activities of FDH and FaldDH when compared to free enzyme systems.

As perspectives, discovering more active and/or robust enzymes from diverse organisms or engineering existing enzymes for improved stability and activity is crucial for advancing current strategies. Additionally, the development of efficient co-factor regeneration systems is essential to establish an energetically sustainable and cost-effective process. The design of an effective co-immobilized system for enzymes coupled with a co-factor regeneration process remains undisclosed. An attractive approach involves substituting the natural co-factor NADH with a more sustainable electron and proton supplier system, as previously demonstrated in the biocatalyzed generation of formate or methanol from CO_2.[11b,213] Similarly, electrochemically driven enzymatic systems represent a promising avenue. Finally, the biocatalyzed four-electron reduction of CO_2 to formaldehyde has yet to be explored in subsequent transformations. While such processes are enticing, the undefined form taken by the generated formaldehyde and its instability in the enzymatic reaction medium have so far hindered its isolation or utilization in subsequent transformations for the synthesis of more complex products.

9. General conclusions

In this comprehensive review, we have examined the reduction of CO_2 with four electrons, leading to the production of formaldehyde and acetal derivatives through thermal (hydrogenation or hydroelementation reactions), electrochemical, photoelectrochemical, and bio-driven processes. Formaldehyde holds considerable appeal for both energy carrier applications and use as a chemical feedstock. Particularly noteworthy is its versatility for the latter application compared to formic acid, methanol, or methane obtained from the CO_2 reduction reaction (CO_2RR). Despite its promising attributes, synthesizing and isolating formaldehyde from the CO_2RR remains significantly more challenging than the aforementioned C_1 compounds. To date, only a limited number of systems have been reported to generate formaldehyde from CO_2 as the major product, and in many cases, conclusive evidence regarding the origin of formaldehyde is lacking. The most notable performances of these systems are summarized in Table 9.

Table 9 Best catalytic performances of the different reduction systems reported for the generation of formaldehyde from electro-, photoelectrochemical, enzymatic and hydrogenation processes and further use as a C_1 source in subsequent transformations

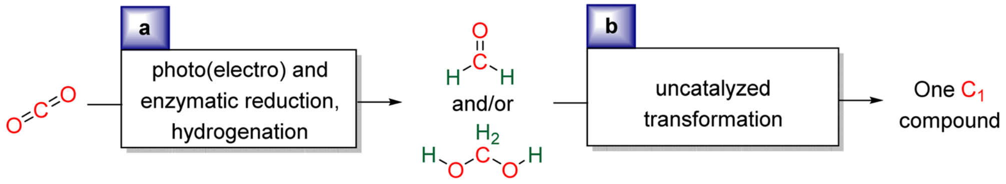

Reduction system	Hydrogenation	Electroreduction	Photoelectroreduction
Yield	0.037 M g_{cat}^{-1} h^{-1}		400–500 µmol h^{-1} g_{cat}^{-1} (1 bar CO_2) 16 500 µmol h^{-1} g_{cat}^{-1} (7 bars CO_2)
TON	—	10^4	
Selectivity (%)	—	90	60–70
Faradaic efficiency (%)	n.a	85–90	NA
Current density (mA cm^{-2})	n.a	0.1–0.2	NA
C_1 source	✗	✗	CH_2–N
C_n source	✗	✗	✗
Asymmetric C center	✗	✗	✗

Table 10 Best catalytic performances of the different reduction systems reported for the generation of acetal compounds and further use of the acetals as C_1 and/or C_n sources in subsequent transformations

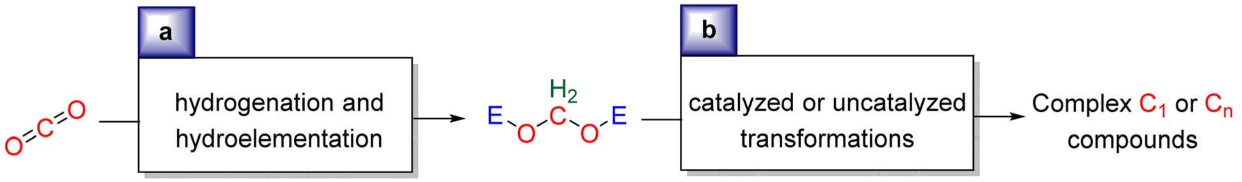

Reduction system	Hydrogenation	Hydrosilylation	Hydroboration	Hydrozirconation
TON	3874	3400	690	—
TOF (h^{-1})	194	10.4	516	—
Yield (%)	—	99	97	—
Scale	2.88 mmol	4.70 mmol	0.55 mmol	
C_1 source	✗	CH_2–N, –O, –S, –C	CH_2–N, –O, -P, –C	CH_2–C
C_n source	✗	✗	C_2, C_3, C_4	✗
Asymmetric C center	✗	✗	Diastereo- and enantio-selective transformations	✗

In hydrogenation reactions, the highest reported yield of formaldehyde (HCHO) was 0.037 M g_{cat}^{-1} h^{-1} achieved with a Ru-based heterogeneous catalyst in an aqueous medium.[148] Another notable instance involved electroreduction, where a film of electropolymerized chromium vinylterpyridine complex exhibited 90% faradaic efficiency (FE) and a turnover number (TON) of 10^4.[170] In photoelectroreduction, optimal performances were observed at 16 500 μmol h^{-1} g_{cat}^{-1} under 7 bars of CO_2 and 80 °C with a TiO_2 catalyst, achieving 70% selectivity.[189] Remarkably, in all these systems, the generated formaldehyde was utilized only once as a substrate in a cascade reaction to form a C–N bond, leaving significant untapped potential in this area for future exploration.[194] Further investigations are thus imperative, both for fundamental understanding and catalyst development, and it is crucial to gather solid evidence regarding the origin of the generated formaldehyde in each case. In addition to the challenge of generating formaldehyde, detecting and isolating it proves to be a formidable task due to its reactive nature.

On the other hand, the reduction of CO_2 into acetal products has seen successful developments in thermic processes, specifically in (i) the hydrogenation of CO_2 in the presence of alcohol and (ii) hydroelementation reactions involving hydrosilanes, hydroboranes, and early transition metal hydride species. In contrast to the synthesis of formaldehyde, numerous acetal compounds were selectively and efficiently generated, and eventually isolated. Notably, the formation of acetals from the CO_2RR currently stands as the sole pathway to formaldehyde, enabling its consistent use not only as a C_1 source but also as a C_n source. Bis(silyl)acetal (BSA) and bis(boryl)acetal (BBA) were indeed shown to release formaldehyde, which was then employed in subsequent C_1 and C_n transformations. It was also demonstrated that these acetals could serve as a formaldehyde surrogate without releasing formaldehyde. The primary drawback of the acetal approach is its lack of atom efficiency. While the regeneration of hydroborane or hydrosilane in a sustainable reduction process would be an ideal solution, the formation of high value-added compounds *via* complex transformations may compensate for this issue to some extent. Table 10 compiles the highest reported performances (TON, TOF, yield, selectivity) in each of the reductive processes leading to acetal compounds. While the chemistry of formaldehyde is well-established and developed, the acetal compounds obtained from the four-electron reduction of CO_2 are, for the most part, novel molecules, and their reactivities are still under investigation. Pioneering studies on their reactivity have led to the utilization of several BSA, BBA, and **BZrA 1** as a C_1 source in multicomponent reactions. This facilitated the incorporation of one carbon atom from CO_2 into very diverse molecules in the form of methylene. Table 10 also summarizes the types of C–E bonds (E = N, O, S, P) formed from BSA, BBA, and **BZrA 1**. Moreover, two BBA compounds (**BBA 2** and **4**) were employed as a C_n source, generating C_2, C_3, and C_4 carbohydrates. In the case of the latter two, asymmetric carbon centres were even generated in a diastereo- and enantioselective manner, respectively. Formaldehyde was directly observed only once in 4% yield with hydrosilanes and only once among a mixture of other products with hydroboranes. The intermediary of acetals (**BSA 3**, **BBA 2** and **4**, **BZrA 1**) was essential for the selective generation of formaldehyde, as it was quantitatively released either spontaneously, from hydrolysis, or from CsF activation depending on the acetal properties.

To conclude, the $4e^-$ reduction of CO_2 is a two-face journey. On one hand, the generation of acetal compounds witnessed important advances both to control this challenging reduction stage and to use it in subsequent complex transformations but at the expense of low atom-efficiency. On the other hand, the generation of formaldehyde from hydrogenation or photo(electro) reduction is more sustainable, but still in its infancy compared to other C_1 reduction compounds such as CO or methanol.

We believe that intertwined processes from the different fields involved in the CO_2RR (single *vs.* cascade processes, coupling between electro- and organo-catalysis) may be instrumental in addressing the challenging and sustainability issues associated with the $4e^-$ reduction of CO_2.

Data availability

Correspondence and requests should be addressed to julien.bonin@sorbonne-universite.fr, sebastien.bontemps@lcc-toulouse.fr or marc.robert@sorbonne-universite.fr.

Author contributions

S. B. conceptualized the review. S. B, S. D., J. B. and M. R. wrote and edited the review.

Conflicts of interest

The authors declare no competing financial interest.

Acknowledgements

Partial financial support to M. R. from the Institut Universitaire de France (IUF) is warmly thanked. S. D. thanks Région Midi-Pyrénées and Université Fédérale de Toulouse for a doctoral fellowship. S. B. thanks the CNRS for financial and technical support.

References

1 (*a*) H. Arakawa, M. Aresta, J. N. Armor, M. A. Barteau, E. J. Beckman, A. T. Bell, J. E. Bercaw, C. Creutz, E. Dinjus, D. A. Dixon, K. Domen, D. L. DuBois, J. Eckert, E. Fujita, D. H. Gibson, W. A. Goddard, D. W. Goodman, J. Keller, G. J. Kubas, H. H. Kung, J. E. Lyons, L. E. Manzer, T. J. Marks, K. Morokuma, K. M. Nicholas, R. Periana, L. Que, J. Rostrup-Nielson, W. M. H. Sachtler, L. D. Schmidt, A. Sen, G. A. Somorjai, P. C. Stair, B. R. Stults and W. Tumas, Catalysis Research of Relevance to Carbon Management: Progress, Challenges, and Opportunities, *Chem. Rev.*, 2001, **101**, 953–996; (*b*) E. Fujita, Photochemical carbon dioxide reduction with metal complexes, *Coord. Chem. Rev.*, 1999, **185–186**, 373–384; (*c*) W. Leitner, The coordination chemistry of carbon dioxide and its relevance for catalysis: A critical study, *Coord. Chem. Rev.*, 1996, **155**, 247; (*d*) D. H. Gibson, The organometallic chemistry of carbon dioxide, *Chem. Rev.*, 1996, **96**, 2063–2095; (*e*) P. Braunstein, D. Matt and D. Nobel, Reactions of carbon dioxide with carbon-carbon bond formation catalyzed by transition-metal complexes, *Chem. Rev.*, 1988, **88**, 747–764; (*f*) D. B. Dell'Amico, F. Calderazzo, L. Labella, F. Marchetti and G. Pampaloni, Converting Carbon Dioxide into Carbamato Derivatives, *Chem. Rev.*, 2003, **103**, 3857–3898.

2 (*a*) A. Goeppert, M. Czaun, J.-P. Jones, G. K. Surya Prakash and G. A. Olah, Recycling of carbon dioxide to methanol and derived products - closing the loop, *Chem. Soc. Rev.*, 2014, **43**, 7995–8048; (*b*) M. Aresta, A. Dibenedetto and A. Angelini, Catalysis for the Valorization of Exhaust Carbon: from CO_2 to Chemicals, Materials, and Fuels. Technological Use of CO_2, *Chem. Rev.*, 2014, **114**, 1709–1742; (*c*) C. Costentin, M. Robert and J.-M. Saveant, Catalysis of the electrochemical reduction of carbon dioxide, *Chem. Soc. Rev.*, 2013, **42**, 2423–2436; (*d*) A. M. Appel, J. E. Bercaw, A. B. Bocarsly, H. Dobbek, D. L. DuBois, M. Dupuis, J. G. Ferry, E. Fujita, R. Hille, P. J. A. Kenis, C. A. Kerfeld, R. H. Morris, C. H. F. Peden, A. R. Portis, S. W. Ragsdale, T. B. Rauchfuss, J. N. H. Reek, L. C. Seefeldt, R. K. Thauer and G. L. Waldrop, Frontiers, Opportunities, and Challenges in Biochemical and Chemical Catalysis of CO_2 Fixation, *Chem. Rev.*, 2013, **113**, 6621–6658; (*e*) G. Centi and S. Perathoner, Opportunities and prospects in the chemical recycling of carbon dioxide to fuels, *Catal. Today*, 2009, **148**, 191–205; (*f*) E. E. Benson, C. P. Kubiak, A. J. Sathrum and J. M. Smieja, Electrocatalytic and homogeneous approaches to conversion of CO_2 to liquid fuels, *Chem. Soc. Rev.*, 2009, **38**, 89–99; (*g*) T. Sakakura, J.-C. Choi and H. Yasuda, Transformation of Carbon Dioxide, *Chem. Rev.*, 2007, **107**, 2365–2387; (*h*) M. Aresta and A. Dibenedetto, Utilisation of CO_2 as a chemical feedstock: opportunities and challenges, *Dalton Trans.*, 2007, 2975–2992; (*i*) M. Aresta, in *Activation of small molecules*, ed. W. B. Tolman, Wiley, Weiheim, Germany, 2006, pp. 1–42; (*j*) M. D. Burkart, N. Hazari, C. L. Tway and E. L. Zeitler, Opportunities and Challenges for Catalysis in Carbon Dioxide Utilization, *ACS Catal.*, 2019, **9**, 7937–7956.

3 (*a*) A. Modak, P. Bhanja, S. Dutta, B. Chowdhury and A. Bhaumik, Catalytic reduction of CO_2 into fuels and fine chemicals, *Green Chem.*, 2020, **22**, 4002–4033; (*b*) F. Marques Mota and D. H. Kim, From CO_2 methanation to ambitious long-chain hydrocarbons: alternative fuels paving the path to sustainability, *Chem. Soc. Rev.*, 2019, **48**, 205–259; (*c*) X. Li, J. Yu, M. Jaroniec and X. Chen, Cocatalysts for Selective Photoreduction of CO_2 into Solar Fuels, *Chem. Rev.*, 2019, **119**, 3962–4179; (*d*) K. Sordakis, C. Tang, L. K. Vogt, H. Junge, P. J. Dyson, M. Beller and G. Laurenczy, Homogeneous Catalysis for Sustainable Hydrogen Storage in Formic Acid and Alcohols, *Chem. Rev.*, 2018, **118**, 372–433; (*e*) S. Remiro-Buenamañana and H. García, Photoassisted CO_2 Conversion to Fuels, *ChemCatChem*, 2018, **11**, 342–356; (*f*) J. Qiao, Y. Liu, F. Hong and J. Zhang, A review of catalysts for the electroreduction of carbon dioxide to produce low-carbon fuels, *Chem. Soc. Rev.*, 2014, **43**, 631–675; (*g*) A. J. Morris, G. J. Meyer and E. Fujita, Molecular Approaches to the Photocatalytic Reduction of Carbon Dioxide for Solar Fuels, *Acc. Chem. Res.*, 2009, **42**, 1983–1994.

4 (*a*) F. Della Monica and A. W. Kleij, Mechanistic guidelines in nonreductive conversion of CO_2: the case of cyclic carbonates, *Catal. Sci. Technol.*, 2020, **10**, 3483–3501; (*b*) Y. Yang and J.-W. Lee, Toward ideal carbon dioxide functionalization, *Chem. Sci.*, 2019, **10**, 3905–3926; (*c*) S. Wang and C. Xi, Recent advances in nucleophile-triggered CO_2-incorporated cyclization leading to heterocycles, *Chem. Soc. Rev.*, 2019, **48**, 382–404; (*d*) A. Cherubini-Celli, J. Mateos, M. Bonchio, L. Dell'Amico

and X. Companyó, Transition Metal-Free CO_2 Fixation into New Carbon–Carbon Bonds, *ChemSusChem*, 2018, **11**, 3056–3070; (*e*) J. Luo and I. Larrosa, C—H Carboxylation of Aromatic Compounds through CO_2 Fixation, *ChemSusChem*, 2017, **10**, 3317–3332; (*f*) T. Janes, Y. Yang and D. Song, Chemical reduction of CO_2 facilitated by C-nucleophiles, *Chem. Commun.*, 2017, **53**, 11390–11398; (*g*) F.-G. Fontaine, M.-A. Courtemanche, M.-A. Légaré and É. Rochette, Design principles in frustrated Lewis pair catalysis for the functionalization of carbon dioxide and heterocycles, *Coord. Chem. Rev.*, 2017, **334**, 124–135; (*h*) Y. Li, X. Cui, K. Dong, K. Junge and M. Beller, Utilization of CO_2 as a C_1 Building Block for Catalytic Methylation Reactions, *ACS Catal.*, 2016, 1077–1086, DOI: 10.1021/acscatal.6b02715; (*i*) D. Yu, S. P. Teong and Y. Zhang, Transition metal complex catalyzed carboxylation reactions with CO_2, *Coord. Chem. Rev.*, 2015, **293–294**, 279–291; (*j*) Q. Liu, L. Wu, R. Jackstell and M. Beller, Using carbon dioxide as a building block in organic synthesis, *Nat. Commun.*, 2015, **6**, 1–15; (*k*) L. Wu, Q. Liu, R. Jackstell and M. Beller, Carbonylations of Alkenes with CO Surrogates, *Angew. Chem., Int. Ed.*, 2014, **53**, 6310–6320; (*l*) I. Omae, Recent developments in carbon dioxide utilization for the production of organic chemicals, *Coord. Chem. Rev.*, 2012, **256**, 1384–1405; (*m*) K. Huang, C.-L. Sun and Z.-J. Shi, Transition-metal-catalyzed C-C bond formation through the fixation of carbon dioxide, *Chem. Soc. Rev.*, 2011, **40**, 2435–2452; (*n*) M. Cokoja, C. Bruckmeier, B. Rieger, W. A. Herrmann and F. E. Kühn, Transformation of Carbon Dioxide with Homogeneous Transition-Metal Catalysts: A Molecular Solution to a Global Challenge?, *Angew. Chem., Int. Ed.*, 2011, **50**, 8510–8537; (*o*) S. N. Riduan and Y. Zhang, Recent developments in carbon dioxide utilization under mild conditions, *Dalton Trans.*, 2010, **39**, 3347–3357.

5 (*a*) G. Garcia-Garcia, M. C. Fernandez, K. Armstrong, S. Woolass and P. Styring, Analytical Review of Life-Cycle Environmental Impacts of Carbon Capture and Utilization Technologies, *ChemSusChem*, 2021, **14**, 995–1015; (*b*) A. Sternberg, C. M. Jens and A. Bardow, Life cycle assessment of CO_2-based C_1-chemicals, *Green Chem.*, 2017, **19**, 2244–2259; (*c*) J. A. Martens, A. Bogaerts, N. De Kimpe, P. A. Jacobs, G. B. Marin, K. Rabaey, M. Saeys and S. Verhelst, The Chemical Route to a Carbon Dioxide Neutral World, *ChemSusChem*, 2017, **10**, 1039–1055; (*d*) N. von der Assen, P. Voll, M. Peters and A. Bardow, Life cycle assessment of CO_2 capture and utilization: a tutorial review, *Chem. Soc. Rev.*, 2014, **43**, 7982–7994.

6 R. I. Masel, Z. Liu, H. Yang, J. J. Kaczur, D. Carrillo, S. Ren, D. Salvatore and C. P. Berlinguette, An industrial perspective on catalysts for low-temperature CO_2 electrolysis, *Nat. Nanotechnol.*, 2021, **16**, 118–128.

7 (*a*) J. Klankermayer, S. Wesselbaum, K. Beydoun and W. Leitner, Selective Catalytic Synthesis Using the Combination of Carbon Dioxide and Hydrogen: Catalytic Chess at the Interface of Energy and Chemistry, *Angew. Chem., Int. Ed.*, 2016, **55**, 7296–7343; (*b*) W.-H. Wang, Y. Himeda, J. T. Muckerman, G. F. Manbeck and E. Fujita, CO_2 Hydrogenation to Formate and Methanol as an Alternative to Photo- and Electrochemical CO_2 Reduction, *Chem. Rev.*, 2015, **115**, 12936–12973; (*c*) W. Wang, S. Wang, X. Ma and J. Gong, Recent advances in catalytic hydrogenation of carbon dioxide, *Chem. Soc. Rev.*, 2011, **40**, 3703–3727; (*d*) P. G. Jessop, F. Joo and C.-C. Tai, Recent advances in the homogeneous hydrogenation of carbon dioxide, *Coord. Chem. Rev.*, 2004, **248**, 2425–2442; (*e*) T. Schaub, CO_2-based hydrogen storage: CO_2 hydrogenation to formic acid, formaldehyde and methanol, *Phys. Sci. Rev.*, 2018, **3**, 20170015.

8 (*a*) S. Bontemps, Boron-Mediated Activation of Carbon Dioxide, *Coord. Chem. Rev.*, 2016, **308**(Part 2), 117–130; (*b*) C. C. Chong and R. Kinjo, Catalytic Hydroboration of Carbonyl Derivatives, Imines, and Carbon Dioxide, *ACS Catal.*, 2015, **5**, 3238–3259.

9 (*a*) F. J. Fernández-Alvarez and L. A. Oro, Homogeneous Catalytic Reduction of CO_2 with Silicon-Hydrides, State of the Art, *ChemCatChem*, 2018, **10**, 4783–4796; (*b*) F. J. Fernandez-Alvarez, A. M. Aitani and L. A. Oro, Homogeneous catalytic reduction of CO_2 with hydrosilanes, *Catal. Sci. Technol.*, 2014, **4**, 611–624.

10 (*a*) E. Boutin, L. Merakeb, B. Ma, B. Boudy, M. Wang, J. Bonin, E. Anxolabéhère-Mallart and M. Robert, Molecular catalysis of CO_2 reduction: recent advances and perspectives in electrochemical and light-driven processes with selected Fe, Ni and Co aza macrocyclic and polypyridine complexes, *Chem. Soc. Rev.*, 2020, **49**, 5772–5809; (*b*) S. Fukuzumi, Y.-M. Lee, H. S. Ahn and W. Nam, Mechanisms of catalytic reduction of CO_2 with heme and nonheme metal complexes, *Chem. Sci.*, 2018, **9**, 6017–6034; (*c*) K. M. Waldie, A. L. Ostericher, M. H. Reineke, A. F. Sasayama and C. P. Kubiak, Hydricity of Transition-Metal Hydrides: Thermodynamic Considerations for CO_2 Reduction, *ACS Catal.*, 2017, **8**, 1313–1324; (*d*) N. Elgrishi, M. B. Chambers, X. Wang and M. Fontecave, Molecular polypyridine-based metal complexes as catalysts for the reduction of CO_2, *Chem. Soc. Rev.*, 2017, **46**, 761–796; (*e*) H. Takeda, C. Cometto, O. Ishitani and M. Robert, Electrons, Photons, Protons and Earth-Abundant Metal Complexes for Molecular Catalysis of CO_2 Reduction, *ACS Catal.*, 2016, **7**, 70–88; (*f*) A. M. Appel and M. L. Helm, Determining the Overpotential for a Molecular Electrocatalyst, *ACS Catal.*, 2014, **4**, 630–633; (*g*) Y. Dong, P. Duchesne, A. Mohan, K. K. Ghuman, P. Kant, L. Hurtado, U. Ulmer, J. Y. Y. Loh, A. A. Tountas, L. Wang, A. Jelle, M. Xia, R. Dittmeyer and G. A. Ozin, Shining light on CO_2: from materials discovery to photocatalyst, photoreactor and process engineering, *Chem. Soc. Rev.*, 2020, **49**, 5648–5663; (*h*) C. S. Yeung, Photoredox Catalysis as a Strategy for CO_2 Incorporation: Direct Access to Carboxylic Acids from a Renewable Feedstock, *Angew. Chem., Int. Ed.*, 2019, **58**, 5492–5502; (*i*) L. j. Guo, Y. j. Wang and T. He, Photocatalytic Reduction of CO_2 over Heterostructure Semiconductors into Value-Added Chemicals, *Chem. Rec.*, 2016, **16**, 1918–1933;

(*j*) X. Chang, T. Wang and J. Gong, CO_2 photo-reduction: insights into CO_2 activation and reaction on surfaces of photocatalysts, *Energy Environ. Sci.*, 2016, **9**, 2177–2196; (*k*) J. L. White, M. F. Baruch, J. E. Pander Iii, Y. Hu, I. C. Fortmeyer, J. E. Park, T. Zhang, K. Liao, J. Gu, Y. Yan, T. W. Shaw, E. Abelev and A. B. Bocarsly, Light-Driven Heterogeneous Reduction of Carbon Dioxide: Photocatalysts and Photoelectrodes, *Chem. Rev.*, 2015, **115**, 12888–12935; (*l*) S. Nitopi, E. Bertheussen, S. B. Scott, X. Liu, A. K. Engstfeld, S. Horch, B. Seger, I. E. L. Stephens, K. Chan, C. Hahn, J. K. Nørskov, T. F. Jaramillo and I. Chorkendorff, Progress and Perspectives of Electrochemical CO_2 Reduction on Copper in Aqueous Electrolyte, *Chem. Rev.*, 2019, **119**, 7610–7672.

11 (*a*) M. Yuan, M. J. Kummer and S. D. Minteer, Strategies for Bioelectrochemical CO_2 Reduction, *Chem.–Eur. J.*, 2019, **25**, 14258–14266; (*b*) S. Schlager, A. Dibenedetto, M. Aresta, D. H. Apaydin, L. M. Dumitru, H. Neugebauer and N. S. Sariciftci, Biocatalytic and Bioelectrocatalytic Approaches for the Reduction of Carbon Dioxide using Enzymes, *Energy Technol.*, 2017, **5**, 812–821.

12 (*a*) K. A. Grice, Carbon dioxide reduction with homogenous early transition metal complexes: Opportunities and challenges for developing CO_2 catalysis, *Coord. Chem. Rev.*, 2017, **336**, 78–95; (*b*) A. Pinaka and G. C. Vougioukalakis, Using sustainable metals to carry out "green" transformations: Fe- and Cu-catalyzed CO_2 monetization, *Coord. Chem. Rev.*, 2015, **288**, 69–97; (*c*) L. Zhang and Z. Hou, N-Heterocyclic carbene (NHC)-copper-catalysed transformations of carbon dioxide, *Chem. Sci.*, 2013, **4**, 3395–3403; (*d*) S. P and S. K. Mandal, From CO_2 activation to catalytic reduction: a metal-free approach, *Chem. Sci.*, 2020, **11**, 10571–10593.

13 (*a*) K. Liu, P. Cao, W. Chen, C. I. Ezeh, Z. Chen, Y. Luo, Q. Liu, H. Zhao, Z. Rui, S. Gao, Z. Yin, X. Sun and X. Yu, Electrocatalysis enabled transformation of earth-abundant water, nitrogen and carbon dioxide for a sustainable future, *Mater. Adv.*, 2022, **3**, 1359–1400; (*b*) H. Lu, J. Tournet, K. Dastafkan, Y. Liu, Y. H. Ng, S. K. Karuturi, C. Zhao and Z. Yin, Noble-Metal-Free Multicomponent Nanointegration for Sustainable Energy Conversion, *Chem. Rev.*, 2021, **121**, 10271–10366; (*c*) F. Naseem, P. Lu, J. Zeng, Z. Lu, Y. H. Ng, H. Zhao, Y. Du and Z. Yin, Solid Nanoporosity Governs Catalytic CO2 and N2 Reduction, *ACS Nano*, 2020, **14**, 7734–7759; (*d*) L. Wang, W. Chen, D. Zhang, Y. Du, R. Amal, S. Qiao, J. Wu and Z. Yin, Surface strategies for catalytic CO2 reduction: from two-dimensional materials to nanoclusters to single atoms, *Chem. Soc. Rev.*, 2019, **48**, 5310–5349; (*e*) H. Yin, K. Xing, Y. Zhang, D. M. A. S. Dissanayake, Z. Lu, H. Zhao, Z. Zeng, J.-H. Yun, D.-C. Qi and Z. Yin, Periodic nanostructures: preparation, properties and applications, *Chem. Soc. Rev.*, 2021, **50**, 6423–6482; (*f*) A. Álvarez, A. Bansode, A. Urakawa, A. V. Bavykina, T. A. Wezendonk, M. Makkee, J. Gascon and F. Kapteijn, Challenges in the Greener Production of Formates/Formic Acid, Methanol, and DME by Heterogeneously Catalyzed CO_2 Hydrogenation Processes, *Chem. Rev.*, 2017, **117**, 9804–9838; (*g*) L. Zhang, Z.-J. Zhao, T. Wang and J. Gong, Nano-designed semiconductors for electro- and photoelectro-catalytic conversion of carbon dioxide, *Chem. Soc. Rev.*, 2018, **47**, 5423–5443; (*h*) J. Zhong, X. Yang, Z. Wu, B. Liang, Y. Huang and T. Zhang, State of the art and perspectives in heterogeneous catalysis of CO_2 hydrogenation to methanol, *Chem. Soc. Rev.*, 2020, **49**, 1385–1413.

14 (*a*) S. Liang, L. Huang, Y. Gao, Q. Wang and B. Liu, Electrochemical Reduction of CO_2 to CO over Transition Metal/N-Doped Carbon Catalysts: The Active Sites and Reaction Mechanism, *Adv. Sci.*, 2021, **8**, 2102886; (*b*) S. Jin, Z. Hao, K. Zhang, Z. Yan and J. Chen, Advances and Challenges for the Electrochemical Reduction of CO_2 to CO: From Fundamentals to Industrialization, *Angew. Chem., Int. Ed.*, 2021, **60**, 20627–20648; (*c*) R. Küngas, Electrochemical CO_2 Reduction for CO Production: Comparison of Low- and High-Temperature Electrolysis Technologies, *J. Electrochem. Soc.*, 2020, **167**, 044508; (*d*) F.-Y. Gao, R.-C. Bao, M.-R. Gao and S.-H. Yu, Electrochemical CO_2-to-CO conversion: electrocatalysts, electrolytes, and electrolyzers, *J. Mater. Chem. A*, 2020, **8**, 15458–15478.

15 (*a*) R. Sun, Y. Liao, S.-T. Bai, M. Zheng, C. Zhou, T. Zhang and B. F. Sels, Heterogeneous catalysts for CO_2 hydrogenation to formic acid/formate: from nanoscale to single atom, *Energy Environ. Sci.*, 2021, **14**, 1247–1285; (*b*) P. Duarah, D. Haldar, V. S. K. Yadav and M. K. Purkait, Progress in the electrochemical reduction of CO_2 to formic acid: A review on current trends and future prospects, *J. Environ. Chem. Eng.*, 2021, **9**, 106394; (*c*) M. F. Philips, G.-J. M. Gruter, M. T. M. Koper and K. J. P. Schouten, Optimizing the Electrochemical Reduction of CO_2 to Formate: A State-of-the-Art Analysis, *ACS Sustain. Chem. Eng.*, 2020, **8**, 15430–15444; (*d*) P. Ding, H. Zhao, T. Li, Y. Luo, G. Fan, G. Chen, S. Gao, X. Shi, S. Lu and X. Sun, Metal-based electrocatalytic conversion of CO_2 to formic acid/formate, *J. Mater. Chem. A*, 2020, **8**, 21947–21960; (*e*) W. Leitner, Carbon-Dioxide as a Raw-Material - the Synthesis of Formic-Acid and Its Derivatives from CO_2, *Angew. Chem., Int. Ed.*, 1995, **34**, 2207–2221.

16 (*a*) X. Jiang, X. Nie, X. Guo, C. Song and J. G. Chen, Recent Advances in Carbon Dioxide Hydrogenation to Methanol via Heterogeneous Catalysis, *Chem. Rev.*, 2020, **120**, 7984–8034; (*b*) E. Alberico and M. Nielsen, Towards a methanol economy based on homogeneous catalysis: methanol to H_2 and CO_2 to methanol, *Chem. Commun.*, 2015, **51**, 6714–6725; (*c*) Y.-N. Li, R. Ma, L.-N. He and Z.-F. Diao, Homogeneous hydrogenation of carbon dioxide to methanol, *Catal. Sci. Technol.*, 2014, **4**, 1498–1512; (*d*) G. A. Olah, Towards Oil Independence Through Renewable Methanol Chemistry, *Angew. Chem., Int. Ed.*, 2012, **52**, 104–107.

17 (*a*) S. W. Sheehan, Electrochemical methane production from CO_2 for orbital and interplanetary refueling, *iScience*,

2021, **24**, 102230; (*b*) C. Vogt, M. Monai, G. J. Kramer and B. M. Weckhuysen, The renaissance of the Sabatier reaction and its applications on Earth and in space, *Nat. Catal.*, 2019, **2**, 188–197; (*c*) P. Melo Bravo and D. P. Debecker, Combining CO_2 capture and catalytic conversion to methane, *Waste Dispos. Sustain. Energy.*, 2019, **1**, 53–65.

18 S. Bagherzadeh and N. P. Mankad, Catalyst Control of Selectivity in CO2 Reduction Using a Tunable Heterobimetallic Effect, *J. Am. Chem. Soc.*, 2015, **137**(34), 10898–10901.

19 (*a*) H. Zhao, Z. Lin and T. B. Marder, Density Functional Theory Studies on the Mechanism of the Reduction of CO_2 to CO Catalyzed by Copper(I) Boryl Complexes, *J. Am. Chem. Soc.*, 2006, **128**, 15637–15643; (*b*) D. S. Laitar, P. Mueller and J. P. Sadighi, Efficient Homogeneous Catalysis in the Reduction of CO_2 to CO, *J. Am. Chem. Soc.*, 2005, **127**, 17196–17197.

20 (*a*) Y. Zhang, T. Zhang and S. Das, Catalytic transformation of CO_2 into C_1 chemicals using hydrosilanes as a reducing agent, *Green Chem.*, 2020, **22**, 1800–1820; (*b*) M. Hulla and P. J. Dyson, Pivotal Role of the Basic Character of Organic and Salt Catalysts in C—N Bond Forming Reactions of Amines with CO_2, *Angew. Chem., Int. Ed.*, 2020, **59**, 1002–1017; (*c*) A. Tlili, E. Blondiaux, X. Frogneux and T. Cantat, Reductive functionalization of CO_2 with amines: an entry to formamide, formamidine and methylamine derivatives, *Green Chem.*, 2015, **17**, 157–168.

21 (*a*) T. K. Todorova, M. W. Schreiber and M. Fontecave, Mechanistic Understanding of CO_2 Reduction Reaction (CO2RR) Toward Multicarbon Products by Heterogeneous Copper-Based Catalysts, *ACS Catal.*, 2020, **10**, 1754–1768; (*b*) G. Prieto, Carbon Dioxide Hydrogenation into Higher Hydrocarbons and Oxygenates: Thermodynamic and Kinetic Bounds and Progress with Heterogeneous and Homogeneous Catalysis, *ChemSusChem*, 2017, **10**, 1056–1070; (*c*) M. D. Porosoff, B. Yan and J. G. Chen, Catalytic reduction of CO_2 by H_2 for synthesis of CO, methanol and hydrocarbons: challenges and opportunities, *Energy Environ. Sci.*, 2016, **9**, 62–73; (*d*) S. A. Fors and C. A. Malapit, Homogeneous Catalysis for the Conversion of CO_2, CO, CH_3OH, and CH_4 to C_{2+} Chemicals via C–C Bond Formation, *ACS Catal.*, 2023, **13**, 4231–4249.

22 (*a*) L. E. Heim, H. Konnerth and M. H. G. Prechtl, Future Perspectives for Formaldehyde: Pathways for Reductive Synthesis and Energy Storage, *Green Chem.*, 2017, **19**, 2347–2355; (*b*) G. Reuss, W. Disteldorf, A. O. Gamer and A. Hilt, *Formaldehyde in Ullmann's Encyclopedia of Industrial Chemistry*, Wiley, Weinheim, 2003; (*c*) M. Trincado, H. Grützmacher and M. H. G. Prechtl, CO_2-based hydrogen storage – Hydrogen generation from formaldehyde/water, *Phys. Sci. Rev.*, 2018, **3**, 20170013.

23 A. W. Franz, H. Kronemayer, D. Pfeiffer, R. D. Pilz, G. Reuss, W. Disteldorf, A. O. Gamer and A. Hilt, in *Ullmann's Encyclopedia of Industrial Chemistry*, 2016, pp. 1–34, DOI: **10.1002/14356007.a11_619.pub2**.

24 S. Desmons, R. Fauré and S. Bontemps, Formaldehyde as a Promising C_1 Source: The Instrumental Role of Biocatalysis for Stereocontrolled Reactions, *ACS Catal.*, 2019, **9**, 9575–9588.

25 S. Meninno and A. Lattanzi, Asymmetric Aldol Reaction with Formaldehyde: a Challenging Process, *Chem. Rec.*, 2016, **16**, 2016–2030.

26 (*a*) I. Zafar and N. Senad, The Formose Reaction: A Tool to Produce Synthetic Carbohydrates Within a Regenerative Life Support System, *Curr. Org. Chem.*, 2012, **16**, 769–788; (*b*) I. V. Delidovich, A. N. Simonov, O. P. Taran and V. N. Parmon, Catalytic Formation of Monosaccharides: From the Formose Reaction towards Selective Synthesis, *ChemSusChem*, 2014, **7**, 1833–1846.

27 T. Nash, The colorimetric estimation of formaldehyde by means of the Hantzsch reaction, *Biochem. J.*, 1953, **55**, 416–421.

28 T. Chatterjee, E. Boutin and M. Robert, Manifesto for the routine use of NMR for the liquid product analysis of aqueous CO_2 reduction: from comprehensive chemical shift data to formaldehyde quantification in water, *Dalton Trans.*, 2020, **49**, 4257–4265.

29 (*a*) M. Rauch, Z. Strater and G. Parkin, Selective Conversion of Carbon Dioxide to Formaldehyde via a Bis(silyl)acetal: Incorporation of Isotopically Labeled C_1 Moieties Derived from Carbon Dioxide into Organic Molecules, *J. Am. Chem. Soc.*, 2019, **141**, 17754–17762; (*b*) D. Zhang, C. Jarava-Barrera and S. Bontemps, Selective Reductive Dimerization of CO_2 into Glycolaldehyde, *ACS Catal.*, 2021, **11**, 4568–4575.

30 S. Desmons, K. Grayson-Steel, N. Nuñez-Dallos, L. Vendier, J. Hurtado, P. Clapés, R. Fauré, C. Dumon and S. Bontemps, Enantioselective Reductive Oligomerization of Carbon Dioxide into L-Erythrulose via a Chemoenzymatic Catalysis, *J. Am. Chem. Soc.*, 2021, **143**, 16274–16283.

31 T. Cai, H. Sun, J. Qiao, L. Zhu, F. Zhang, J. Zhang, Z. Tang, X. Wei, J. Yang, Q. Yuan, W. Wang, X. Yang, H. Chu, Q. Wang, C. You, H. Ma, Y. Sun, Y. Li, C. Li, H. Jiang, Q. Wang and Y. Ma, Cell-free chemoenzymatic starch synthesis from carbon dioxide, *Science*, 2021, **373**, 1523–1527.

32 S. Zhao, H.-Q. Liang, X.-M. Hu, S. Li and K. Daasbjerg, Challenges and Prospects in the Catalytic Conversion of Carbon Dioxide to Formaldehyde, *Angew. Chem., Int. Ed.*, 2022, **61**, e202204008.

33 A. Béthegnies, Y. Escudié, N. Nuñez-Dallos, L. Vendier, J. Hurtado, I. del Rosal, L. Maron and S. Bontemps, Reductive CO_2 Homocoupling: Synthesis of a Borylated C_3 Carbohydrate, *ChemCatChem*, 2019, **11**, 760–765.

34 (*a*) H. Maciejewski, C. Pietraszuk, P. Pawluć and B. Marciniec, *Hydrosilylation - A Comprehensive Review on Recent Advances*, Springer, Berlin, 2010; (*b*) B. Marciniec, Catalysis by transition metal complexes of alkene silylation–recent progress and mechanistic implications, *Coord. Chem. Rev.*, 2005, **249**, 2374–2390.

35 C. Hühn, A. Erlebach, D. Mey, L. Wondraczek and M. Sierka, Ab Initio energetics of Si-O bond cleavage, *J. Comput. Chem.*, 2017, **38**, 2349–2353.

36 (*a*) G. Sussfink and J. Reiner, Anionic Ruthenium Clusters as Catalysts in the Hydrosilylation of Carbon-Dioxide, *J. Organomet. Chem.*, 1981, **221**, C36–C38; (*b*) H. Koinuma, F. Kawakami, H. Kato and H. Hirai, Hydrosilylation of carbon dioxide catalysed by ruthenium complexes, *J. Chem. Soc., Chem. Commun.*, 1981, 213–214.

37 T. C. Eisenschmid and R. Eisenberg, The iridium complex catalyzed reduction of carbon dioxide to methoxide by alkylsilanes, *Organometallics*, 1989, **8**, 1822–1824.

38 T. Matsuo and H. Kawaguchi, From Carbon Dioxide to Methane: Homogeneous Reduction of Carbon Dioxide with Hydrosilanes Catalyzed by Zirconium−Borane Complexes, *J. Am. Chem. Soc.*, 2006, **128**, 12362–12363.

39 P. Rios, N. Curado, J. Lopez-Serrano and A. Rodriguez, Selective reduction of carbon dioxide to bis(silyl)acetal catalyzed by a PBP-supported nickel complex, *Chem. Commun.*, 2016, **52**, 2114–2117.

40 T. T. Metsänen and M. Oestreich, Temperature-Dependent Chemoselective Hydrosilylation of Carbon Dioxide to Formaldehyde or Methanol Oxidation State, *Organometallics*, 2015, **34**, 543–546.

41 S. N. Riduan, Y. Zhang and J. Y. Ying, Conversion of Carbon Dioxide into Methanol with Silanes over N-Heterocyclic Carbene Catalysts, *Angew. Chem., Int. Ed.*, 2009, **48**, 3322–3325.

42 M. L. Scheuermann, S. P. Semproni, I. Pappas and P. J. Chirik, Carbon Dioxide Hydrosilylation Promoted by Cobalt Pincer Complexes, *Inorg. Chem.*, 2014, **53**, 9463–9465.

43 M. Tolzmann, L. Schürmann, A. Hepp, W. Uhl and M. Layh, Hydrosilylation and Hydrogermylation of CO_2 and CS_2 by Al and Ga Functionalized Silanes and Germanes – Cooperative Reactivity with Formation of Silyl Formates and Disilylacetals, *Eur. J. Inorg. Chem.*, 2020, **2020**, 4024–4036.

44 Y. Jiang, O. Blacque, T. Fox and H. Berke, Catalytic CO_2 Activation Assisted by Rhenium Hydride/$B(C_6F_5)_3$ Frustrated Lewis Pairs—Metal Hydrides Functioning as FLP Bases, *J. Am. Chem. Soc.*, 2013, **135**, 7751–7760.

45 F. A. LeBlanc, W. E. Piers and M. Parvez, Selective Hydrosilation of CO_2 to a Bis(silylacetal) Using an Anilido Bipyridyl-Ligated Organoscandium Catalyst, *Angew. Chem., Int. Ed.*, 2014, **53**, 789–792.

46 Z. Lu, H. Hausmann, S. Becker and H. A. Wegner, Aromaticity as Stabilizing Element in the Bidentate Activation for the Catalytic Reduction of Carbon Dioxide, *J. Am. Chem. Soc.*, 2015, **137**, 5332–5335.

47 N. Del Rio, M. Lopez-Reyes, A. Baceiredo, N. Saffon-Merceron, D. Lutters, T. Müller and T. Kato, N,P-Heterocyclic Germylene/$B(C_6F_5)_3$ Adducts: A Lewis Pair with Multi-reactive Sites, *Angew. Chem., Int. Ed.*, 2017, **56**, 1365–1370.

48 L. Luconi, A. Rossin, G. Tuci, Z. Gafurov, D. M. Lyubov, A. A. Trifonov, S. Cicchi, H. Ba, C. Pham-Huu, D. Yakhvarov and G. Giambastiani, Benzoimidazole-Pyridylamido Zirconium and Hafnium Alkyl Complexes as Homogeneous Catalysts for Tandem Carbon Dioxide Hydrosilylation to Methane, *ChemCatChem*, 2019, **11**, 495–510.

49 W. Huang, T. Roisnel, V. Dorcet, C. Orione and E. Kirillov, Reduction of CO_2 by Hydrosilanes in the Presence of Formamidinates of Group 13 and 12 Elements, *Organometallics*, 2020, **39**, 698–710.

50 T. González and J. J. García, Catalytic CO_2 hydrosilylation with $[Mn(CO)_5Br]$ under mild reaction conditions, *Polyhedron*, 2021, **203**, 115242.

51 A. Caise, J. Hicks, M. Ángeles Fuentes, J. M. Goicoechea and S. Aldridge, Partnering a Three-Coordinate Gallium Cation with a Hydroborate Counter-Ion for the Catalytic Hydrosilylation of CO_2, *Chem.–Eur. J.*, 2021, **27**, 2138–2148.

52 K. Chang, I. del Rosal, X. Zheng, L. Maron and X. Xu, Hydrosilylative reduction of carbon dioxide by a homoleptic lanthanum aryloxide catalyst with high activity and selectivity, *Dalton Trans.*, 2021, **50**, 7804–7809.

53 S. Park, D. Bézier and M. Brookhart, An Efficient Iridium Catalyst for Reduction of Carbon Dioxide to Methane with Trialkylsilanes, *J. Am. Chem. Soc.*, 2012, **134**, 11404–11407.

54 M. Rauch and G. Parkin, Zinc and Magnesium Catalysts for the Hydrosilylation of Carbon Dioxide, *J. Am. Chem. Soc.*, 2017, **139**, 18162–18165.

55 Q. Zhang, N. Fukaya, T. Fujitani and J.-C. Choi, Carbon Dioxide Hydrosilylation to Methane Catalyzed by Zinc and Other First-Row Transition Metal Salts, *Bull. Chem. Soc. Jpn.*, 2019, **92**, 1945–1949.

56 M.-A. Courtemanche, M.-A. Legare, E. Rochette and F.-G. Fontaine, Phosphazenes: efficient organocatalysts for the catalytic hydrosilylation of carbon dioxide, *Chem. Commun.*, 2015, **51**, 6858–6861.

57 (*a*) B. H. Rotstein, S. H. Liang, M. S. Placzek, J. M. Hooker, A. D. Gee, F. Dolle, A. A. Wilson and N. Vasdev, $^{11}C{=}O$ bonds made easily for positron emission tomography radiopharmaceuticals, *Chem. Soc. Rev.*, 2016, **45**, 4708–4726; (*b*) B. H. Rotstein, S. H. Liang, J. P. Holland, T. L. Collier, J. M. Hooker, A. A. Wilson and N. Vasdev, $^{11}CO_2$ fixation: a renaissance in PET radiochemistry, *Chem. Commun.*, 2013, **49**, 5621–5629; (*c*) M. Ahamed, J. Verbeek, U. Funke, J. Lecina, A. Verbruggen and G. Bormans, Recent Progress in Metal Catalyzed Direct Carboxylation of Aryl Halides and Pseudo Halides Employing CO_2: Opportunities for ^{11}C Radiochemistry, *ChemCatChem*, 2016, **8**, 3692–3700; (*d*) S. Monticelli, A. Talbot, P. Gotico, F. Caillé, O. Loreau, A. Del Vecchio, A. Malandain, A. Sallustrau, W. Leibl, A. Aukauloo, F. Taran, Z. Halime and D. Audisio, Unlocking full and fast conversion in photocatalytic carbon dioxide reduction for applications in radio-carbonylation, *Nat. Commun.*, 2023, **14**, 4451; (*e*) A. Malandain, M. Molins, A. Hauwelle, A. Talbot, O. Loreau, T. D'Anfray, S. Goutal, N. Tournier, F. Taran, F. Caillé and D. Audisio, Carbon Dioxide Radical Anion by Photoinduced Equilibration between Formate Salts and $[^{11}C, ^{13}C, ^{14}C]CO_2$: Application to Carbon Isotope Radiolabeling, *J. Am. Chem. Soc.*, 2023, **145**,

16760–16770; (*f*) G. Destro, K. Horkka, O. Loreau, D.-A. Buisson, L. Kingston, A. Del Vecchio, M. Schou, C. S. Elmore, F. Taran, T. Cantat and D. Audisio, Transition-Metal-Free Carbon Isotope Exchange of Phenyl Acetic Acids, *Angew. Chem., Int. Ed.*, 2020, **59**, 13490–13495; (*g*) G. Destro, O. Loreau, E. Marcon, F. Taran, T. Cantat and D. Audisio, Dynamic Carbon Isotope Exchange of Pharmaceuticals with Labeled CO2, *J. Am. Chem. Soc.*, 2019, **141**, 780–784; (*h*) P. Gotico, A. Del Vecchio, D. Audisio, A. Quaranta, Z. Halime, W. Leibl and A. Aukauloo, Visible-Light-Driven Reduction of CO_2 to CO and Its Subsequent Valorization in Carbonylation Chemistry and ^{13}C Isotope Labeling, *ChemPhotoChem*, 2018, **2**, 715–719.

58 A. Berkefeld, W. E. Piers and M. Parvez, Tandem Frustrated Lewis Pair/Tris(pentafluorophenyl)borane-Catalyzed Deoxygenative Hydrosilylation of Carbon Dioxide, *J. Am. Chem. Soc.*, 2010, **132**, 10660–10661.

59 A. Berkefeld, W. E. Piers, M. Parvez, L. Castro, L. Maron and O. Eisenstein, Decamethylscandocinium-hydrido-(perfluorophenyl)borate: fixation and tandem tris(perfluorophenyl)borane catalysed deoxygenative hydrosilation of carbon dioxide, *Chem. Sci.*, 2013, **4**, 2152–2162.

60 F. Bertini, M. Glatz, B. Stöger, M. Peruzzini, L. F. Veiros, K. Kirchner and L. Gonsalvi, Carbon Dioxide Reduction to Methanol Catalyzed by Mn(I) PNP Pincer Complexes under Mild Reaction Conditions, *ACS Catal.*, 2019, **9**, 632–639.

61 D. S. Morris, C. Weetman, J. T. C. Wennmacher, M. Cokoja, M. Drees, F. E. Kühn and J. B. Love, Reduction of carbon dioxide and organic carbonyls by hydrosilanes catalysed by the perrhenate anion, *Catal. Sci. Technol.*, 2017, **7**, 2838–2845.

62 X. Zhang, J. Sun, G. Wei, Z. Liu, H. Yang, K. Wang and H. Fei, In Situ Generation of an N-Heterocyclic Carbene Functionalized Metal–Organic Framework by Postsynthetic Ligand Exchange: Efficient and Selective Hydrosilylation of CO_2, *Angew. Chem., Int. Ed.*, 2019, **58**, 2844–2849.

63 J. Chen, L. Falivene, L. Caporaso, L. Cavallo and E. Y. X. Chen, Selective Reduction of CO_2 to CH_4 by Tandem Hydrosilylation with Mixed Al/B Catalysts, *J. Am. Chem. Soc.*, 2016, **138**, 5321–5333.

64 D. W. Beh, W. E. Piers, B. S. Gelfand and J.-B. Lin, Tandem deoxygenative hydrosilation of carbon dioxide with a cationic scandium hydridoborate and $B(C_6F_5)_3$, *Dalton Trans.*, 2020, **49**, 95–101.

65 F. Huang, G. Lu, L. Zhao, H. Li and Z.-X. Wang, The Catalytic Role of N-Heterocyclic Carbene in a Metal-Free Conversion of Carbon Dioxide into Methanol: A Computational Mechanism Study, *J. Am. Chem. Soc.*, 2010, **132**, 12388–12396.

66 (*a*) T. Robert and M. Oestreich, Si-H Bond Activation: Bridging Lewis Acid Catalysis with Brookhart's Iridium(III) Pincer Complex and $B(C_6F_5)_3$, *Angew. Chem., Int. Ed.*, 2013, **52**, 5216–5218; (*b*) D. J. Parks, J. M. Blackwell and W. E. Piers, Studies on the Mechanism of $B(C_6F_5)_3$-Catalyzed Hydrosilation of Carbonyl Functions, *J. Org. Chem.*, 2000, **65**, 3090–3098; (*c*) V. Gevorgyan, M. Rubin, S. Benson, J.-X. Liu and Y. Yamamoto, A Novel $B(C_6F_5)_3$-Catalyzed Reduction of Alcohols and Cleavage of Aryl and Alkyl Ethers with Hydrosilanes, *J. Org. Chem.*, 2000, **65**, 6179–6186; (*d*) D. J. Parks and W. E. Piers, Tris(pentafluorophenyl)boron-Catalyzed Hydrosilation of Aromatic Aldehydes, Ketones, and Esters, *J. Am. Chem. Soc.*, 1996, **118**, 9440–9441.

67 S. Fang, H. Chen and H. Wei, Insight into catalytic reduction of CO_2 to methane with silanes using Brookhart's cationic Ir(III) pincer complex, *RSC Adv.*, 2018, **8**, 9232–9242.

68 M. Wen, F. Huang, G. Lu and Z.-X. Wang, Density Functional Theory Mechanistic Study of the Reduction of CO_2 to CH_4 Catalyzed by an Ammonium Hydridoborate Ion Pair: CO_2 Activation via Formation of a Formic Acid Entity, *Inorg. Chem.*, 2013, **52**, 12098–12107.

69 P. Ríos, A. Rodríguez and J. López-Serrano, Mechanistic Studies on the Selective Reduction of CO_2 to the Aldehyde Level by a Bis(phosphino)boryl (PBP)-Supported Nickel Complex, *ACS Catal.*, 2016, **6**, 5715–5723.

70 T. Stahl, H. F. T. Klare and M. Oestreich, $C(sp^3)$–F Bond Activation of CF_3-Substituted Anilines with Catalytically Generated Silicon Cations: Spectroscopic Evidence for a Hydride-Bridged Ru–S Dimer in the Catalytic Cycle, *J. Am. Chem. Soc.*, 2013, **135**, 1248–1251.

71 H. H. Cramer, S. Ye, F. Neese, C. Werlé and W. Leitner, Cobalt-Catalyzed Hydrosilylation of Carbon Dioxide to the Formic Acid, Formaldehyde, and Methanol Level—How to Control the Catalytic Network?, *JACS Au*, 2021, **1**, 2058–2069.

72 (*a*) K. Fujiwara, S. Yasuda and T. Mizuta, Reduction of CO_2 to Trimethoxyboroxine with BH_3 in THF, *Organometallics*, 2014, **33**, 6692–6695; (*b*) I. Knopf and C. C. Cummins, Revisiting CO_2 Reduction with $NaBH_4$ under Aprotic Conditions: Synthesis and Characterization of Sodium Triformatoborohydride, *Organometallics*, 2015, **34**, 1601–1603.

73 Y. Zhao, X. Liu, L. Zheng, Y. Du, X. Shi, Y. Liu, Z. Yan, J. You and Y. Jiang, One-Pot Methylenation–Cyclization Employing Two Molecules of CO_2 with Arylamines and Enaminones, *J. Org. Chem.*, 2020, **85**, 912–923.

74 (*a*) O. Jacquet, C. Das Neves Gomes, M. Ephritikhine and T. Cantat, Recycling of Carbon and Silicon Wastes: Room Temperature Formylation of N–H Bonds Using Carbon Dioxide and Polymethylhydrosiloxane, *J. Am. Chem. Soc.*, 2012, **134**, 2934–2937; (*b*) C. Das Neves Gomes, O. Jacquet, C. Villiers, P. Thuéry, M. Ephritikhine and T. Cantat, A Diagonal Approach to Chemical Recycling of Carbon Dioxide: Organocatalytic Transformation for the Reductive Functionalization of CO_2, *Angew. Chem., Int. Ed.*, 2012, **51**, 187–190.

75 S. Schreiner, J. Y. Yu and L. Vaska, Reversible homogeneous catalysis of carbon dioxide hydrogenation/reduction at

room temperature and low pressures, *J. Chem. Soc., Chem. Commun.*, 1988, 602–603.

76 M. Khandelwal and R. J. Wehmschulte, Deoxygenative Reduction of Carbon Dioxide to Methane, Toluene, and Diphenylmethane with $[Et_2Al]^+$ as Catalyst, *Angew. Chem., Int. Ed.*, 2012, **51**, 7323–7326.

77 X. Frogneux, E. Blondiaux, P. Thuéry and T. Cantat, Bridging Amines with CO_2: Organocatalyzed Reduction of CO_2 to Aminals, *ACS Catal.*, 2015, **5**, 3983–3987.

78 D.-Y. Zhu, L. Fang, H. Han, Y. Wang and J.-B. Xia, Reductive CO_2 Fixation via Tandem C–C and C–N Bond Formation: Synthesis of Spiro-indolepyrrolidines, *Org. Lett.*, 2017, **19**, 4259–4262.

79 Y. Zhao, X. Guo, X. Ding, Z. Zhou, M. Li, N. Feng, B. Gao, X. Lu, Y. Liu and J. You, Reductive CO_2 Fixation via the Selective Formation of C–C Bonds: Bridging Enaminones and Synthesis of 1,4-Dihydropyridines, *Org. Lett.*, 2020, **22**, 8326–8331.

80 W.-D. Li, J. Chen, D.-Y. Zhu and J.-B. Xia, Fe-Catalyzed Pictet-Spengler-Type Cyclization via Selective Four-Electron Reductive Functionalization of CO_2, *Chin. J. Chem.*, 2021, **39**, 614–620.

81 D.-Y. Zhu, W.-D. Li, C. Yang, J. Chen and J.-B. Xia, Transition-Metal-Free Reductive Deoxygenative Olefination with CO_2, *Org. Lett.*, 2018, **20**, 3282–3285.

82 X.-Y. Li, S.-S. Zheng, X.-F. Liu, Z.-W. Yang, T.-Y. Tan, A. Yu and L.-N. He, Waste Recycling: Ionic Liquid-Catalyzed 4-Electron Reduction of CO_2 with Amines and Polymethylhydrosiloxane Combining Experimental and Theoretical Study, *ACS Sustain. Chem. Eng.*, 2018, **6**, 8130–8135.

83 Z.-J. Mu, X. Ding, Z.-Y. Chen and B.-H. Han, Zwitterionic Covalent Organic Frameworks as Catalysts for Hierarchical Reduction of CO_2 with Amine and Hydrosilane, *ACS Appl. Mater. Interfaces*, 2018, **10**, 41350–41358.

84 (*a*) R. Köster and I. Borverbindungen, Darstellung von Bortrialkylen und ihre Reaktionen mit Olefinen, *Justus Liebigs Ann. Chem.*, 1958, **618**, 31–43; (*b*) H. C. Brown and G. Zweifel, Hydroboration. VII. Directive Effects in the Hydroboration of Olefins, *J. Am. Chem. Soc.*, 1960, **82**, 4708–4712; (*c*) H. C. Brown and B. C. S. Rao, A new technique for the conversion of olefins into organoboranes and related alcohols, *J. Am. Chem. Soc.*, 1956, **78**, 5694–5695.

85 (*a*) E. J. Corey, R. K. Bakshi and S. Shibata, Highly enantioselective borane reduction of ketones catalyzed by chiral oxazaborolidines. Mechanism and synthetic implications, *J. Am. Chem. Soc.*, 1987, **109**, 5551–5553; (*b*) E. J. Corey and C. J. Helal, Reduction of Carbonyl Compounds with Chiral Oxazaborolidine Catalysts: A New Paradigm for Enantioselective Catalysis and a Powerful New Synthetic Method, *Angew. Chem., Int. Ed.*, 1998, **37**, 1986–2012.

86 A. Suzuki, Cross-Coupling Reactions Of Organoboranes: An Easy Way To Construct C-C Bonds (Nobel Lecture), *Angew. Chem., Int. Ed.*, 2011, **50**, 6722–6737.

87 Y.-R. Luo and Editor, *Comprehensive Handbook of Chemical Bond Energies*, CRC Press, 2007.

88 S. Chakraborty, J. Zhang, J. A. Krause and H. Guan, An Efficient Nickel Catalyst for the Reduction of Carbon Dioxide with a Borane, *J. Am. Chem. Soc.*, 2010, **132**, 8872–8873.

89 F. Huang, C. Zhang, J. Jiang, Z.-X. Wang and H. Guan, How Does the Nickel Pincer Complex Catalyze the Conversion of CO_2 to a Methanol Derivative? A Computational Mechanistic Study, *Inorg. Chem.*, 2011, **50**, 3816–3825.

90 S. Bontemps, L. Vendier and S. Sabo-Etienne, Borane-Mediated Carbon Dioxide Reduction at Ruthenium: Formation of C_1 and C_2 Compounds, *Angew. Chem., Int. Ed.*, 2012, **51**, 1671–1674.

91 S. Bontemps, L. Vendier and S. Sabo-Etienne, Ruthenium-Catalyzed Reduction of Carbon Dioxide to Formaldehyde, *J. Am. Chem. Soc.*, 2014, **136**, 4419–4425.

92 S. Desmons, Y. Zhou, D. Zhang, C. Jarava-Barrera, A. Coffinet, A. Simonneau, L. Vendier, G. Luo and S. Bontemps, CO_2 Hydroboration: Impact of the Boryl Moieties on the Reactivity of Four Bis(boryl)acetal Compounds toward 2,6-Diisopropylaniline, *Eur. J. Org Chem.*, 2023, **26**, e202300525.

93 G. Jin, C. G. Werncke, Y. Escudié, S. Sabo-Etienne and S. Bontemps, Iron-Catalyzed Reduction of CO_2 into Methylene: Formation of C–N, C–O, and C–C Bonds, *J. Am. Chem. Soc.*, 2015, **137**, 9563–9566.

94 L. J. Murphy, H. Hollenhorst, R. McDonald, M. Ferguson, M. D. Lumsden and L. Turculet, Selective Ni-Catalyzed Hydroboration of CO_2 to the Formaldehyde Level Enabled by New PSiP Ligation, *Organometallics*, 2017, **36**, 3709–3720.

95 H.-W. Suh, L. M. Guard and N. Hazari, Synthesis and reactivity of a masked PSiP pincer supported nickel hydride, *Polyhedron*, 2014, **84**, 37–43.

96 R. Pal, T. L. Groy and R. J. Trovitch, Conversion of Carbon Dioxide to Methanol Using a C–H Activated Bis(imino) pyridine Molybdenum Hydroboration Catalyst, *Inorg. Chem.*, 2015, **54**, 7506–7515.

97 M. R. Espinosa, D. J. Charboneau, A. Garcia de Oliveira and N. Hazari, Controlling Selectivity in the Hydroboration of Carbon Dioxide to the Formic Acid, Formaldehyde, and Methanol Oxidation Levels, *ACS Catal.*, 2019, **9**, 301–314.

98 M. D. Anker, M. Arrowsmith, P. Bellham, M. S. Hill, G. Kociok-Kohn, D. J. Liptrot, M. F. Mahon and C. Weetman, Selective reduction of CO_2 to a methanol equivalent by $B(C_6F_5)_3$-activated alkaline earth catalysis, *Chem. Sci.*, 2014, **5**, 2826–2830.

99 L. Li, H. Zhu, L. Liu, D. Song and M. Lei, A Hydride-Shuttle Mechanism for the Catalytic Hydroboration of CO_2, *Inorg. Chem.*, 2018, **57**, 3054–3060.

100 (*a*) Y. Yang, L. Yan, Q. Xie, Q. Liang and D. Song, Zwitterionic indenylammonium with carbon-centred reactivity towards reversible CO_2 binding and catalytic reduction, *Org. Biomol. Chem.*, 2017, **15**, 2240–2245; (*b*) T. Janes, K. M. Osten, A. Pantaleo, E. Yan, Y. Yang and D. Song, Insertion of CO_2 into the carbon-boron bond of a boronic ester ligand, *Chem. Commun.*, 2016, **52**, 4148–

4151; (*c*) Y. Yang, M. Xu and D. Song, Organocatalysts with carbon-centered activity for CO_2 reduction with boranes, *Chem. Commun.*, 2015, **51**, 11293–11296; (*d*) C. Weetman, A. Porzelt, P. Bag, F. Hanusch and S. Inoue, Dialumenes – aryl vs. silyl stabilisation for small molecule activation and catalysis, *Chem. Sci.*, 2020, **11**, 4817–4827; (*e*) J. Fan, J.-Q. Mah, M.-C. Yang, M.-D. Su and C.-W. So, A N-Phosphinoamidinato NHC-Diborene Catalyst for Hydroboration, *J. Am. Chem. Soc.*, 2021, **143**, 4993–5002.

101 C. Das Neves Gomes, E. Blondiaux, P. Thuéry and T. Cantat, Metal-Free Reduction of CO_2 with Hydroboranes: Two Efficient Pathways at Play for the Reduction of CO_2 to Methanol, *Chem.–Eur. J.*, 2014, **20**, 7098–7106.

102 A. Aloisi, J.-C. Berthet, C. Genre, P. Thuery and T. Cantat, Complexes of the tripodal phosphine ligands PhSi(XPPh2) 3 (X = CH2, O): synthesis, structure and catalytic activity in the hydroboration of CO_2, *Dalton Trans.*, 2016, **45**, 14774–14788.

103 A. Ramos, A. Antinolo, F. Carrillo-Hermosilla, R. Fernandez-Galan, A. Rodriguez-Dieguez and D. Garcia-Vivo, Carbodiimides as catalysts for the reduction of CO_2 with boranes, *Chem. Commun.*, 2018, **54**, 4700–4703.

104 A. Ramos, A. Antiñolo, F. Carrillo-Hermosilla and R. Fernández-Galán, $Ph_2PCH_2CH_2B(C_8H_{14})$ and Its Formaldehyde Adduct as Catalysts for the Reduction of CO_2 with Hydroboranes, *Inorg. Chem.*, 2020, **59**, 9998–10012.

105 S. C. Sau, R. Bhattacharjee, P. K. Vardhanapu, G. Vijaykumar, A. Datta and S. K. Mandal, Metal-Free Reduction of CO_2 to Methoxyborane under Ambient Conditions through Borondiformate Formation, *Angew. Chem., Int. Ed.*, 2016, **55**, 15147–15151.

106 X. Wang, K. Chang and X. Xu, Hydroboration of carbon dioxide enabled by molecular zinc dihydrides, *Dalton Trans.*, 2020, **49**, 7324–7327.

107 M. Frick, J. Horn, H. Wadepohl, E. Kaifer and H. J. Himmel, Catalyst-Free Hydroboration of CO_2 With a Nucleophilic Diborane(4), *Chem.–Eur. J.*, 2018, **24**, 16983–16986.

108 J. Li, C. G. Daniliuc, G. Kehr and G. Erker, Preparation of the Borane (Fmes)BH2 and its Utilization in the FLP Reduction of Carbon Monoxide and Carbon Dioxide, *Angew. Chem. Int. Ed.*, 2019, **58**, 6737–6741.

109 (*a*) R. Declercq, G. Bouhadir, D. Bourissou, M.-A. Légaré, M.-A. Courtemanche, K. S. Nahi, N. Bouchard, F.-G. Fontaine and L. Maron, Hydroboration of Carbon Dioxide using Ambiphilic Phosphine-Borane Catalysts: On the Role of the Formaldehyde Adduct, *ACS Catal.*, 2015, **5**, 2513–2520; (*b*) S. Y. F. Ho, C.-W. So, N. Saffon-Merceron and N. Mezailles, Formation of a zwitterionic boronium species from the reaction of a stable carbenoid with borane: CO_2 reduction, *Chem. Commun.*, 2015, **51**, 2107–2110.

110 M.-A. Courtemanche, A. P. Pulis, E. Rochette, M.-A. Legare, D. W. Stephan and F.-G. Fontaine, Intramolecular B/N frustrated Lewis pairs and the hydrogenation of carbon dioxide, *Chem. Commun.*, 2015, **51**, 9797–9800.

111 J. H. W. LaFortune, Z. W. Qu, K. L. Bamford, A. Trofimova, S. A. Westcott and D. W. Stephan, Double Phosphinoboration of CO_2: A Facile Route to Diphospha-Ureas, *Chem.–Eur. J.*, 2019, **25**, 12063–12067.

112 S. Bontemps and S. Sabo-Etienne, Trapping Formaldehyde in the Homogeneous Catalytic Reduction of Carbon Dioxide, *Angew. Chem., Int. Ed.*, 2013, **52**, 10253–10255.

113 (*a*) C. Dong, M. Ji, X. Yang, J. Yao and H. Chen, Reaction Mechanisms of CO_2 Reduction to Formaldehyde Catalyzed by Hourglass Ru, Fe, and Os Complexes: A Density Functional Theory Study, *Catalysts*, 2017, **7**, 5; (*b*) F. Huang, Q. Wang, J. Guo, M. Wen and Z.-X. Wang, Computational mechanistic study of Ru-catalyzed CO_2 reduction by pinacolborane revealing the σ-π coupling mechanism for CO_2 decarbonylation, *Dalton Trans.*, 2018, **47**, 4804–4819.

114 A. Caise, D. Jones, E. L. Kolychev, J. Hicks, J. M. Goicoechea and S. Aldridge, On the Viability of Catalytic Turnover via Al–O/B–H Metathesis: The Reactivity of β-Diketiminate Aluminium Hydrides towards CO_2 and Boranes, *Chem.–Eur. J.*, 2018, **24**, 13624–13635.

115 N. Ma, C. Tu, Q. Xu, W. Guo, J. Zhang and G. Zhang, Computational study on the mechanism of hydroboration of CO_2 catalysed by POCOP pincer nickel thiolate complexes: concerted catalysis and hydride transfer by a shuttle, *Dalton Trans.*, 2021, **50**, 2903–2914.

116 (*a*) X. Wan, M. Li and R.-Z. Liao, Ligand-assisted Hydride Transfer: A Pivotal Step for CO_2 Hydroboration Catalyzed by a Mononuclear Mn(I) PNP Complex, *Chem.–Asian J.*, 2021, **16**, 2529–2537; (*b*) C. Erken, A. Kaithal, S. Sen, T. Weyhermüller, M. Hölscher, C. Werlé and W. Leitner, Manganese-catalyzed hydroboration of carbon dioxide and other challenging carbonyl groups, *Nat. Commun.*, 2018, **9**, 4521.

117 H. Sabet-Sarvestani, M. Izadyar and H. Eshghi, Theoretical evaluation of the organocatalytic behavior of the negatively charged carbon atom in a fused five-member ring in carbon dioxide transformation to methanol, *Energy*, 2017, **134**, 493–503.

118 (*a*) M.-A. Courtemanche, M.-A. Légaré, L. Maron and F.-G. Fontaine, Reducing CO_2 to Methanol Using Frustrated Lewis Pairs: On the Mechanism of Phosphine–Borane-Mediated Hydroboration of CO_2, *J. Am. Chem. Soc.*, 2014, **136**, 10708–10717; (*b*) M.-A. Courtemanche, M.-A. Légaré, L. Maron and F.-G. Fontaine, A Highly Active Phosphine–Borane Organocatalyst for the Reduction of CO_2 to Methanol Using Hydroboranes, *J. Am. Chem. Soc.*, 2013, **135**, 9326–9329.

119 Z.-W. Qu, H. Zhu and S. Grimme, Frustrated Lewis Pair Catalyzed Reduction of Carbon Dioxide Using Hydroboranes: New DFT Mechanistic Insights, *ChemCatChem*, 2020, **12**, 3656–3660.

120 T. Wang and D. W. Stephan, Phosphine catalyzed reduction of CO_2 with boranes, *Chem. Commun.*, 2014, **50**, 7007–7010.

121 Y. C. A. Sokolovicz, O. Nieto Faza, D. Specklin, B. Jacques, C. S. López, J. H. Z. dos Santos, H. S. Schrekker and S. Dagorne, Acetate-catalyzed hydroboration of CO_2 for

the selective formation of methanol-equivalent products, *Catal. Sci. Technol.*, 2020, **10**, 2407–2414.

122 Z. M. Heiden and A. P. Lathem, Establishing the Hydride Donor Abilities of Main Group Hydrides, *Organometallics*, 2015, **34**, 1818–1827.

123 H. Gao, J. Jia, C.-H. Tung and W. Wang, Iron-Catalyzed Selective Hydroboration of CO_2 by Cooperative B–H Bond Activation, *Organometallics*, 2023, **42**, 944–951.

124 W. Huadsai, M. Westerhausen and S. Bontemps, Alkaline Earth Catalyzed CO_2 Hydroboration into Acetal Derivatives Leading to C–S Bond Formation, *Organometallics*, 2023, **42**, 2921–2926.

125 A. Butlerow, Formation synthétique d'une substance sucrée, *Cr. Acad. Sci.*, 1861, **53**, 145–147.

126 J. Henrique Teles, J.-P. Melder, K. Ebel, R. Schneider, E. Gehrer, W. Harder, S. Brode, D. Enders, K. Breuer and G. Raabe, The Chemistry of Stable Carbenes. Part 2. Benzoin-type condensations of formaldehyde catalyzed by stable carbenes, *Helv. Chim. Acta*, 1996, **79**, 61–83.

127 A. M. Fajardo, N. Queyriaux, A. Camy, L. Vendier, M. Grellier, I. del Rosal, L. Maron and S. Bontemps, A Masked Form of an O-Borylated Breslow Intermediate for the Diastereoselective FLP-Type Activation of Aldehydes, *Chem.–Eur. J.*, 2022, **28**, e202104122.

128 (*a*) I. V. Delidovich, A. N. Simonov, O. P. Pestunova and V. N. Parmon, Catalytic condensation of glycolaldehyde and glyceraldehyde with formaldehyde in neutral and weakly alkaline aqueous media: Kinetics and mechanism, *Kinet. Catal.*, 2009, **50**, 297–303; (*b*) J. Castells, F. Geijo and F. López-Calahorra, The "formoin reaction" : A promising entry to carbohydrates from formaldehyde, *Tetrahedron Lett.*, 1980, **21**, 4517–4520.

129 J. J. A. G. Kamps, R. J. Hopkinson, C. J. Schofield and T. D. W. Claridge, How formaldehyde reacts with amino acids, *Commun. Chem.*, 2019, **2**, 126.

130 (*a*) T. Zhou, J. J. Vallooran, S. Assenza, A. Szekrenyi, P. Clapés and R. Mezzenga, Efficient Asymmetric Synthesis of Carbohydrates by Aldolase Nano-Confined in Lipidic Cubic Mesophases, *ACS Catal.*, 2018, **8**, 5810–5815; (*b*) A. Szekrenyi, X. Garrabou, T. Parella, J. Joglar, J. Bujons and P. Clapés, Asymmetric Assembly of Aldose Carbohydrates from Formaldehyde and Glycolaldehyde by Tandem Biocatalytic Aldol Reactions, *Nat. Chem.*, 2015, **7**, 724–729; (*c*) J. A. Castillo, C. Guérard-Hélaine, M. Gutiérrez, X. Garrabou, M. Sancelme, M. Schürmann, T. Inoue, V. Hélaine, F. Charmantray, T. Gefflaut, L. Hecquet, J. Joglar, P. Clapés, G. A. Sprenger and M. Lemaire, A Mutant D-Fructose-6-Phosphate Aldolase (Ala129Ser) with Improved Affinity towards Dihydroxyacetone for the Synthesis of Polyhydroxylated Compounds, *Adv. Synth. Catal.*, 2010, **352**, 1039–1046; (*d*) S. Güner, V. Wegat, A. Pick and V. Sieber, Design of a synthetic enzyme cascade for the in vitro fixation of a C_1 carbon source to a functional C_4 sugar, *Green Chem.*, 2021, **23**, 6583–6590; (*e*) T. Li, Z. Tang, H. Wei, Z. Tan, P. Liu, J. Li, Y. Zheng, J. Lin, W. Liu, H. Jiang, H. Liu, L. Zhu and Y. Ma, Totally atom-economical synthesis of lactic acid from formaldehyde: combined bio-carboligation and chemo-rearrangement without the isolation of intermediates, *Green Chem.*, 2020, **22**, 6809–6814; (*f*) J. B. Siegel, A. L. Smith, S. Poust, A. J. Wargacki, A. Bar-Even, C. Louw, B. W. Shen, C. B. Eiben, H. M. Tran, E. Noor, J. L. Gallaher, J. Bale, Y. Yoshikuni, M. H. Gelb, J. D. Keasling, B. L. Stoddard, M. E. Lidstrom and D. Baker, Computational Protein Design Enables a Novel one-Carbon Assimilation Pathway, *Proc. Natl. Acad. Sci. U. S. A.*, 2015, **112**, 3704–3709; (*g*) S. Poust, J. Piety, A. Bar-Even, C. Louw, D. Baker, J. D. Keasling and J. B. Siegel, Mechanistic Analysis of an Engineered Enzyme that Catalyzes the Formose Reaction, *ChemBioChem*, 2015, **16**, 1950–1954.

131 X. Garrabou, J. A. Castillo, C. Guérard-Hélaine, T. Parella, J. Joglar, M. Lemaire and P. Clapés, Asymmetric Self- and Cross-Aldol Reactions of Glycolaldehyde Catalyzed by D-Fructose-6-phosphate Aldolase, *Angew. Chem., Int. Ed.*, 2009, **121**, 5629–5633.

132 J. Yang, S. Sun, Y. Men, Y. Zeng, Y. Zhu, Y. Sun and Y. Ma, Transformation of Formaldehyde into Functional Sugars via Multi-Enzyme Stepwise Cascade Catalysis, *Catal. Sci. Technol.*, 2017, **7**, 3459–3463.

133 J.-C. Berthet and M. Ephritikhine, Reactions of the uranium (IV) hydride $(C_5H_4SiMe_3)_3UH$ including the first transformation : 2 [M]-H + CO_2 -> [M]-O-CH_2-O-[M], *New J. Chem.*, 1992, **16**, 767–768.

134 (*a*) N. E. Schlörer, E. J. Cabrita and S. Berger, Characterization of Reactive Intermediates by Diffusion-Ordered NMR Spectroscopy: A Snapshot of the Reaction of $^{13}CO_2$ with $[Cp_2Zr(Cl)H]$, *Angew. Chem., Int. Ed.*, 2002, **41**, 107–109; (*b*) N. E. Schlörer and S. Berger, First Spectroscopical Evidence of a Dioxomethylene Intermediate in the Reaction of CO_2 with $Cp_2Zr(H)Cl$: A ^{13}C NMR Study, *Organometallics*, 2001, **20**, 1703–1704.

135 (*a*) A. Mendiratta, J. S. Figueroa and C. C. Cummins, Synthesis of a four-coordinate titanium(iv) oxoanion via deprotonation and decarbonylation of complexed formate, *Chem. Commun.*, 2005, 3403–3405; (*b*) M. A. Rankin and C. C. Cummins, Carbon Dioxide Reduction by Terminal Tantalum Hydrides: Formation and Isolation of Bridging Methylene Diolate Complexes, *J. Am. Chem. Soc.*, 2010, **132**, 10021–10023.

136 J. Ballmann, F. Pick, L. Castro, M. D. Fryzuk and L. Maron, Reduction of Carbon Dioxide Promoted by a Dinuclear Tantalum Tetrahydride Complex, *Inorg. Chem.*, 2013, **52**, 1685–1687.

137 O. Tardif, D. Hashizume and Z. Hou, Hydrogenation of Carbon Dioxide and Aryl Isocyanates by a Tetranuclear Tetrahydrido Yttrium Complex. Isolation, Structures, and CO_2 Insertion Reactions of Methylene Diolate and μ3-Oxo Yttrium Complexes, *J. Am. Chem. Soc.*, 2004, **126**, 8080–8081.

138 (*a*) K.-C. Lau, B. J. Petro, S. Bontemps and R. F. Jordan, Comparative Reactivity of Zr– and Pd–Alkyl Complexes with Carbon Dioxide, *Organometallics*, 2013, **32**, 6895–6898; (*b*) M. Hill and O. F. Wendt, Reactivity of Carbon

Dioxide toward Zirconocene Cations, *Organometallics*, 2005, **24**, 5772–5775; (*c*) N. Hazari and J. E. Heimann, Carbon Dioxide Insertion into Group 9 and 10 Metal–Element σ Bonds, *Inorg. Chem.*, 2017, **56**(22), 13655–13678; (*d*) A. P. Deziel, M. R. Espinosa, L. Pavlovic, D. J. Charboneau, N. Hazari, K. H. Hopmann and B. Q. Mercado, Ligand and solvent effects on CO_2 insertion into group 10 metal alkyl bonds, *Chem. Sci.*, 2022, **13**, 2391–2404.

139 (*a*) S. Gambarotta, S. Strologo, C. Floriani, A. Chiesi-Villa and C. Guastini, Stepwise reduction of carbon dioxide to formaldehyde and methanol: reactions of carbon dioxide and carbon dioxide like molecules with hydridochlorobis(cyclopentadienyl)zirconium(IV), *J. Am. Chem. Soc.*, 1985, **107**, 6278–6282; (*b*) G. Fachinetti, C. Floriani and S. Pucci, Stoicheiometric reduction of CO and CO_2 to methanol: evidence for carbon monoxide insertion into zirconium–hydrogen bond, *J. Chem. Soc., Chem. Commun.*, 1978, 269–270; (*c*) J. A. Labinger, Titanium, zirconium and hafnium: Annual survey covering the year 1976, *J. Organomet. Chem.*, 1977, **138**, 185–210; (*d*) G. Fachinetti, C. Floriani, A. Chiesi-Villa and C. Guastini, Carbon dioxide activation. Deoxygenation and disproportionation of carbon dioxide promoted by bis(cyclopentadienyl)titanium and -zirconium derivatives. A novel bonding mode of the carbonato and a trimer of the zirconyl unit, *J. Am. Chem. Soc.*, 1979, **101**, 1767–1775.

140 D. Spencer and T. Henshall, The Kinetics and Mechanism of the Reaction of Formaldehyde with Dimedone. Part I, *J. Am. Chem. Soc.*, 1955, **77**, 1943–1948.

141 C. C. Chong and R. Kinjo, Hydrophosphination of CO_2 and Subsequent Formate Transfer in the 1,3,2-Diazaphospholene-Catalyzed N-Formylation of Amines, *Angew. Chem., Int. Ed.*, 2015, **54**, 12116–12120.

142 D. Gudat, in *Encyclopedia of Inorganic and Bioinorganic Chemistry*, 2018, pp. 1–23, DOI: **10.1002/9781119951438.eibc2642**.

143 J. Wei, R. Yao, Y. Han, Q. Ge and J. Sun, Towards the development of the emerging process of CO_2 heterogenous hydrogenation into high-value unsaturated heavy hydrocarbons, *Chem. Soc. Rev.*, 2021, **50**, 10764–10805.

144 M. M. T. Khan, S. B. Halligudi and S. Shukla, Reduction of CO_2 by molecular hydrogen to formic acid and formaldehyde and their decomposition to CO and H_2O, *J. Mol. Catal.*, 1989, **57**, 47–60.

145 D.-K. Lee, D.-S. Kim and S.-W. Kim, Selective formation of formaldehyde from carbon dioxide and hydrogen over $PtCu/SiO_2$, *Appl. Organomet. Chem.*, 2001, **15**, 148–150.

146 S. Carenco, C.-H. Wu, A. Shavorskiy, S. Alayoglu, G. A. Somorjai, H. Bluhm and M. Salmeron, Synthesis and Structural Evolution of Nickel–Cobalt Nanoparticles Under H_2 and CO_2, *Small*, 2015, **11**, 3045–3053.

147 F. L. Chan, G. Altinkaya, N. Fung and A. Tanksale, Low temperature hydrogenation of carbon dioxide into formaldehyde in liquid media, *Catal. Today*, 2018, **309**, 242–247.

148 L. Deng, X. Liu, J. Xu, Z. Zhou, S. Feng, Z. Wang and M. Xu, Transfer hydrogenation of CO_2 into formaldehyde from aqueous glycerol heterogeneously catalyzed by Ru bound to LDH, *Chem. Commun.*, 2021, **57**, 5167–5170.

149 U. Kleeberg and W. Klinger, Sensitive formaldehyde determination with NASH's reagent and a 'tryptophan reaction', *J. Pharmacol. Methods*, 1982, **8**, 19–31.

150 J. Zhang, C. Xing, B. Tiwari and Y. R. Chi, Catalytic Activation of Carbohydrates as Formaldehyde Equivalents for Stetter Reaction with Enones, *J. Am. Chem. Soc.*, 2013, **135**, 8113–8116.

151 (*a*) K. Thenert, K. Beydoun, J. Wiesenthal, W. Leitner and J. Klankermayer, Ruthenium-Catalyzed Synthesis of Dialkoxymethane Ethers Utilizing Carbon Dioxide and Molecular Hydrogen, *Angew. Chem., Int. Ed.*, 2016, **55**, 12266–12269; (*b*) B. G. Schieweck and J. Klankermayer, Tailor-made Molecular Cobalt Catalyst System for the Selective Transformation of Carbon Dioxide to Dialkoxymethane Ethers, *Angew. Chem., Int. Ed.*, 2017, **56**, 10854–10857.

152 (*a*) F. A. Long and D. McIntyre, Acid-catalyzed Hydrolysis of Methylal. II. Kinetic and Equilibrium Salt Effects and Correlation with H_0, *J. Am. Chem. Soc.*, 1954, **76**, 3243–3247; (*b*) D. McIntyre and F. A. Long, Acid-catalyzed Hydrolysis of Methylal. I. Influence of Strong Acids and Correlation with Hammett Acidity Function, *J. Am. Chem. Soc.*, 1954, **76**, 3240–3242.

153 (*a*) S. Dabral and T. Schaub, The Use of Carbon Dioxide (CO_2) as a Building Block in Organic Synthesis from an Industrial Perspective, *Adv. Synth. Catal.*, 2019, **361**, 223–246; (*b*) Z. Wei, X. Tian, M. Bender, M. Beller and H. Jiao, Mechanisms of CoII and Acid Jointly Catalyzed Domino Conversion of CO_2, H_2, and CH_3OH to Dialkoxymethane: A DFT Study, *ACS Catal.*, 2021, 6908–6919.

154 M. Siebert, M. Seibicke, A. F. Siegle, S. Kräh and O. Trapp, Selective Ruthenium-Catalyzed Transformation of Carbon Dioxide: An Alternative Approach toward Formaldehyde, *J. Am. Chem. Soc.*, 2019, **141**, 334–341.

155 M. Siebert, G. Krennrich, M. Seibicke, A. F. Siegle and O. Trapp, Identifying high-performance catalytic conditions for carbon dioxide reduction to dimethoxymethane by multivariate modelling, *Chem. Sci.*, 2019, **10**, 10466–10474.

156 M. Seibicke, M. Siebert, A. F. Siegle, S. M. Gutenthaler and O. Trapp, Application of Hetero-Triphos Ligands in the Selective Ruthenium-Catalyzed Transformation of Carbon Dioxide to the Formaldehyde Oxidation State, *Organometallics*, 2019, **38**, 1809–1814.

157 R. Konrath, K. Sekine, I. Jevtovikj, R. A. Paciello, A. S. K. Hashmi and T. Schaub, Performance enhancing additives for reusable ruthenium-triphos catalysts in the reduction of CO_2 to dimethoxymethane, *Green Chem.*, 2020, **22**, 6464–6470.

158 K. Beydoun and J. Klankermayer, Ruthenium-Catalyzed Synthesis of Cyclic and Linear Acetals by the Combined Utilization of CO_2, H_2, and Biomass Derived Diols, *Chem.–Eur. J.*, 2019, **25**, 11412–11415.

159 C. A. Huff and M. S. Sanford, Cascade Catalysis for the Homogeneous Hydrogenation of CO$_2$ to Methanol, *J. Am. Chem. Soc.*, 2011, **133**, 18122–18125.

160 N. M. Rezayee, C. A. Huff and M. S. Sanford, Tandem Amine and Ruthenium-Catalyzed Hydrogenation of CO$_2$ to Methanol, *J. Am. Chem. Soc.*, 2015, **137**, 1028–1031.

161 M. Leopold, M. Siebert, A. F. Siegle and O. Trapp, Reaction Network Analysis of the Ruthenium-Catalyzed Reduction of Carbon Dioxide to Dimethoxymethane, *ChemCatChem*, 2021, **13**, 2807–2814.

162 J. D. Erickson, A. Z. Preston, J. C. Linehan and E. S. Wiedner, Enhanced Hydrogenation of Carbon Dioxide to Methanol by a Ruthenium Complex with a Charged Outer-Coordination Sphere, *ACS Catal.*, 2020, 7419–7423.

163 (*a*) S. Wesselbaum, V. Moha, M. Meuresch, S. Brosinski, K. M. Thenert, J. Kothe, T. vom Stein, U. Englert, M. Holscher, J. Klankermayer and W. Leitner, Hydrogenation of carbon dioxide to methanol using a homogeneous ruthenium-Triphos catalyst: from mechanistic investigations to multiphase catalysis, *Chem. Sci.*, 2015, **6**, 693–704; (*b*) S. Wesselbaum, T. vom Stein, J. Klankermayer and W. Leitner, Hydrogenation of Carbon Dioxide to Methanol by Using a Homogeneous Ruthenium–Phosphine Catalyst, *Angew. Chem., Int. Ed.*, 2012, **51**, 7499–7502; (*c*) K. Beydoun, G. Ghattas, K. Thenert, J. Klankermayer and W. Leitner, Ruthenium-Catalyzed Reductive Methylation of Imines Using Carbon Dioxide and Molecular Hydrogen, *Angew. Chem., Int. Ed.*, 2014, **53**, 11010–11014; (*d*) K. Beydoun, T. vom Stein, J. Klankermayer and W. Leitner, Ruthenium-Catalyzed Direct Methylation of Primary and Secondary Aromatic Amines Using Carbon Dioxide and Molecular Hydrogen, *Angew. Chem., Int. Ed.*, 2013, **52**, 9554–9557; (*e*) Y. Li, T. Yan, K. Junge and M. Beller, Catalytic Methylation of C-H Bonds Using CO$_2$ and H$_2$, *Angew. Chem., Int. Ed.*, 2014, **126**, 10644–10648; (*f*) Y. Li, I. Sorribes, T. Yan, K. Junge and M. Beller, Selective Methylation of Amines with Carbon Dioxide and H$_2$, *Angew. Chem., Int. Ed.*, 2013, **52**, 12156–12160.

164 A. N. Simonov, L. G. Matvienko, O. P. Pestunova, V. N. Parmon, N. A. Komandrova, V. A. Denisenko and V. E. Vas'kovskii, Selective synthesis of erythrulose and 3-pentulose from formaldehyde and dihydroxyacetone catalyzed by phosphates in a neutral aqueous medium, *Kinet. Catal.*, 2007, **48**, 550–555.

165 E. Boutin and M. Robert, Molecular Electrochemical Reduction of CO$_2$ beyond Two Electrons, *Trends Chem.*, 2021, **3**, 359–372.

166 (*a*) H. Nagao, T. Mizukawa and K. Tanaka, Carbon-Carbon Bond Formation in the Electrochemical Reduction of Carbon Dioxide Catalyzed by a Ruthenium Complex, *Inorg. Chem.*, 1994, **33**, 3415–3420; (*b*) N. Hirotaka, M. Tetsunori and T. Koji, Carbon-Carbon Bond Formation in Multi-electron Reduction of Carbon Dioxide Catalyzed by $[Ru(bpy)(trpy)(CO)]^{2+}$ (bpy = 2,2′-bipyridine; trpy = 2,2′:6′,2″-terpyridine), *Chem. Lett.*, 1993, **22**, 955–958.

167 D. Xiang, D. Magana and R. B. Dyer, CO$_2$ Reduction Catalyzed by Mercaptopteridine on Glassy Carbon, *J. Am. Chem. Soc.*, 2014, **136**, 14007–14010.

168 M. Girardi, S. Blanchard, S. Griveau, P. Simon, M. Fontecave, F. Bedioui and A. Proust, Electro-Assisted Reduction of CO$_2$ to CO and Formaldehyde by (TOA)$_6$[α-SiW$_{11}$O$_{39}$Co(_)] Polyoxometalate, *Eur. J. Inorg. Chem.*, 2015, **2015**, 3642–3648.

169 S. Gonglach, S. Paul, M. Haas, F. Pillwein, S. S. Sreejith, S. Barman, R. De, S. Müllegger, P. Gerschel, U.-P. Apfel, H. Coskun, A. Aljabour, P. Stadler, W. Schöfberger and S. Roy, Molecular cobalt corrole complex for the heterogeneous electrocatalytic reduction of carbon dioxide, *Nat. Commun.*, 2019, **10**, 3864.

170 J. A. Ramos Sende, C. R. Arana, L. Hernandez, K. T. Potts, M. Keshevarz-K and H. D. Abruna, Electrocatalysis of CO$_2$ Reduction in Aqueous Media at Electrodes Modified with Electropolymerized Films of Vinylterpyridine Complexes of Transition Metals, *Inorg. Chem.*, 1995, **34**, 3339–3348.

171 K. Kusuda, R. Ishihara, H. Yamaguchi and I. Izumi, Electrochemical investigation of thin films of cobalt phthalocyanine and cobalt-4,4′,4″,4‴-tetracarboxyphthalocyanine and the reduction of carbon monoxide, formic acid and formaldehyde mediated by the Co(I) complexes, *Electrochim. Acta*, 1986, **31**, 657–663.

172 E. Boutin, A. Salamé, L. Merakeb, T. Chatterjee and M. Robert, On the Existence and Role of Formaldehyde During Aqueous Electrochemical Reduction of Carbon Monoxide to Methanol by Cobalt Phthalocyanine, *Chem.–Eur. J.*, 2022, **28**, e202200697.

173 A. Singh, A. Zamader, R. Khakpour, K. Laasonen, M. Busch and M. Robert, Molecular electrochemical catalysis of CO-to-formaldehyde conversion with a Cobalt complex, *J. Am. Chem. Soc.*, 2024, **146**(32), 22129–22133.

174 (*a*) K. Nakata, T. Ozaki, C. Terashima, A. Fujishima and Y. Einaga, High-Yield Electrochemical Production of Formaldehyde from CO$_2$ and Seawater, *Angew. Chem., Int. Ed.*, 2014, **53**, 871–874; (*b*) D. Luo, S. Liu, K. Nakata and A. Fujishima, Electrochemical reduction of CO2 and degradation of KHP on boron-doped diamond electrodes in a simultaneous and enhanced process, *Chin. Chem. Lett.*, 2019, **30**, 509–512.

175 J. Bin Yeo, J. Ho Jang, Y. In Jo, J. Woo Koo and K. Tae Nam, Paired Electrosynthesis of Formaldehyde Derivatives from CO$_2$ Reduction and Methanol Oxidation, *Angew. Chem., Int. Ed.*, 2024, **63**, e202316020.

176 (*a*) M. Shibata and N. Furuya, Electrochemical synthesis of urea at gas-diffusion electrodes: Part VI. Simultaneous reduction of carbon dioxide and nitrite ions with various metallophthalocyanine catalysts, *J. Electroanal. Chem.*, 2001, **507**, 177–184; (*b*) M. Shibata, K. Yoshida and N. Furuya, Electrochemical synthesis of urea on reduction of carbon dioxide with nitrate and nitrite ions using Cu-loaded gas-diffusion electrode, *J. Electroanal. Chem.*, 1995, **387**, 143–145.

177 Y. Wu, Z. Jiang, Z. Lin, Y. Liang and H. Wang, Direct electrosynthesis of methylamine from carbon dioxide and nitrate, *Nat. Sustain.*, 2021, **4**, 725–730.

178 (*a*) B. Kumar, M. Llorente, J. Froehlich, T. Dang, A. Sathrum and C. P. Kubiak, Photochemical and Photoelectrochemical Reduction of CO_2, *Annu. Rev. Phys. Chem.*, 2012, **63**, 541–569; (*b*) J. Wu, Y. Huang, W. Ye and Y. Li, CO_2 Reduction: From the Electrochemical to Photochemical Approach, *Adv. Sci.*, 2017, **4**, 1700194; (*c*) A. U. Pawar, C. W. Kim, M.-T. Nguyen-Le and Y. S. Kang, General Review on the Components and Parameters of Photoelectrochemical System for CO_2 Reduction with in Situ Analysis, *ACS Sustain. Chem. Eng.*, 2019, **7**, 7431–7455; (*d*) P. R. Yaashikaa, P. Senthil Kumar, S. J. Varjani and A. Saravanan, A review on photochemical, biochemical and electrochemical transformation of CO_2 into value-added products, *J. CO_2 Util.*, 2019, **33**, 131–147.

179 T. D. Nguyen, T. Van Tran, S. Singh, P. T. T. Phuong, L. G. Bach, S. Nanda and D.-V. N. Vo, in *Conversion of Carbon Dioxide into Hydrocarbons Vol. 2 Technology*, ed. Inamuddin, A. M. Asiri and E. Lichtfouse, Springer International Publishing, Cham, 2020, ch. 6, pp. 159–183, DOI: **10.1007/978-3-030-28638-5_6**.

180 M. Bonchio, J. Bonin, O. Ishitani, T.-B. Lu, T. Morikawa, A. J. Morris, E. Reisner, D. Sarkar, F. M. Toma and M. Robert, Best practices for experiments and reporting in photocatalytic CO_2 reduction, *Nat. Catal.*, 2023, **6**, 657–665.

181 E. C. C. Baly, I. M. Heilbron and W. F. Barker, CX.—Photocatalysis. Part I. The synthesis of formaldehyde and carbohydrates from carbon dioxide and water, *J. Chem. Soc., Trans.*, 1921, **119**, 1025–1035.

182 T. Inoue, A. Fujishima, S. Konishi and K. Honda, Photoelectrocatalytic reduction of carbon dioxide in aqueous suspensions of semiconductor powders, *Nature*, 1979, **277**, 637–638.

183 B. Aurian-Blajeni, M. Halmann and J. Manassen, Photoreduction of carbon dioxide and water into formaldehyde and methanol on semiconductor materials, *Sol. Energy*, 1980, **25**, 165–170.

184 M. Ulman, A. H. A. Tinnemans, A. Mackor, B. Aurian-Blajeni and M. Halmann, Photoreduction of Carbon Dioxide to Formic Acid, Formaldehyde, Methanol, Acetaldehyde and Ethanol Using Aqueous Suspensions of Strontium Titanate with Transition Metal Additives, *Int. J. Sol. Energy*, 1982, **1**, 213–222.

185 S. M. Aliwi and K. F. Al-Jubori, Photoreduction of CO_2 by metal sulphide semiconductors in presence of H_2S, *Sol. Energy Mater.*, 1989, **18**, 223–229.

186 F. Solymosi and I. Tombácz, Photocatalytic reaction of H_2O+CO_2 over pure and doped Rh/TiO_2, *Catal. Lett.*, 1994, **27**, 61–65.

187 E. Bahadori, A. Tripodi, A. Villa, C. Pirola, L. Prati, G. Ramis, N. Dimitratos, D. Wang and I. Rossetti, High pressure CO_2 photoreduction using Au/TiO_2: unravelling the effect of co-catalysts and of titania polymorphs, *Catal. Sci. Technol.*, 2019, **9**, 2253–2265.

188 S. Zeng, E. Vahidzadeh, C. G. VanEssen, P. Kar, R. Kisslinger, A. Goswami, Y. Zhang, N. Mahdi, S. Riddell, A. E. Kobryn, S. Gusarov, P. Kumar and K. Shankar, Optical control of selectivity of high rate CO_2 photoreduction via interband- or hot electron Z-scheme reaction pathways in Au-TiO_2 plasmonic photonic crystal photocatalyst, *Appl. Catal., B*, 2020, **267**, 118644.

189 F. Galli, M. Compagnoni, D. Vitali, C. Pirola, C. L. Bianchi, A. Villa, L. Prati and I. Rossetti, CO_2 photoreduction at high pressure to both gas and liquid products over titanium dioxide, *Appl. Catal., B*, 2017, **200**, 386–391.

190 I. Moriya, Converting of CO_2 into low-molecular-weight organic compounds with the TiO_2/ZrO_2 composites under solar irradiation, *Sci. Rep.*, 2017, **7**, 14446.

191 J. M. Mora-Hernandez, A. M. Huerta-Flores and L. M. Torres-Martínez, Photoelectrocatalytic characterization of carbon-doped $NaTaO_3$ applied in the photoreduction of CO_2 towards the formaldehyde production, *J. CO_2 Util.*, 2018, **27**, 179–187.

192 M. Lashgari and S. Soodi, Photocatalytic Conversion of CO_2 into Oxygenate Fuels/Chemicals Using Efficient, Eco-Friendly, Titania/Hematite-Based Nanostructured Solar-Energy Materials, *J. Nanosci. Nanotechnol.*, 2019, **19**, 3237–3243.

193 Z. Zhao, J. Fan, S. Liu and Z. Wang, Optimal design and preparation of titania-supported CoPc using sol–gel for the photo-reduction of CO_2, *Chem. Eng. J.*, 2009, **151**, 134–140.

194 A. Kumar and R. Ananthakrishnan, Visible light-assisted reduction of CO_2 into formaldehyde by heteroleptic ruthenium metal complex–TiO_2 hybrids in an aqueous medium, *Green Chem.*, 2020, **22**, 1650–1661.

195 B. Kim, D. Kwon, J.-O. Baeg, M. Austeria P, G. H. Gu, J.-H. Lee, J. Jeong, W. Kim and W. Choi, Dual-Atom-Site Sn-Cu/C_3N_4 Photocatalyst Selectively Produces Formaldehyde from CO_2 Reduction, *Adv. Funct. Mater.*, 2023, **33**, 2212453.

196 G. Guan, T. Kida, T. Harada, M. Isayama and A. Yoshida, Photoreduction of carbon dioxide with water over $K_2Ti_6O_{13}$ photocatalyst combined with Cu/ZnO catalyst under concentrated sunlight, *Appl. Catal., A*, 2003, **249**, 11–18.

197 M. Guo, F. Gu, L. Meng, Q. Liao, Z. Meng and W. Liu, Synthesis of formaldehyde from CO_2 catalyzed by the coupled photo-enzyme system, *Sep. Purif. Technol.*, 2022, **286**, 120480.

198 S. N. Habisreutinger, L. Schmidt-Mende and J. K. Stolarczyk, Photocatalytic Reduction of CO_2 on TiO_2 and Other Semiconductors, *Angew. Chem., Int. Ed.*, 2013, **52**, 7372–7408.

199 X. Chang, T. Wang, P. Yang, G. Zhang and J. Gong, The Development of Cocatalysts for Photoelectrochemical CO_2 Reduction, *Adv. Mater.*, 2019, **31**, 1804710.

200 B. Aurian-Blajeni, I. Taniguchi and J. O. M. Bockris, Photoelectrochemical reduction of carbon dioxide using polyaniline-coated silicon, *J. Electroanal. Chem.*, 1983, **149**, 291–293.

201 M. Zafrir, M. Ulman, Y. Zuckerman and M. Halmann, Photoelectrochemical reduction of carbon dioxide to formic acid, formaldehyde and methanol on p-gallium arsenide in an aqueous V(II)-V(III) chloride redox system, *J. Electroanal. Chem.*, 1983, **159**, 373–389.

202 G. Qin, Y. Zhang, X. Ke, X. Tong, Z. Sun, M. Liang and S. Xue, Photocatalytic reduction of carbon dioxide to formic acid, formaldehyde, and methanol using dye-sensitized TiO_2 film, *Appl. Catal., B*, 2013, **129**, 599–605.

203 J. F. de Brito, A. R. Araujo, K. Rajeshwar and M. V. B. Zanoni, Photoelectrochemical reduction of CO_2 on Cu/Cu_2O films: Product distribution and pH effects, *Chem. Eng. J.*, 2015, **264**, 302–309.

204 C. W. Kim, M. J. Kang, S. Ji and Y. S. Kang, Artificial Photosynthesis for Formaldehyde Production with 85% of Faradaic Efficiency by Tuning the Reduction Potential, *ACS Catal.*, 2018, **8**, 968–974.

205 A. U. Pawar, U. Pal, J. Y. Zheng, C. W. Kim and Y. S. Kang, Thermodynamically controlled photo-electrochemical CO_2 reduction at Cu/rGO/PVP/Nafion multi-layered dark cathode for selective production of formaldehyde and acetaldehyde, *Appl. Catal., B*, 2022, **303**, 120921.

206 S. Das, S. Biswas, T. Balaraju, S. Barman, R. Pochamoni and S. Roy, Photochemical reduction of carbon dioxide coupled with water oxidation using various soft-oxometalate (SOM) based catalytic systems, *J. Mater. Chem. A*, 2016, **4**, 8875–8887.

207 D. J. Boston, C. Xu, D. W. Armstrong and F. M. MacDonnell, Photochemical Reduction of Carbon Dioxide to Methanol and Formate in a Homogeneous System with Pyridinium Catalysts, *J. Am. Chem. Soc.*, 2013, **135**, 16252–16255.

208 D. J. Boston, Y. M. F. Pachón, R. O. Lezna, N. R. de Tacconi and F. M. MacDonnell, Electrocatalytic and Photocatalytic Conversion of CO_2 to Methanol using Ruthenium Complexes with Internal Pyridyl Cocatalysts, *Inorg. Chem.*, 2014, **53**, 6544–6553.

209 A. Alissandratos and C. J. Easton, Biocatalysis for the application of CO2 as a chemical feedstock, *Beilstein J. Org. Chem.*, 2015, **11**, 2370–2387.

210 E. C. C. Baly, I. M. Heilbron and D. P. Hudson, CXXX.—Photocatalysis. Part II. The photosynthesis of nitrogen compounds from nitrates and carbon dioxide, *J. Chem. Soc., Trans.*, 1922, **121**, 1078–1088.

211 J. A. Bassham, A. A. Benson, L. D. Kay, A. Z. Harris, A. T. Wilson and M. Calvin, The Path of Carbon in Photosynthesis. XXI. The Cyclic Regeneration of Carbon Dioxide Acceptor1, *J. Am. Chem. Soc.*, 1954, **76**, 1760–1770.

212 (*a*) L. F. Li, L. Ljungdahl and H. G. Wood, Properties of Nicotinamide Adenine Dinucleotide Phosphate-Dependent Formate Dehydrogenase from Clostridium thermoaceticum, *J. Bacteriol.*, 1966, **92**, 405–412; (*b*) L. Calzadiaz-Ramirez and A. S. Meyer, Formate dehydrogenases for CO2 utilization, *Curr. Opin. Biotechnol.*, 2022, **73**, 95–100.

213 K. Murashima, H. Yoneda, H. Sumi and Y. Amao, Electrocatalytic production of formaldehyde with formaldehyde dehydrogenase using a viologen redox mediator, *New J. Chem.*, 2022, **46**, 10004–10011.

214 J. Shi, Y. Jiang, Z. Jiang, X. Wang, X. Wang, S. Zhang, P. Han and C. Yang, Enzymatic conversion of carbon dioxide, *Chem. Soc. Rev.*, 2015, **44**, 5981–6000.

215 (*a*) M. Miller, W. E. Robinson, A. R. Oliveira, N. Heidary, N. Kornienko, J. Warnan, I. A. C. Pereira and E. Reisner, Interfacing Formate Dehydrogenase with Metal Oxides for the Reversible Electrocatalysis and Solar-Driven Reduction of Carbon Dioxide, *Angew. Chem., Int. Ed.*, 2019, **58**, 4601–4605; (*b*) B. S. Jayathilake, S. Bhattacharya, N. Vaidehi and S. R. Narayanan, Efficient and Selective Electrochemically Driven Enzyme-Catalyzed Reduction of Carbon Dioxide to Formate using Formate Dehydrogenase and an Artificial Cofactor, *Acc. Chem. Res.*, 2019, **52**, 676–685.

216 (*a*) S. K. Kuk, R. K. Singh, D. H. Nam, R. Singh, J.-K. Lee and C. B. Park, Photoelectrochemical Reduction of Carbon Dioxide to Methanol through a Highly Efficient Enzyme Cascade, *Angew. Chem., Int. Ed.*, 2017, **56**, 3827–3832; (*b*) K. Ma, O. Yehezkeli, E. Park and J. N. Cha, Enzyme Mediated Increase in Methanol Production from Photoelectrochemical Cells and CO_2, *ACS Catal.*, 2016, **6**, 6982–6986; (*c*) R. K. Yadav, G. H. Oh, N.-J. Park, A. Kumar, K.-j. Kong and J.-O. Baeg, Highly Selective Solar-Driven Methanol from CO_2 by a Photocatalyst/Biocatalyst Integrated System, *J. Am. Chem. Soc.*, 2014, **136**, 16728–16731.

217 R. Cazelles, J. Drone, F. Fajula, O. Ersen, S. Moldovan and A. Galarneau, Reduction of CO_2 to methanol by a polyenzymatic system encapsulated in phospholipids–silica nanocapsules, *New J. Chem.*, 2013, **37**, 3721–3730.

218 W. Liu, Y. Hou, B. Hou and Z. Zhao, Enzyme-catalyzed Sequential Reduction of Carbon Dioxide to Formaldehyde, *Chin. J. Chem. Eng.*, 2014, **22**, 1328–1332.

219 J. Shi, L. Zhang and Z. Jiang, Facile Construction of Multicompartment Multienzyme System through Layer-by-Layer Self-Assembly and Biomimetic Mineralization, *ACS Appl. Mater. Interfaces*, 2011, **3**, 881–889.

220 J. Shi, X. Wang, Z. Jiang, Y. Liang, Y. Zhu and C. Zhang, Constructing spatially separated multienzyme system through bioadhesion-assisted bio-inspired mineralization for efficient carbon dioxide conversion, *Bioresour. Technol.*, 2012, **118**, 359–366.

221 J. Shi, X. Wang, W. Zhang, Z. Jiang, Y. Liang, Y. Zhu and C. Zhang, Synergy of Pickering Emulsion and Sol-Gel Process for the Construction of an Efficient, Recyclable Enzyme Cascade System, *Adv. Funct. Mater.*, 2013, **23**, 1450–1458.

222 P. S. Nabavi Zadeh, M. Zezzi do Valle Gomes, B. Åkerman and A. E. C. Palmqvist, Förster Resonance Energy Transfer Study of the Improved Biocatalytic Conversion of CO_2 to Formaldehyde by Coimmobilization of Enzymes in Siliceous Mesostructured Cellular Foams, *ACS Catal.*, 2018, **8**, 7251–7260.

223 J. Zhou, S. Yu, H. Kang, R. He, Y. Ning, Y. Yu, M. Wang and B. Chen, Construction of multi-enzyme cascade

biomimetic carbon sequestration system based on photocatalytic coenzyme NADH regeneration, *Renewable Energy*, 2020, **156**, 107–116.

224 P. Bauler, G. Huber, T. Leyh and J. A. McCammon, Channeling by Proximity: The Catalytic Advantages of Active Site Colocalization Using Brownian Dynamics, *J. Phys. Chem. Lett.*, 2010, **1**, 1332–1335.

225 (*a*) J. Liu and M. Antonietti, Bio-inspired NADH regeneration by carbon nitride photocatalysis using diatom templates, *Energy Environ. Sci.*, 2013, **6**, 1486–1493; (*b*) A. Weckbecker, H. Gröger and W. Hummel, in *Biosystems Engineering I: Creating Superior Biocatalysts*, ed. C. Wittmann and R. Krull, Springer Berlin Heidelberg, Berlin, Heidelberg, 2010, pp. 195–242.